ENDOCANNABINOID METABOLISM AND PEROXISOME PROLIFERATOR-ACTIVATED RECEPTORS SIGNALLING

Mauro Dionisi, MSc.

Thesis submitted to the University of Nottingham for the degree of Doctor of Philosophy

May 2010

ACKNOWLEDGEMENTS

I would first like to thank both my supervisors Dr. Andrew Bennett and Dr. Stephen Alexander for all their support, both scientific and personal. In particular, I would like to thank them for the stimulating discussions we had in these years I spent at the University of Nottingham.

My thanks also go to the entire FRAME lab and in particular to Yan, Bright, Roslina, Paul, Monika, Elke and Nicola for all their help, not only in the lab.

I would also like to thank Michael Garle for bearing with all my questions and for his helping hand. I also thank Dr. Leonie Norris for the LC-MS/MS endocannabinoids measurement.

I acknowledge the MRC and FRAME for funding this project.

Finally, I want to thank my parents for giving me the possibility of studying and getting in love with science. I would also like to thank my girlfriend for always being herself and for being there for me during all this time.

ABSTRACT

The fatty acid amides (FAAs) family includes endocannabinoids, such as anandamide, as well as endocannabinoid-like molecules, such as *N*-palmitoylethanolamine (PEA) and *N*-oleoylethanolamine (OEA). Members of the FAA family show agonist activity at transmitter-gated channels (TRPV1), as well as peroxisome poliferator-activated receptors (PPARs). Given that FAAs appear to be hydrolysed principally through the action of the enzyme fatty acid amide hydrolase, inhibition of FAAH should lead to accumulation of a variety of FAAs. Therefore, in this study it was investigated whether pharmacological inhibition of FAAH could influence PPAR activity in SH-SY5Y human neuroblastoma cells or HeLa human cervical carcinoma cells.

FAAH activity was assessed by monitoring liberation of [^{3}H]-ethanolamine from labelled anandamide. FAAH protein and RNA expression were measured by immunoblotting and qRT-PCR respectively. Endocannabinoid levels were measured by LC-MS/MS. In order to evaluate PPAR activation, a PPRE-linked luciferase construct was co-transfected with expression plasmids for either PPAR α, β or γ. Binding to PPAR receptors was assessed with a competitor displacement assay (Invitrogen).

In intact SH-SY5Y cells, sustained FAAH inhibition by URB597 (~75 %) led to accumulation of AEA, 2AG and PEA, but not OEA. Treatment with URB597, OL135 or PF750, three structurally and functionally distinct FAAH inhibitors, induced activation of endogenously expressed PPARs, while no activation was observed in FAAH-1 negative HeLa cells. Furthermore, exposure to URB597, OL135 or PF750 led to activation of over-expressed

PPARs in SH-SY5Y cells. To rule out direct activation of PPARs by the FAAH inhibitors, cell-free binding assays showed that URB597, OL135 and PF750 could not bind to PPARα, PPARβ or PPARγ. Surprisingly, treatment with URB597 in HeLa cells led to intracellular accumulation of PEA but not AEA, OEA or 2AG. This might be due to inhibition of either FAAH-2 or NAAA, both of which are expressed in HeLa cells. Moreover, the presence of either URB597 or OL135 led to activation of PPARγ receptors over-expressed in HeLa cells.

In conclusion, data in this study showed activation of PPAR nuclear receptors *in vitro* by inhibition of FAAH activity and subsequent augmentation of endocannabinoid tone. These data suggest that, at least in a model setup, it is possible to modulate the endocannabinoid tone without any previous external stimulus of their synthesis and trigger a functional effect.

LIST OF ABBREVIATIONS

AEA: *N*-arachidonoylethanolamine (anandamide)

CNS: Central nervous system

DMSO: Dimethyl sulfoxide

EC: Endocannabinoid

ECL: Endocannabinoid-like molecules

EMT: Endocannabinoid membrane transporter

FAA: Fatty acid amide

FAAH: Fatty acid amide hydrolase

MGL: Monoglyceride lipase

NAAA: *N*-acylethanolamine-hydrolizing acid amidase

ODA: Cis-9,10-octadecanoamide (oleamide)

OEA: *N*-oleoylethanolamine

PEA: *N*-palmitoylethanolamine

PPAR: Peroxisome proliferator-activated receptor

PPRE: PPAR responsive element

2AG: 2-arachidonoylglycerol

1. INTRODUCTION

1.1. Fatty acid amides (FAAs), N-acyl-ethanolamines (NAEs) and Endocannabinoids (ECs)

Fatty acid amides (FAAs, Figure 1.1) are signalling lipids among which the most studied compounds found *in vivo* are: the endogenous cannabinoid *N*-arachinoylethanolamine (anandamide, AEA), the anti-inflammatory *N*-palmitoylethanolamine (PEA), the regulator of food intake *N*-oleoylethanolamine (OEA) and the sleeping inducing factor Cis-9,10-octadecanoamide (oleamide, ODA) (McKinney *et al.*, 2005). AEA, PEA and OEA belong to the *N*-Acyl Ethanolamines (NAEs) family, while ODA is a fatty acid primary amide (FAPA). NAEs have been largely studied in the last few years after the discovery of AEA as an endogenous ligand for the cannabinoid receptors (Devane *et al.*, 1992). In fact, while the main psychoactive compound of *Cannabis Sativa* (-)-Δ^9-tetrahydrocannabinol (THC) has been isolated in the early 1970s (Gaoni *et al.*, 1971), the endogenous cannabinoid system (endocannabinoid system) started to be delineated only in the last two decades (Mechoulam *et al.*, 1995).

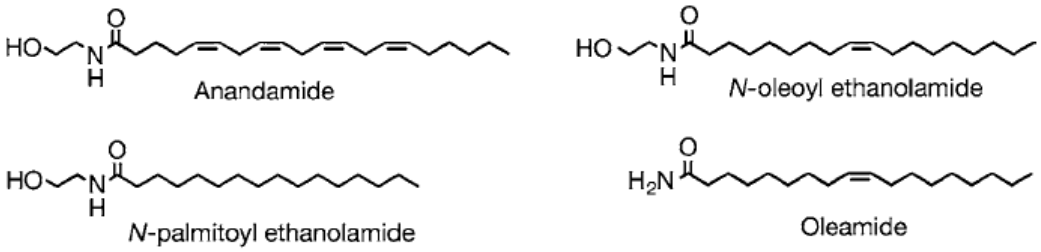

Figure 1.1: Structure of commonly found FAAs (taken from McKinney and Cravatt, 2005)

Endocannabinoids (ECs) are by definition endogenous ligands for the cannabinoid receptors and are believed to follow on-demand biosynthesis. There are at least two cannabinoid receptors (CB_1 and CB_2), and they both belong to the $G_{i/o}$-protein-coupled class of cell surface receptors. Indeed, they are both coupled to pertussis toxin-sensitive inhibition of cAMP formation, implicating $G_{i/o}$-protein as transducers, and to stimulation of p42/p44 mitogen-activated protein kinase activity. CB_1, but not CB_2, receptors signal also via ion channels by inhibiting N- and P/Q-type calcium channels and by activating A-type and inwardly rectifying potassium channels. Furthermore, CB_1 activation stimulates phosphatidylinositol 3-kinase and protein kinase B (Bisogno *et al.*, 2005). There is ample evidence supporting the fact that cannabinoids act as retrograde messengers, and their signalling through CB_1 receptors inhibits neurotransmitter release and neurotransmission (Straiker *et al.*, 2006). The CB_1 receptor was cloned in 1990 (Matsuda *et al.*, 1990) and it is mainly but not exclusively expressed in the central nervous system; here, it is widely distributed through the forebrain while it has a more localized distribution in the hindbrain and spinal cord (Tsou *et al.*, 1998). The CB_1 receptor is the most abundant GPCR expressed in the brain; however, it is also found in a variety of peripheral tissues such as adipose tissue, liver, the gastrointestinal tract, and pancreas (Di Marzo *et al.*, 2004; Pagotto *et al.*, 2006) (Table 1.1). The CB_2 receptor was cloned in 1993 (Munro *et al.*, 1993) and it is mostly found in peripheral tissues like spleen and testis (Brown *et al.*, 2002) and in the immune system (Klein *et al.*, 2003), but it is also believed to be expressed in the central nervous system (Onaivi *et al.*, 2006). Recently, two

distinct human CB_2 isoforms have been identified, with differential tissue expression and regulation by cannabinoid receptor ligands (Liu *et al.*, 2009).

Central Nervous System	Genitourinary/ Reproductive	Gastrointestinal	Other
Brain	Kidney	Ileum	Adipose
Spinal cord	Placenta	Liver	Lung
	Prostate	Stomach	Skeletal Muscle
	Testis and sperm	Pancreas	Spleen
	Uterus		

Table 1.1: Human tissues and organs expressing the CB_1 receptor RNA (Di Marzo *et al.*, 2004; Pagotto *et al.*, 2006)

ECs are mainly represented by AEA and by 2-arachidonoyl-glycerol (2AG, Figure 1.2). AEA can act as an endogenous ligand for CB_1 and CB_2 receptors (Devane *et al.*, 1992) but it is also an endogenous agonist for the vanilloid TRPV1 receptor channel (Van der Stelt *et al.*, 2005) and the GRP55 receptor (Ryberg *et al.*, 2007). Depending on the tissue and biological response measured, it behaves as a partial or full agonist of CB_1 receptors. It has very low efficacy as CB_2 agonist and may even act as antagonist depending on the G proteins interacting (Gómez-Ruiz *et al.*, 2007). Instead, 2AG is a full CB_1 and CB_2 agonist (Mechoulam *et al.*, 1995) and for this reason many authors believe 2AG to be the true ligand for CB_2 receptors. ECs and in particular

AEA produce a wide range of biological effects. Most notably, AEA plays an important role in a cannabinergic pain-suppression system existing within the dorsal and lateral periaqueductal gray (PAG) (Walker *et al.*, 1999). However, ECs also show antiproliferative, antiemetic, appetite enhancement, and anxiolytic activity as well as neuroprotective effects that have strong clinical implications (Martin *et al.*, 1999).

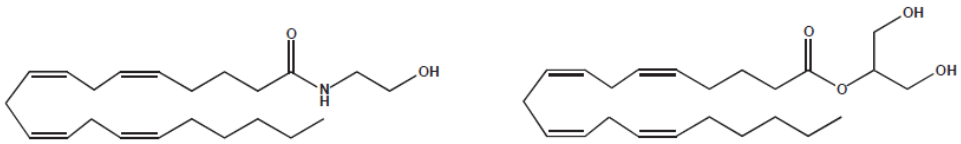

Anandamide
Partial CB_1 agonist, weak CB_2 agonist

2-Arachidonoyl-glycerol
Full CB_1 and CB_2 agonist

Figure 1.2: Chemical structures of the two main endocannabinoids and their binding and functional properties at cannabinoid receptors (Taken from Bisogno *et al.*, 2005)

PEA was extensively studied in the 1950s for its anti-inflammatory properties, but research on this compound sped up after discovery of AEA as an endogenous ligand for the cannabinoid receptors (Devane *et al.*, 1992). Despite being closely related to AEA in terms of structure and belonging to the same family, PEA does not bind the cannabinoid receptors (Lo Verme *et al.*, 2005). OEA binds with a relatively low affinity to the CB_1 but not the CB_2 receptor (Appendino *et al.*, 2006). This monounsaturated FAE decreases food intake

and body weight gain through a cannabinoid receptor-independent mechanism (Fu *et al.*, 2003)

The ability compounds such as PEA and OEA to activate the CB_1/CB_2 receptor system is likely to be caused by *entourage effect* and they may elevate other ECs, by inhibiting their catabolism. For example, PEA was shown to potently enhance the anti-proliferative effects of AEA on human breast cancer cells at least in part by inhibiting the expression of fatty acid amide hydrolase (FAAH) the major enzyme responsible for AEA degradation (Di Marzo *et al.*, 2001). Moreover, PEA could enhance the TRPV1-mediated effects of AEA and capsaicin on calcium influx into cells (De Petrocellis *et al.*, 2002).

Oleamide (octadec-9,10Z-enamide, ODA, Figure 1.1) is a fatty acid primary amide first identified as an endogenous lipoamide in the cerebrospinal fluid of sleep-deprived cats (Cravatt *et al.*, 1995). ODA is a sleep-inducing factor when administered *in vivo*, also eliciting hypothermia, analgesia and hypo-locomotion by acting through either the endocannabinoid, GABAergic and dopaminergic systems (Fedorova *et al.*, 2001). *In vitro*, ODA has also been reported to induce vasorelaxation in the rat small mesenteric artery (Hoi *et al.*, 2006). While the biological effects of ODA are well documented, the molecular mechanisms and site of action remain elusive. However, i*n vitro*, ODA can inhibit gap junction formation (Boger *et al.*, 1998), modulate GABA (Yost *et al.*, 1998) and 5-HT (Thomas *et al.*, 1998) receptors. ODA does not belong to the NAEs family of ECs, but it has been demonstrated to bind to the

CB_1 receptor *in vitro* (Leggett *et al.*, 2004). However, whether it can be classified as an endogenous cannabinoid is still under debate (Fowler, 2004). Recently, it has been proposed to use the appellation of endocannabinoid-like molecules (ECLs) when referring to compounds such as OEA, PEA, ODA and other families of ECs related molecules (Alexander *et al.*, 2007).

1.2. ECs biochemistry

1.2.1. Biosynthesis

ECs biosynthesis can follow various pathways and it is believed to differ from that typical of classical neurotransmitters in which vesicle storage is involved. AEA and 2AG, and more in general all ECLs, exist as preformed precursors in the membrane and thus are enzymatically produced on-demand in response to specific signals, such as an increase in intracellular calcium or activation of phospholipase C β by $G_{q/11}$ metabotropic receptors (Straiker *et al.*, 2006).

1.2.1.1. FAAs and AEA

FAAs biosynthesis has been widely studied. Early work was done on PEA and OEA hydrolysis, while lately much attention has been given to AEA biosynthesis (Schmid, 2000). The major biosynthetic pathway involves a calcium-dependent transacylase that transfers an acyl group from the *sn*-1 position of phospholipids to the N-position of phosphatidylethanolamine to form N-acyl-phosphatidylethanolamine (NAPE, Figure 1.3). A phospholipase D selective for NAPEs (NAPE-PLD) then hydrolyses them to form the

corresponding NAE (Bisogno *et al.*, 2005; McKinney *et al.*, 2005). The activity of NAPE-PLD is regulated by membrane depolarization or by a number of major neurotransmitters, such as dopamine, glutamate and acetylcholine (Giuffrida *et al.*, 1999; Kim *et al.*, 2002; Varma *et al.*, 2001). It is worth mentioning that other pathways have also been proposed (Liu *et al.*, 2008)

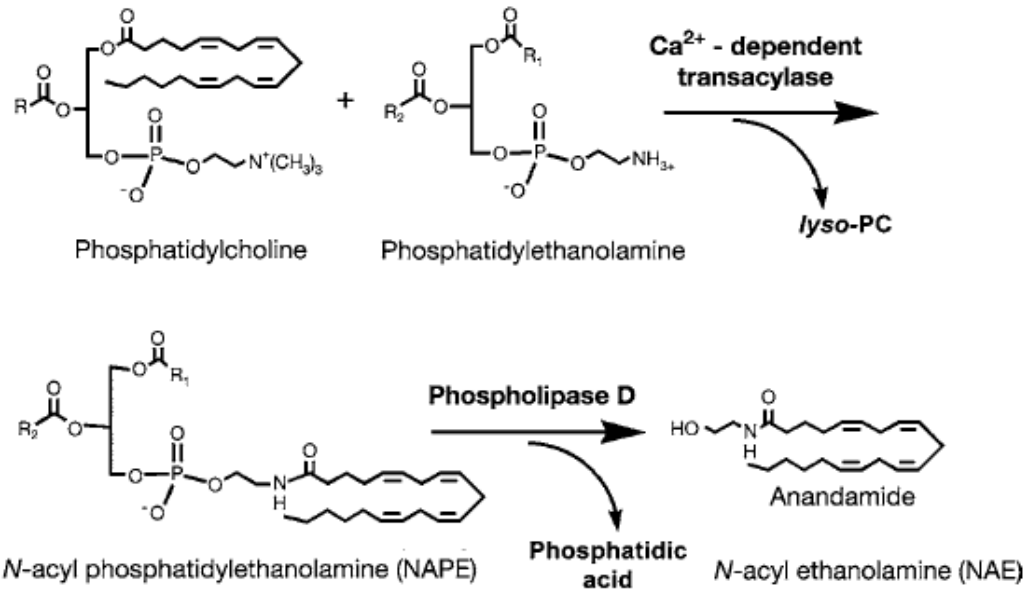

Figure 1.3: Proposed biosynthetic route for NAEs (Taken from McKinney and Cravatt, 2005)

The fatty acid primary amides (FAPAs) and ODA biosynthetic pathway has been less intensively investigated, but is believed to involve the peptidyl glycine α-amidating monooxygenase (PGAM). FAPAs may be generated by oxidative cleavage of *N*-fatty acyl glycines by PGAM (Figure 1.4) (McKinney

and Cravatt, 2005). Recently, Driscoll et al. (2007) suggested that cytochrome C may also be a route for ODA synthesis.

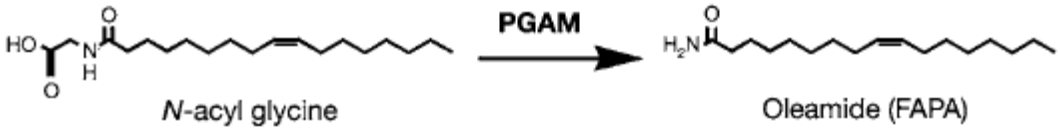

Figure 1.4: Biosynthetic pathway for FAPAs (Taken from McKinney and Cravatt, 2005)

1.2.1.2. 2AG

In unstimulated tissues and cells the levels of the other main endogenous cannabinoid 2AG are higher than those of AEA (Sugiura *et al.*, 1995) and its biosynthetic pathway follows a separate route from that of AEA. In most cases, 2AG is produced from the hydrolysis of diacylglycerols containing arachidonate in the 2 position (DAGs), catalysed by a DAG lipase selective for the sn-1 position (Figure 1.5). Two sn-1 DAG lipase isozymes (DAGLα and DAGLβ) have been cloned (Bisogno *et al.*, 2003). DAGs, in turn, can be produced from the hydrolysis either of phosphoinositides (PI), catalysed by a PI-selective phospholipase C (PI-PLC), as in macrophages, platelets and cortical neurons, or of phosphatidic acid (PA), catalysed by a PA phosphohydrolase, in mouse neuroblastoma cells N18TG2 and in a rat microglial RTMGL1 cell line (Bisogno *et al.*, 2005).

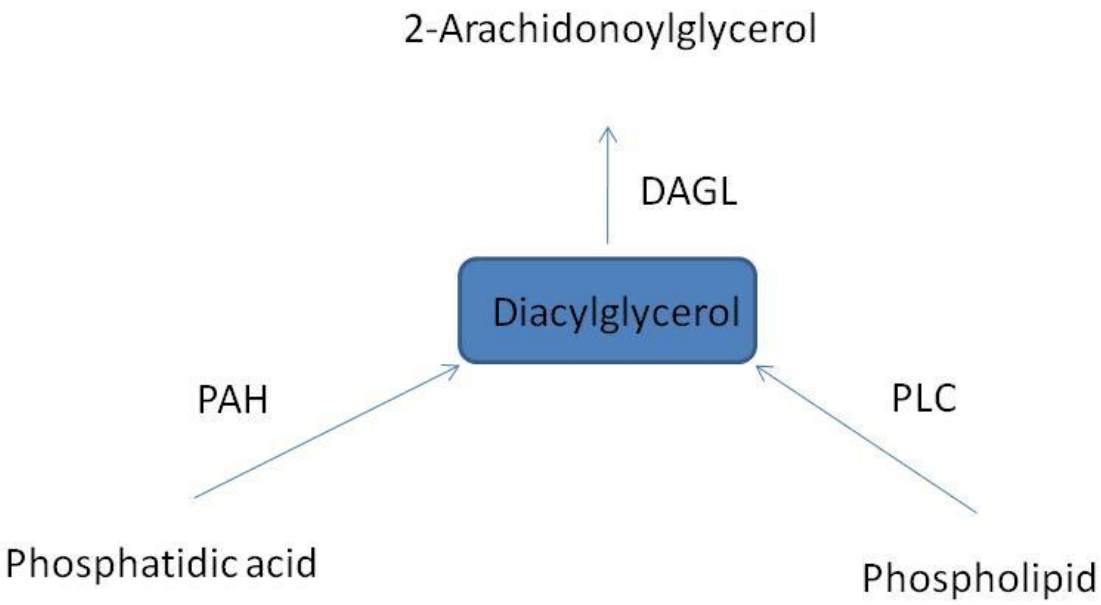

Figure 1.5: Biosynthetic pathways for the endocannabinoid 2-arachidonoylglycerol. PAH: phosphatidic acid hydrolase, PLC: phospholipase C.

1.2.2. Catabolism

Cessation of AEA and 2-AG signaling is believed to occur via a two-step process: transport of endocannabinoids from the extracellular to the intracellular space, and intracellular degradation by hydrolysis or oxidation.

1.2.2.1. Transport

Although the majority of these models were developed based on data from AEA uptake studies, there is some evidence to suggest that AEA and 2-AG uptake occur via a common mechanism.

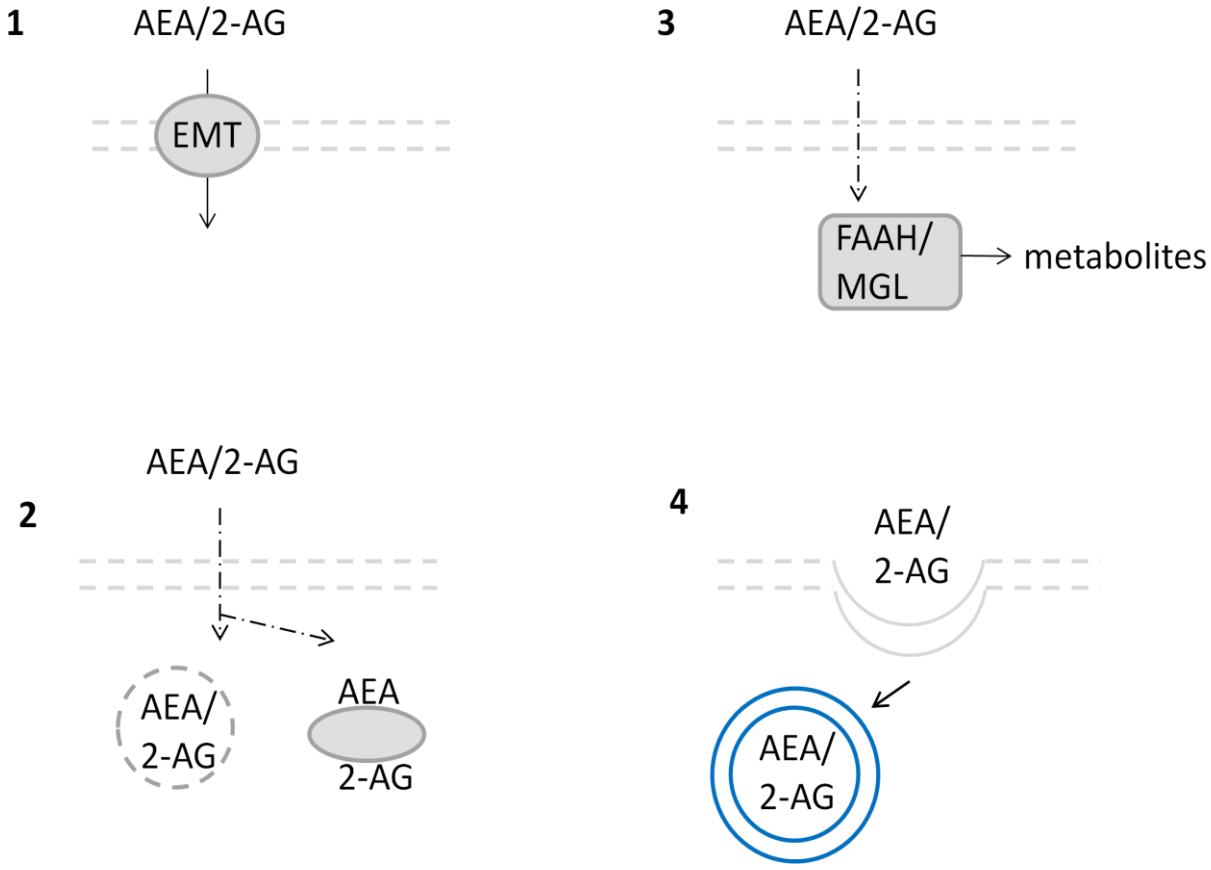

Figure 1.6: Various proposed models for EC transport: 1) EMT: putative EC membrane transporter. 2) Passive diffusion and intracellular sequestration model. 3) FAAH/MGL driven passive diffusion. 4) Carrier-mediated caveolae-Related endocytosis.

Various uptake mechanisms have been proposed in the recent years for both AEA and 2AG (Figure 1.6). The first model requires a yet to be cloned putative EC membrane transporter (EMT) assisting in the translocation of ECs across the plasma membrane. Another theory counts on ECs passively diffusing across the plasma membrane along a catabolism-driven concentration gradient. ECs are sequestered in an intracellular compartment or by binding to an intracellular binding protein prior to metabolism. Alternatively, ECs might passively diffuse across the plasma membrane along a concentration gradient that is driven by their rapid metabolism. Finally, ECs might be transported into cells via a protein carrier-mediated caveolae-related endocytic event (Yates *et al.*, 2009).

1.2.2.2. Hydrolysis

FAAs and AEAs signalling is mainly terminated by the Fatty Acid Amide Hydrolase (FAAH, Figure 1.7), the major enzyme controlling their signalling and concentration *in vivo*. Early work on this enzyme was done on OEA hydrolysis in rat liver (Schmid *et al.*, 1985). AEA was then showed to be hydrolysed by FAAH and the first inhibitor of this enzyme was discovered (Deutsch *et al.*, 1993). FAAH is a member of an unusual class of serine hydrolases termed the amidase signature family that utilizes a serine-serine-lysine catalytic triad (McKinney and Cravatt, 2005). FAAH enzyme activity is highest at alkaline pH and, amongst the FAAs, AEA seems to be the preferred substrate (McKinney and Cravatt, 2005). FAAH hydrolyses AEA to ethanolamine and arachidonic acid and this latter metabolite in particular has

been demonstrated to be involved at least in some of the AEA effects in mice in a tetrad of tests sensitive to ECs (Wiley, 2006).

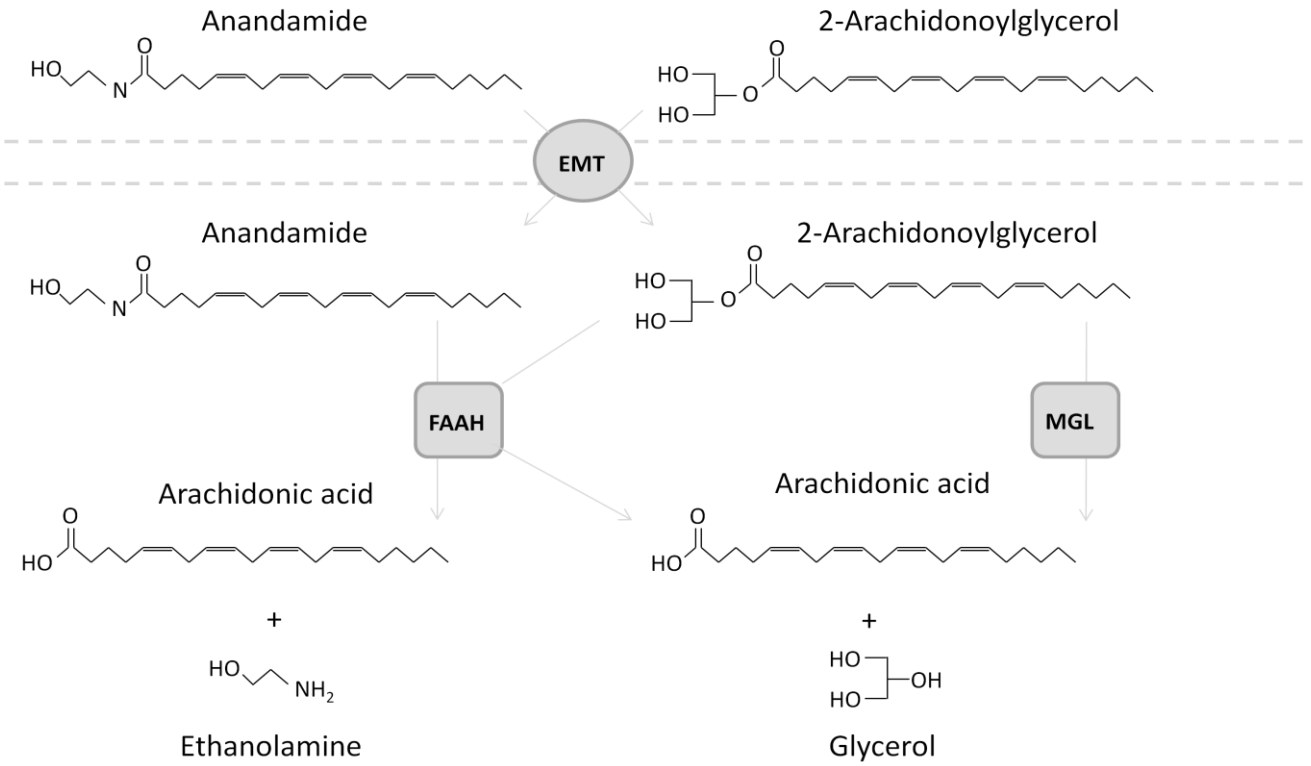

Figure 1.7: Mechanisms for endocannabinoids inactivation. FAAH: fatty acid amide hydrolase; MGL: monoacylglycerol lipase; EMT: putatitve EC membrane transporter.

Recently, a second FAAH widely distributed in mammalian tissues and not expressed in rodents has been isolated and named FAAH-2. This enzyme works at alkaline pH but the preferred substrate seems to be ODA, a primary fatty acid amide (Wei *et al.*, 2006). These two hydrolytic enzymes show a differential pattern of expression in human tissues, FAAH being mainly expressed in the brain, kidney, liver, small intestine, lung, prostate and testis while FAAH-2 being mostly found in the kidneys, liver, lung, prostate, heart

and ovaries (Table 1.2) (Wei *et al.*, 2006). A third enzyme, *N*-Acylethanolamine-hydrolizing Acid Amidase (NAAA) was recently discovered. NAAA works at a more acidic pH and PEA appears to be the major substrate for this enzyme (Tsuboi *et al.*, 2005).

FAAH	FAAH-2
Brain	**Heart**
Kidney	**Kidney**
Liver	**Liver**
Small intestine	**Lung**
Lung	**Prostate**
Prostate	**Ovary**
Testis	

Table 1.2: Tissue distribution of human FAAH and FAAH-2 RNA (Wei *et al.*, 2006)

2AG, the other main endogenous cannabinoid, is mainly hydrolysed to glycerol and arachidonic acid by the enzyme monoglyceride lipase (MGL, Figure 1.7). MGL is a serine hydrolase and is unevenly present in the rat brain, with highest levels in regions where CB_1 cannabinoid receptors are also expressed (hippocampus, cortex, anterior thalamus and cerebellum) (Dinh *et al.*, 2002). However, 2AG has been previously showed to be hydrolysed also by FAAH under particular circumstances (Di Marzo *et al.*, 2008).

1.2.2.3. Oxidation

Because of their fatty acid chain, both AEA and 2AG can also be metabolised by the same enzymes that are responsible for arachidonic acid oxidation. COX-2 is responsible for catalyzing the oxidation of AEA and 2AG into various prostaglandin-ethanolamides (or prostamides) and prostaglandin-glycerol esters, respectively (Fig. 1.8) (Yates *et al.*, 2009)

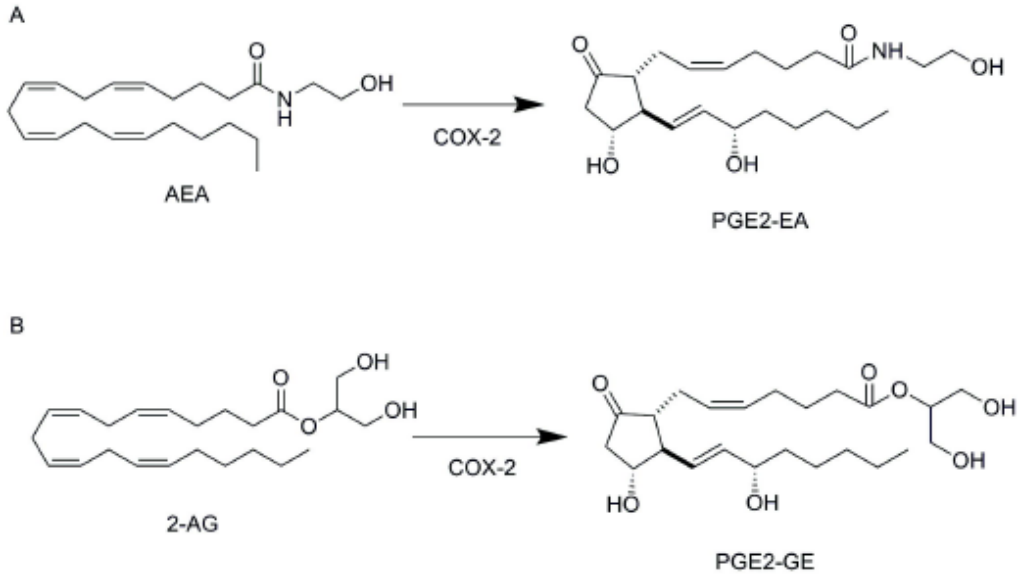

Figure 1.8: The major metabolites generated via COX-2-mediated oxidation of the endocannabinoids A) AEA and B) 2-AG. Prostaglandin E2 ethanolamide, PGE2-EA; prostaglandin E2 glycerol esther, PGE2-GE. Taken from (Yates *et al.*, 2009)

12-LOX and 15-LOX have also been identified as enzymes metabolising both AEA and 2-AG in intact cells. Oxidative metabolism of AEA by 12-LOX and

15-LOX results respectively in the formation of 12- and 15 hydroperoxyeicosatetraenoylethanolamide (12-HETE-EA and 15-HETE-EA), while 12-LOX- and 15-LOX-mediated oxidation of 2AG results in the formation of 12- and 15-hydroperoxyeicosatetraenoic acid glycerol ester (12 HETE-GE and 15-HETE-GE), respectively (Figure 1.9) (Yates *et al.*, 2009). Cytochrome P450 is also been shown to be involved in anandamide metabolism (Snider *et al.*, 2009).

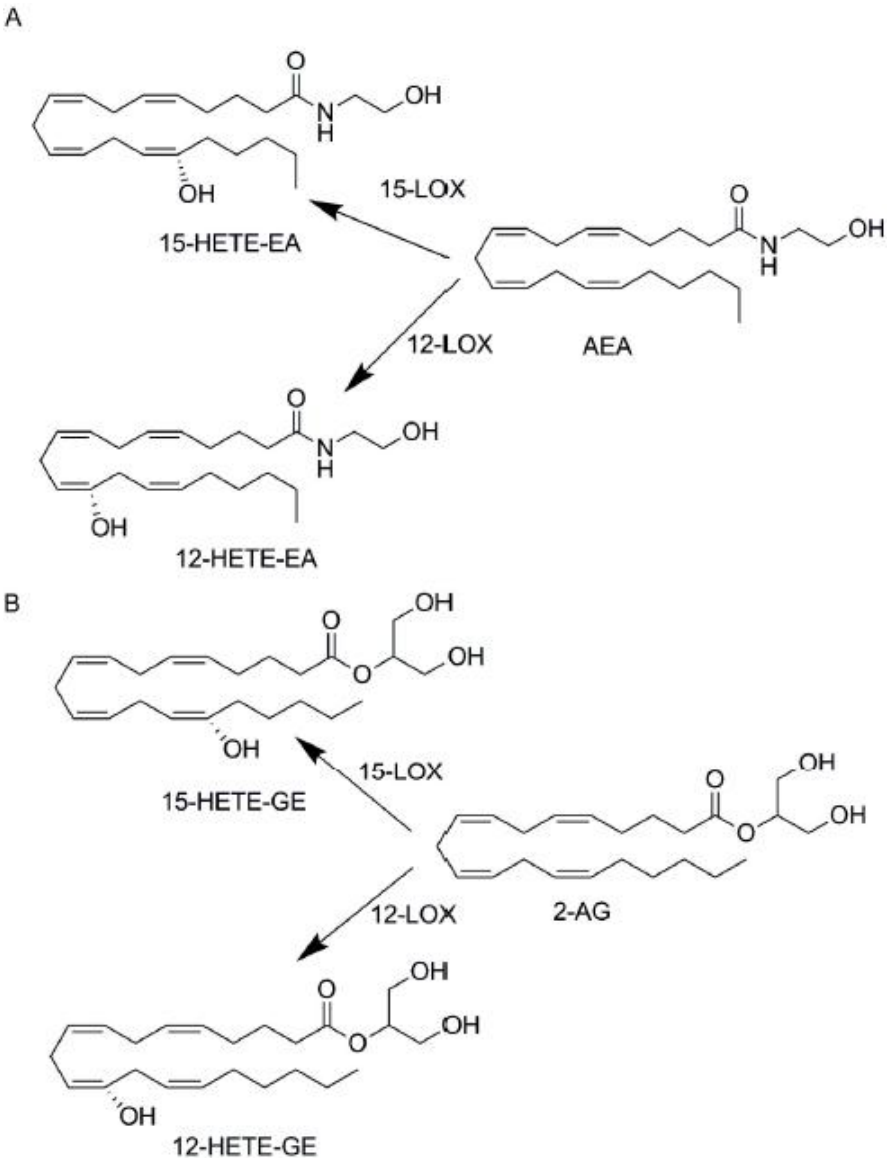

Figure 1.9: The major metabolites generated via oxidation of A) AEA and B) 2-AG by the 12- and 15-LOXs. Hydroperoxyeicosatetraenoylethanolamide, HETE-EA; hydroperoxyeicosatetraenoic acid glycerol ester, HETE-GE. Taken from (Yates *et al.*, 2009)

1.2.3. FAAH inhibitors

In the recent years, much attention has been given to the possibility of manipulating the endogenous cannabinoid system, and in particular FAAH enzyme activity, in order to augment the intracellular levels of the endocannabinoids and increase their activity. One of the most promising applications of this pharmacological modulation may be in the treatment of inflammatory pain (Fowler, 2006). Cannabinoids and endocannabinoids can indeed mediate antihyperalgesia and antinociception, but their mechanism of action is still poorly understood. Although the mechanism by which these compounds can evoke antinociception in the CNS seems to be mediated primarily by the CB_1 receptors, the peripheral mechanism by which some cannabinoids mediate antihyperalgesia appears to be indirect or possibly involve non-CB_1 or –CB_2 receptors (Patwardhan *et al.*, 2006). FAAH is a promising drug target for pain treatment because it might allow the avoidance of undesirable central side effects associated with CB receptor activation (Table 1.3). For example, its pharmacological inhibition increases AEA levels in the brain without inducing immobility, hypothermia or over-eating at doses that are effective at abrogating pain (Kathuria *et al.*, 2003; Piomelli *et al.*, 2006). FAAH knockout mice have higher levels of AEA in the brain and show

signs of an exaggerated endocannabinoid tone, such as reduced pain sensation (Cravatt *et al.*, 2001). Various authors reported that FAAH inhibition is anti-nociceptive in models of acute and inflammatory pain (Fegley *et al.*, 2005; Holt *et al.*, 2005; Kathuria *et al.*, 2003; Russo *et al.*, 2007). However, while FAAH inhibition consistently seems to reduce the response to acute and chronic inflammatory pain through an endocannabinoid related mechanism, its role in neuropathic pain is still unclear (Jhaveri *et al.*, 2006).

	CB1 agonist	FAAH(−/−) mice	FAAH NS mice	Chemical FAAH inhibitor
Potential therapeutic effects				
Analgesia	Yes	Yes	No	Yes
Anxiolysis	Yes/no	Unknown	Unknown	Yes
Anti-inflammation	Yes	Yes	Yes	Unknown
Antispasticity	Yes	Unknown	Unknown	Unknown
Anti-emesis	Yes	Unknown	Unknown	Unknown
Decrease intraocular pressure	Yes	Unknown	Unknown	Unknown
Side Effects				
Hypomotility	Yes	No	No	No
Hypothermia	Yes	No	No	No
Catalepsy	Yes	No	No	No

Table 1.3: Comparison of behavioral effects of CB_1 agonists versus the genetic [global (−/−) or peripheral (NS)] or chemical (inhibitor) inactivation of FAAH (Taken from McKinney and Cravatt, 2005)

1.2.3.1. URB597

URB597 (cyclohexyl carbamic acid 3'-carbamoyl-biphenyl-3-yl ester, Figure 1.10) is a potent and selective FAAH and FAAH-2 inhibitor (Wei *et al.*, 2006). It exhibits selectivity for FAAH compared to Monoacyl Glycerol lipase (MAG

lipase), the principal catabolic enzyme for 2-AG and has been shown not to bind to cannabinoid receptors (Kathuria *et al.*, 2003). URB597 and related carbamate compound inhibit FAAH by covalent modification of the active site (Alexander *et al.*, 2005).

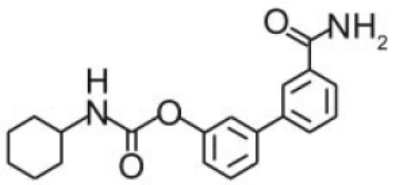

Fig 1.10: Chemical structure of URB597 (Taken Fegley *et al.*, 2005)

URB597 caused the augmentation of AEA, PEA and OEA levels in the brain of rats and wild-type mice but failed to have this effect in FAAH null mice (Fegley *et al.*, 2005). It has also been demonstrated that URB597 dose-dependently reduces oedema formation in carrageenan-induced hind paw inflammation by reducing FAAH activity (Holt *et al.*, 2005).

1.2.3.2. OL135

OL135 is a α-keto-heterocycle (Figure 1.11) that belongs to a potent and reversible class of FAAH inhibitors that show strong selectivity for FAAH relative to other mammalian hydrolases (Boger *et al.*, 2005). As URB597, even OL135 has been proven to inhibit FAAH-2 (Wei *et al.*, 2006). When administered to rodents, OL135 raise central nervous system levels of AEA

and promote cannabinoid receptor 1-dependent analgesia (Chang *et al.*, 2006; Lichtman *et al.*, 2004). Moreover, inhibition of FAAH by OL135 enhances the anti-allodynic actions of ECs in a mouse model of acute pain (Palmer *et al.*, 2008).

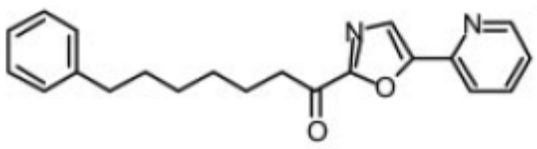

Fig 1.11: Chemical structure of OL135. Taken from (Lichtman *et al.*, 2004)

1.2.3.3. PF-750

Recently, both URB597 and OL135 have been demonstrated to have some off-targets. Indeed, activity-based protein profiling (ABPP) and enzymatic assays showed that they can inhibit various carboxylesterases (Zhang *et al.*, 2007). On the contrary, ABPP showed that PF-750 (N-phenyl-4-(quinolin-3-ylmethyl)piperidine-1-carboxamide, Figure 1.12) was completely selective for FAAH relative to other mammalian serine hydrolases. PF750 belongs to a novel class of piperidine ureas irreversible FAAH inhibitors that show higher *in vitro* potencies than previously established classes of FAAH inhibitors (Ahn *et al.*, 2007).

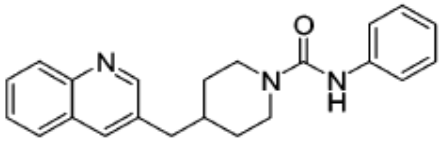

Fig 1.12: Chemical structure of PF-750. Taken from (Ahn *et al.*, 2007)

1.3. Peroxisome proliferator-activated receptors

Recently, it has been demonstrated that ECs are not only ligands for the cannabinoid receptors. In fact, their activity cannot always be explained by the sole interaction with cannabinoid receptors and they have been demonstrated to modulate the activation of several other receptor types including opioid receptors, vanilloid TRPV1 receptor, serotonin $(5\text{-HT})_3$ receptor, N-methyl-D-aspartate (NMDA) receptor, glycine receptors and nicotinic acetylcholine receptors (nAChR) (Demuth *et al.*, 2006). Moreover, ECs modulate the functional properties of voltage-gated ion channels including Ca^{2+} channels, Na^{+} channels, various types of K^{+} channels (Oz, 2006). Recent findings have also highlighted the interaction of the endocannabinoid system and related compounds with the peroxisome proliferators-activated receptors PPARs (O'Sullivan, 2007).

PPARs are nuclear hormone receptors. They act as ligand-activated transcription factors and they are principally linked to lipid metabolism, glucose homeostasis, apoptosis, immune response modulation and inflammation. There are three types of PPARs and they are all encoded by

different genes. PPARα is mainly expressed in brown adipose tissue, liver, kidney, heart and skeletal muscle. PPARγ is highly expressed in adipose tissue but it is also expressed in other tissues like muscle, colon, kidney, pancreas and spleen. PPARβ (also called PPARδ) is almost ubiquitous but it is markedly expressed in brain, adipose tissue and skin. PPARα is the least selective in terms of ligand binding among the three receptors and its natural ligands are various saturated and unsaturated fatty acids. PPARγ is the most selective of the PPARs. Fatty acids and eicosanoid derivatives can bind this receptor, but PPARγ markedly prefers polyunsaturated fatty acids like linoleic acid, linolenic acid and arachidonic acid. Natural ligands of PPARβ are prostacyclin and unsaturated fatty acids with a selectivity that is intermediate between that of PPARγ and PPARα. Among the synthetic ligands, PPARγ ligands thiazolidinediones like rosiglitazone are used in patients with type 2 diabetes while fibrates, PPARα ligands, are used to treat dislipidemia (Berger *et al.*, 2002).

Until recently, it was believed that upon binding of a ligand to the ligand binding domain (LBD), the PPAR receptor changes its conformation and forms an heterodimer with retinoid X receptor (RXR, a nuclear receptor for 9-cis-retinoic acid) (Michalik *et al.*, 2006). However, it has been shown that *in vivo* a high percentage of PPARs and RXR receptors is associated even in the absence of ligand (Tudor *et al.*, 2007). This complex binds to the DNA through the PPAR's DNA binding domain (DBD) and act as a transcription factor. The DBD binds specific response elements (PPREs) located within the promoter regions of downstream genes. Presence of a number of co-repressors and co-

activators can either stimulate or inhibit receptor-mediated gene expression (Michalik *et al.*, 2006). Notably, it has been demonstrated that co-regulator recruitment more than DNA binding plays a crucial role in receptor mobility, suggesting that the transcriptional complexes are formed prior to promoter binding (Tudor *et al.*, 2007).

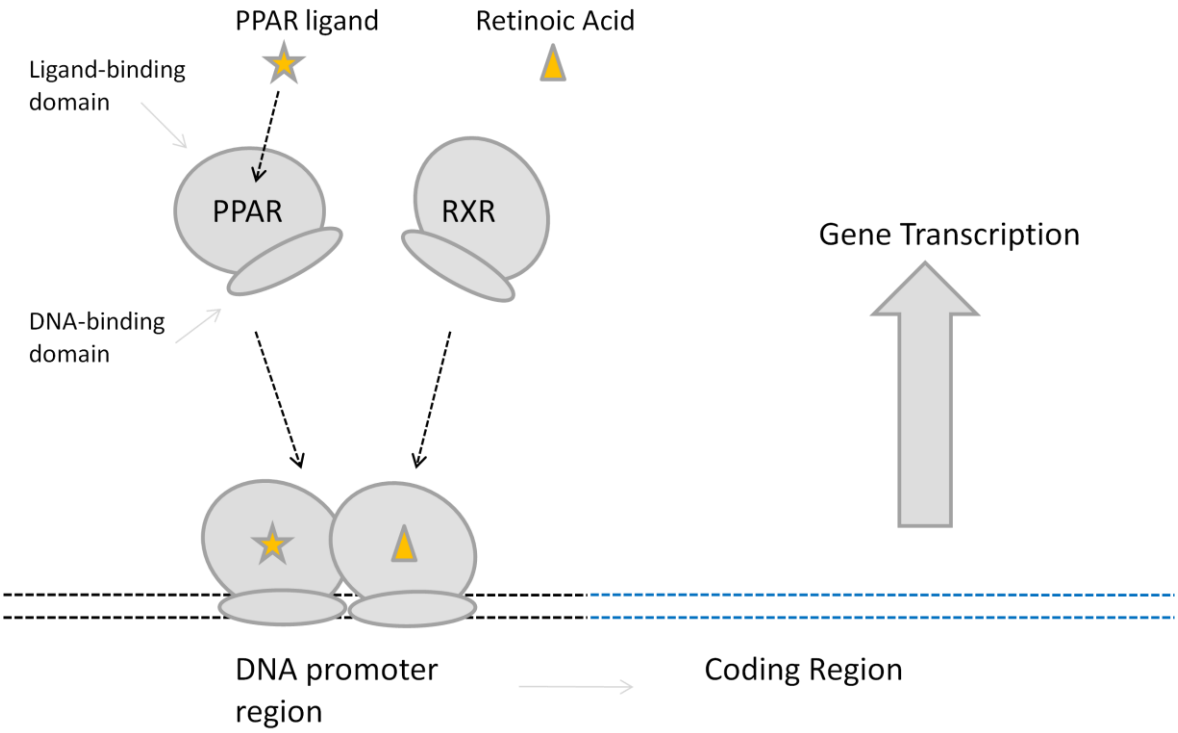

Figure 1.13: Schematic diagram of PPARs function as ligand-activated transcription factors

1.3.1. ECs and PPARs

Recent findings suggested an interaction of the endocannabinoid system and related compounds (NAEs) with the nuclear receptors PPARs. Indeed, various authors reported how a variety of ECs can bind to and activate PPARs when

administered exogenously (O'Sullivan, 2007). AEA has been previously reported to transactivate and bind to both PPARα and PPARγ (Bouaboula *et al.*, 2005; Sun *et al.*, 2006). 2AG was also demonstrated to transactivate both PPARα and PPARγ (Kozak *et al.*, 2002; Rockwell *et al.*, 2006a). Moreover, the anti-inflammatory properties of PEA have been shown to be PPARα-dependent *in vitro* and PEA stimulates PPARα gene expression when topically applied to mouse skin (Lo Verme *et al.*, 2005). It has also been proposed that OEA elicits satiety in rodents by activating PPARα in the vagal nerve (Guzman *et al.*, 2004). OEA also causes lipolysis in adipose tissue by a PPARα-dependent route (Guzman et al., 2004). Finally, THC and cannabidiol (CBD) have both been reported to elicit vasorelaxation through a PPARγ dependent mechanism (O'Sullivan *et al.*, 2009; O'Sullivan *et al.*, 2005).

Recently, *in vivo* effects of FAAH inhibition by URB597 such as analgesia, enhancement of memory acquisition and suppression of nicotine-induced excitation of dopamine cells have been linked to PPAR activation (Jhaveri *et al.*, 2008; Mazzola *et al.*, 2009; Melis *et al.*, 2008). Growing interest has been given in recent years to the ability of PPARs to modulate neuroinflammation and neurodegeneration. PPAR signalling can have an important role in several diseases of the central nervous system, amongst them Multiple Sclerosis, Parkinson's and Alzheimer's disease (Drew *et al.*, 2006). In particular, activation of PPARγ is thought to play an important role in brain inflammatory conditions inhibiting the production of proinflammatory mediators like cytokines and inducible nitric oxide synthase (García-Bueno *et al.*, 2005).

1.4. Aim of the study

The aim of the present work was to dissect the mechanism by which inhibition of NAEs catabolism can modulate PPARs activation. The possibility of elevating intracellular levels of ECs by inhibiting their metabolism and whether this augmentation would lead to activation of PPARs nuclear receptors was tested (Figure 1.14). This issue was addressed by using the potent and selective FAAH inhibitor URB597 alongside OL135 and PF750, two structurally and functionally distinct FAAH inhibitors, to determine whether the intracellular elevation of FAA levels can lead to activation of PPARs nuclear receptors. Human neuroblastoma cells (SH-SY5Y) were used as a model of neuronal cells. HeLa cells, a cell line derived from a human cervical cancer, are widely used in the literature as a cell line lacking FAAH (Day *et al.*, 2001) and were used in the present study as a negative control.

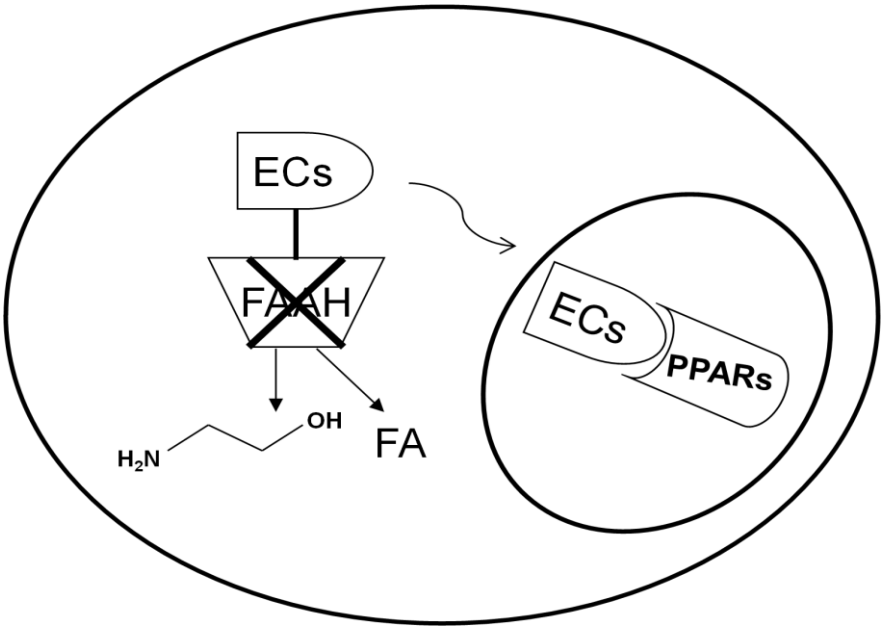

Figure 1.14: Schematic view of the hypothesis of the present study: pharmacological inhibition of FAAH should lead to an increase in intracellular ECLs that would in turn activate PPARs nuclear receptors. FA: fatty acid

2. MATERIALS AND METHODS

2.1. Materials

2.1.1. Reagents

All the reagents used in the study were purchased from Sigma (St. Louis, MO/USA), unless otherwise stated. AEA, 2-AG, OEA, PEA, arachidonic acid, palmitic acid, oleic acid, WY14643, GW0742, GW6471, GW9662 were purchased from Tocris Cookson (Bristol, UK). ODA was prepared by Dr Stephen Alexander by condensation of oleoylchloride with saturated ammonia solution and purification over silica. OL135 was a kind gift from Prof Ben Cravatt (San Diego, CA/USA). GSK0660 and rosiglitazone were donated by GlaxoSmithKline (London, UK). CCP was synthesised by Dr Stephen Alexander. Radiolabeled anandamide [ethanolamine-1-^{3}H] ([^{3}H]AEA, (specific activity 2.2x10^{12} Bq/mmol) and 2-mono-oleoylglycerol [glycerol-1,2,3-^{3}H] ([^{3}H]2OG, specific activity 7.4x10^{11} Bq/mmol) were obtained from American Radiolabeled Chemicals (St. Louis, MO/USA).

2.1.2. Enzymes and antibodies

Molecular biology enzymes used in this study were all purchased from Promega (Madison, WI/USA) unless otherwise stated. Because of time limitations, a single protocol has been used for all antibodies used in the study.

Rabbit polyclonal anti-FAAH antibody was from Millipore (Billerica, MA/USA); mouse monoclonal anti-PPARα antibody was from Sigma (Poole, UK); rabbit polyclonal anti-PPARβ was from Santa Cruz (Santa Cruz, CA/USA), rabbit polyclonal anti-PPARγ was from Cell Signaling (Beverly,

MA/USA); mouse monoclonal anti-β-actin and mouse polyclonal anti-actin were from Sigma (Poole, UK).

2.1.3. Vectors and cell lines

Name	Origin	Insert Length
pcDNA3.1/Zeo-hPPARα	Invitrogen	1.4 kbp
pcDNA3.1/Zeo-hPPARβ	Invitrogen	1.3 kbp
pcDNA3.1/Zeo-hPPARγ2	Invitrogen	1.5 kbp

Human neuroblastoma SH-SY5Y cells, human cervical adenocarcinoma HeLa cells, Chinese hamster ovary CHO cells and mouse embryonic fibroblast 3T3-L1 cells were all purchased from ECACC (Salisbury, UK).

2.2. qRT-PCR

2.2.1. First strand cDNA synthesis

Primers and probes for the target gene and for reference genes were designed using Primer Express 2 (Applied Biosystems, Foster City, CA/USA). A list of all primers and probes used in this study is available in Appendix.

mRNA or total RNA was extracted with either the mRNA extraction kit (Invitrogen, Carlsbad, CA/USA) or RNA cleaning kit (QIAGEN, Valencia, CA/USA). Purified total/mRNA concentrations were detected with the NanoDrop spectrophotometer (Thermo scientific, Waltham, MA/USA).

Similar amounts of RNA (usually 1 μg total RNA or 100 ng mRNA) from different samples were then used as a template for RT-PCR synthesis of first strand cDNA using either M-MLV or SuperScript (Invitrogen, Carlsbad, CA/USA) reverse transcriptase according to the manufacturer's protocol. Samples were then diluted 5 times with HPLC water.

2.2.2. Relative Standard Curve Method

Standard cDNA dilutions are required in order to quantify relative concentrations of the target and reference gene in the samples. Serial dilutions (4-fold) of either a mix of cDNA from different samples or cDNA from a tissue known to express the gene of interest were used as standard cDNA.

Serial dilutions of the standard cDNA and a non-template control (NTC) were run in triplicate for both the reference and the target gene in order to construct two standard curves. A master mix was prepared for both the reference gene and the target gene using TaqMan Rox-UDG mix (Applied Biosystems, Foster City, CA/USA) according to the manufacturer's protocol. Samples were loaded into a 96-well plate (Applied Biosystems, Foster City, CA/USA) and the final reaction volume was 25 μL. The plate was sealed with transparent film (Applied Biosystems, Foster City, CA/USA) and the qRT-PCR reaction was then carried out in a 7700 detection system (Applied Biosystems, Foster City, CA/USA).

2.3. Protein quantitation

2.3.1. Bradford Method

Bradford protein determination was carried out using the Bio-Rad (Hercules, CA/USA) Protein Assay Dye Reagent Concentrate according to the manufacturer's protocol.

2.3.2. BCA Method

Bicinchoninic acid (BCA) protein determination was carried out using the Thermo scientific (Waltham, MA/USA) BCA Protein Assay Reagent according to the manufacturer's protocol.

2.3.3. SDS polyacrylamide gel electrophoresis and immunoblot

The procedure was essentially as described by (Laemmli, 1970) and carried out using 10 % slab gels in Bio-Rad Minigel System (Hercules, CA/USA). Gels were run at 100 mA until the dye front reached the bottom of the gel. Gels were then removed from the glass plates and proteins were transferred to a nitrocellulose membrane (Hybond, Escondido, CA/USA) by electrophoresis at 200 mA for 1 hour. The membrane was incubated in 5 % (w/v) non-fat dried milk Marvel (Cadbury, London, UK) in phosphate buffered saline (PBS) for 1 hour at room temperature. The membrane was then incubated overnight at 4 ºC with primary antibody in 5 % (w/v) Marvel in PBS Tween (0.1 % v/v). The membrane was rinsed three times followed by a further four 20 minute washes

in PBS Tween. The membrane was incubated for 1 hour with the appropriate secondary antibody in 1 % (w/v) Marvel, PBS Tween (0.1 % v/v). The membrane was rinsed three times followed by four 20 minutes washes in PBS Tween and a further wash of 10 minutes in dH_2O. The membrane was either developed using the Amersham ECL Western blotting detection system (GE Healthcare Life Sciences, Uppsala, Sweden) or transferred to an Odyssey scanner (LI-COR Biosciences, Lincoln, NE/USA) according to the manufacturer's protocol.

2.4. Enzymatic activity

2.4.1. [^{3}H]-AEA hydrolysis – Cell homogenate

Incubation buffer: Hanks/Hepes buffer: NaCl 116 mM, KCl 5.4 mM, $CaCl_2 \cdot 2H_2O$ 1.8 mM, HEPES 25 mM, $MgSO_4$ 0.8mM, $NaH_2PO_4 \cdot 2\ H_2O$ 1 mM, supplemented with 1 mg/ml defatted bovine albumin serum from Sigma, pH 7.4

This method is based on the hydrolysis of AEA tritiated in the ethanolamide moiety ([^{3}H]-AEA) adapted from (Holt *et al.*, 2005) and (Boldrup *et al.*, 2004). Cell pellets (-80 °C) from 75 cm^2 flasks were thawed and re-suspended in 50 µL homogenising buffer (50 mM Tris, 1 mM EDTA, 5 mM $MgSO_4$, pH 7.4). Samples were then sonicated on ice in two 5 seconds burst to avoid over-heating. Fifty µL of homogenate was diluted in 950 µL incubation buffer.

A 250 µL aliquot was pre incubated with URB597 (1 µM in Dimethyl sulfoxide, DMSO). The DMSO concentration did not exceed 1 % (v/v). The

remaining 750 µL aliquot and the 250 µL aliquot were incubated at 37 °C for 30 min. 200 µL aliquots of pre-incubated homogenates were then further incubated for 30 min at 37 °C in 1.5 mL Eppendorf tubes with [^{3}H]-AEA (2 µM final AEA concentration, spiked with 1% [^{3}H]-AEA).

0.4 mL activated charcoal (4 % w/v in 0.5 M HCl) was then added and the mixture was centrifuged at 13000 rpm for 5 mins. 200 µL aliquots of supernatant layerswere then added to 3.5 ml scintillation fluid (Emulsifier-Safe, PerkinElmer, Waltham, CA/USA) and counted for [^{3}H] (minimum of 3 min) with quench correction using a scintillation analyzer (Tri-Carb, PACKARD, Palo Alto, CA/USA). The protein content of homogenates (mg/mL) was determined by Bradford methods (see Section 3.1). Activity was expressed in pmoles/(min x mg protein).

2.4.2. [^{3}H]-AEA/ [^{3}H]-2OG hydrolysis – Intact cells

Washing buffer: Hanks/Hepes buffer: NaCl 116 mM, KCl 5.4 mM, $CaCl_2 \cdot 2H_2O$ 1.8 mM, HEPES 25 mM, $MgSO_4$ 0.8mM, $NaH_2PO_4 \cdot 2H_2O$ 1 mM, pH 7.4
Incubation buffer: Washing buffer supplemented with 1 mg/ml defatted bovine albumin serum from Sigma.

This method is based on the hydrolysis of either AEA tritiated in the ethanolamide moiety ([^{3}H]-AEA) or 2OG tritiated in the glycerol moiety ([^{3}H]-2OG, adapted from (Holt *et al.*, 2005). Cells were seeded on the day before the experiment in 24-well plates at a density of $2x10^5$ cells/well in complete growth medium and placed in the incubator at 37 ºC and 5 % CO_2 overnight.

Cells were then treated with the appropriate compound in complete growth medium for the indicated time. DMSO concentration never exceeded 0.1%.

After the treatment, cells were incubated at 37 ºC for the rest of the experiment. Cells were washed with washing buffer. Incubation buffer was then added to the wells. In experiments with pre-incubation treatment, the appropriate compound was added to a final volume of 350 µL and cells were incubated at 37 °C for 15 minutes. [^{3}H]-AEA or [^{3}H]-2OG (8 µM) solution was prepared by adding 0.8 µL [^{3}H]-AEA or [^{3}H]-2OG respectively, per each 2 mL of solution. The appropriate tritiated compound was then added to the cells to a final concentration of 2 µM and a final volume of 400 µL. Cells were incubated at 37 ºC for 10 minutes and the reaction was stopped by placing them on ice for the rest of the experiment. Cells were washed and 400 µl of ice-cold methanol was added. Cells were scraped and the suspension was transferred to Eppendorf tubes where 400 µL of chloroform and 200 µL of H_2O were added. Samples were vortexed and centrifuged at 13000 rpm for 5 minutes. 300 µL aliquots of the liquid upper phase were then added to 3 mL of scintillation fluid Emulsifier-Safe (PerkinElmer, Waltham, MA/USA) and counted for [^{3}H] with a long count (minimum of 3 min) using a scintillation analyzer (Tri-Carb, PACKARD, Palo Alto, CA/USA). Tissue blanks were measured in empty wells following the same procedure described so far. Standards were measured in triplicates by adding the tritiated compound directly to 3 mL of scintillation fluid. Activity was expressed in pmoles/(min x well).

2.4.3. ODA hydrolysis – Cell Homogenate

Phosphate buffer/EDTA (NaH_2PO_4 5.92g/l, Na_2HPO_4 28g/l, EDTA 370g/l, pH=7.4)
Potassium phosphate solution: K_3PO_4 42g/l and K_2HPO_4 34g/l
OPA/sulphite: OPA 0.65g/l and Na_2SO_3 0.85 g/l

Cells were grown to confluence and collected with 5 mM EDTA in PBS. The cell pellet was re-suspended in phosphate buffer/EDTA (pH 7.4) and homogenised by sonication. The suspension was then spun at 30 000 g for 15 minutes and the resultant particulate preparation was re-suspended in phosphate buffer/EDTA (pH 7.4) and homogenised by sonication. Ammonia was then determined in the presence of excess ortho-phthalaldehyde (Ahn *et al.*) and sulphite following an adaptation from (Mana *et al.*, 2001). Homogenate was incubated at 37 °C for 30 minutes together with ODA (100 µM) and either URB597 (1 µM) or DMSO (5 %). Tissue blanks were incubated alongside. Substrate blanks were prepared by adding ODA (100 µM) after the incubation. The reaction was stopped by putting the sample on ice and adding trichloroacetic acid to a final concentration of 1 % (w/v). After centrifugation at 5000 g for 5 minutes, aliquots of deproteinised supernatant layer were dispensed into a 96-well microtitre plate together with 2 volumes of OPA/sulphite in potassium phosphate solution, pH 11.5. Reaction was allowed to run for 30 minutes and fluorescence was read at 390nm excitation 460nm emission. Standards were obtained by adding 2 volumes of OPA/sulphite solution to 16 µmol $(NH_4)_2SO_3$ in phosphate/EDTA buffer. Hydrolysis rate was expressed as nmoles/min/mg protein.

2.5. RNA interference

2.5.1. miRNA

Cells were seeded the day before transfection in 6-well plates in order to reach a confluency of 80-90 % on the day of transfection. Four separate miRNA constructs (Invitrogen, Carlsbad, CA/USA: two constructs against FAAH, two individual preparations each) were transfected with TransFast transfection reagent (Promega, Madison, WI/USA) according to the manufacturers' instructions. Cells were harvested after 24 hours and mRNA was extracted with mRNA extraction kit (Invitrogen, Carlsbad, CA/USA).

2.5.2. siRNA

2.5.2.1. Electroporation

Cells were passaged three days before transfection and grown to around 80 % confluency in T75 flasks. siRNAs (Ambion, Austin, TX/USA) were delivered by electroporation with Nucleofector (Amaxa, Germany). Cells were nucleofected in suspension and subsequently plated in 6-well dishes with complete culture medium.

A positive construct against β-actin and a mix of the best two constructs out of three preliminarily tested against FAAH were used. Cells were harvested after 48 hours and total RNA was extracted with RNeasy columns (QIAGEN, Valencia, CA/USA).

2.5.2.2. Transfection

Cells were seeded in 24-well plates to reach around 25 % confluency on the day of transfection. siRNAs (Dharmacon, Lafayette, CO/USA) were delivered with Dharmacon modified medium.

A positive control against GAPDH, four individual constructs and a SmartPool of the four constructs were tested. Total RNA was extracted after 72 hours with RNeasy columns (QIAGEN, Valencia, CA/USA).

2.5.3. shRNA

Cells were seeded in 24-well plates in order to reach around 50 % of confluency on the day of transduction. Cells were treated with the viral particles (Sigma, Poole, UK) overnight.

A positive control against beta 2-microglobulin gene (B2M) and five individual constructs (both at Multiplicity of Infection MOI=1 and MOI=3) were tested. Total RNA was extracted after 48 hours directly on the plates with Nano-scale RNA purification kit.

2.6. Neutral Red Assay

Destain solution: 50% ethanol, 49% dH_2O, 1% glacial acetic acid, V/V

A neutral red uptake was performed in intact cells following a protocol adapted from Repetto *et al.*, 2008. On the day before the experiment, cells were seeded

in 24-well plates at a density of $2x10^5$ cells/well in 1 ml of medium and placed in the incubator at 37 ºC and 5 % CO_2 overnight. Cells were then treated with increasing concentrations of the appropriate compound in complete growth medium. As a positive control, cells were treated with saponin 0.1%, or vehicle (DMSO 0.3%) as a negative control.

After 24 hours incubation, cells were quickly washed with PBS and medium was replaced with a solution of neutral red in 1 ml growth medium (33 mg/ml, no additives). Cells were then incubated for 3 hours at 37 ºC and 5 % CO_2. Neutral red medium was then removed and cells were washed again with PBS. 1 ml of destain solution was then added to the cells and the plate was shaken for 10 minutes. Aliquots of 100 µl were then dispensed to a 96-well plate in triplicates and absorbance was read at 550 nm.

2.7. LC-MS/MS endocannabinoid measurement

A liquid chromatography-tandem electrospray ionisation mass spectrometry (LC-MS/MS) method was employed for measurement of endocannabinoids (ECs) in cells by Dr Leonie Norris in the School of Pharmacy (University of Nottingham). In brief, lipids were extracted using ice cold acetonitrile with internal standards (0.42 nmol d8-AEA, 1.5 nmol d8-2-AG) based on the method of Richardson *et al*. (2007). Simultaneous measurement of ECs and related compounds was then performed using LC-MS/MS. Chromatographic separation was carried out on an Shimadzu system (Shimadzu, Milton Keynes, UK) using a Thermo Hypersil-Keystone BDS C18 (150 x 1 mm internal diameter, 5 µm particle size; Thermo Fisher Scientific, Runcorn, UK) with a

mobile phase flow rate of 0.15 ml/min. Gradient elution chromatography with mobile phases consisting of A (water, 1 g/L ammonium acetate, 0.1% formic acid) and B (acetonitrile, 1 g/L ammonium acetate, 0.1% formic acid) was used over the range 15% B to 100% B. Samples were injected from a cooled auto sampler maintained at 4^{o}C. Mass spectrometry detection used a 4000 QTRAP MS (Applied Biosystems, California, USA) in electrospray positive mode with multiple reaction monitoring of specific precursor and product mass to charge (*m/z*) ratios of AEA, 2-AG, PEA and OEA.

Cells in each sample were counted with a haemocytometer and data are expressed as pmol/10^5 cells.

2.8. Calcium mobilization

Loading buffer: HBSS ($MgCl_2$ 1 mM, $CaCl_2$ 0.1 mM) with 5 mM glucose and 0.1% BSA

Cells were seeded in 96-well plates the day before the experiment in order to reach confluency close to 100 %. The measurements were carried out with the calcium-sensitive dye Fluo-4 (Invitrogen, Carlsbad, CA/USA) according to the vendor's instructions. Some adjustments to the original protocol were required to avoid the washing step after addition of the dye. The loading buffer was HBSS with glucose and BSA rather than media and FBS, as serum contains

different factors which would stimulate calcium release. 1 mM Brilliant Black was added to the loading buffer in order to quench the background fluorescence. The organic anion-transport inhibitor probenecid (2.5 mM) was added to reduce leakage of the de-esterified indicator.

Fluo-4 was solubilised in 10 % pluronic acid in DMSO (1 mM stock solution). This non-ionic detergent assists in dispersion of the non-polar acetoxymethyl (AM) ester in aqueous media. The stock solution was diluted to 2 µM in loading buffer and added to the cells in a volume of 100 µl/well. Cells were incubated at 37 °C for 30 minutes.

Drugs were prepared in loading buffer at the required concentrations. DMSO concentration never exceeded 0.1%. Fluorescence was read using a 96-well Flexstation (Molecular Devices, Sunnyvale, CA/USA). Data are expressed as percentage of the carbachol response (Peak-trough interval), with the vehicle control set as 0 %.

2.9. Molecular biology methods

2.9.1. Preparation and transformation of competent *E. Coli*

LB medium: 10g tryptone, 5g yeast extract, 10g NaCl per litre

A single bacterial colony was picked from a plate that was incubated for 16-20 hours at 37 ºC and the colony was inoculated into 100 mL LB medium in a 1-

litre flask. The culture was incubated at 37 ºC for 3 hours with vigorous agitation. The bacterial cells were transferred into sterile, ice-cold 50 mL polypropylene tubes. The cells were recovered by centrifugation at 2700 g for 10 minutes at 4 ºC. The medium was decanted and the cell pellets were resuspended in 30 mL ice-cold 0.1 M sterile $CaCl_2$ solution and recovered by centrifugation. The cells were washed in $CaCl_2$ solution two more times as previously described. The cell pellets were then re-suspended in 2 ml $CaCl_2$ solution containing 12 % (v/v) DMSO and kept on ice for 1 hour before aliquoting and freezing at -80 ºC. For transformation, 100 ng DNA was added to 200 µL thawed competent cells. The mixture was stored on ice for 30 minutes. LB medium (800 µL) was added to each tube and the cells were incubated for 1 hour with shaking at 37 ºC to allow the bacteria to express the antibiotic resistance marker encoded by the plasmid. Transformed competent cells were spread onto LB agar plates containing the appropriate antibiotic. The plates were incubated at 37 ºC until the transformed colonies appeared (15-20 hours).

2.9.2. Plasmid DNA Maxi-Prep

All Maxi-preps of plasmid DNA were carried out using Plasmid Maxi Kit (QIAGEN, Valencia, CA/USA) according to manufacturer's protocol.

2.10. PPAR transactivation assay

A luciferase reporter construct under the control of 3xPPRE was transfected into SH-SY5Y, HeLa and CHO cells either alone or together with a pcDNA3.1 plasmid expressing the human PPARα, PPARβ or PPARγ gene. SH-SH5Y and HeLa cells were transiently transfected using TransFast transfection reagent (Promega, Madison, WI/USA) according to the manufacturer's instructions. Cells were transfected in 6-well plates with 1 µg luciferase plasmid and 1 µg PPAR expressing plasmid per well with a 1:1 DNA:reagent ratio. Transient transfection of CHO cells was carried out by the polyethyleneimine method with the ratio nitrogen (N) to DNA phosphate (P) of N/P=15 as previously described (Sun *et al.*, 2007) 1 hour after transfection, HeLa cells were treated with the appropriate compounds while CHO cells were treated 4 hours after transfection. DMSO concentrations never exceeded 0.1%.

Twenty-four hours after treatment, cells were harvested and lysed with Passive Lysis Buffer (Promega, Madison, WI/USA) and luciferase expression was monitored using the Luciferase Assay System (Promega, Madison, WI/USA) and a luminometer (TD-20/20, Turner Biosystems, Sunnyvale, CA/USA). Data were expressed as Relative Luciferase Units (RLU)/mg protein.

2.11. PPAR ligand binding

2.11.1. PPARα

To assess the binding properties of URB597, displacement of cis-parinaric acid (CPA) from mPPARα LBD was monitored by measuring the fluorescence of

CPA (Causevic *et al.*, 1999). Purified mPPARα LBD protein was diluted to 1 µM in TBS buffer; diluted proteins were mixed with 2 µM CPA from concentrated stock solution in ethanol, followed by addition of potential ligands from concentrated stock solutions in either DMSO or ethanol. Protein-CPA-ligand mixtures (330 µL/well) were loaded into 96-well solid black microplates (Fisher Scientific, Loughborough, Leicestershire, UK). Fluorescence (excitation: 315 nm; emission: 415 nm) emission spectra were obtained by reading the plate from above using a Flexstation® II (Molecular Devices, Sunnyvale, CA/USA) at 25 ºC and corrected for background (fluorescent ligand only). The displacement of bound fluorescent ligand was calculated from the decrease in CPA fluorescence intensity with increasing concentrations of non-fluorescent ligand. Displacement curves were analyzed by fitting a curve to the data using a one-site competition binding model (Prism, GraphPad software, La Jolla, CA/USA).

Binding experiments for ODA were carried out with LanthaScreen™ PPARα Competitor Assay (Invitrogen, Carlsbad, CA/USA) following the manufacturer's instructions. Black 384-well plates (Nunc, Denmark) were read with EnVision multilabel plate reader (PerkinElmer, Waltham, CA/USA). Data are calculated as emission ratio 520 nm/495 nm and reported as percentage of control. Displacement curves were analyzed by fitting a curve to the data using a one-site competition binding model (Prism, GraphPad software, La Jolla, CA/USA).

2.11.2. PPARβ

Binding experiments were carried out with LanthaScreen™ PPARβ Competitor Assay (Invitrogen, Carlsbad, CA/USA) following the manufacturer's instructions. Black 384-well plates (Nunc, Denmark) were read with EnVision multilabel plate reader (PerkinElmer, Waltham, CA/USA). Data are calculated as emission ratio 520 nm/495 nm and reported as percentage of control. Displacement curves were analyzed by fitting a curve to the data using a one-site competition binding model (Prism, GraphPad software, La Jolla, CA/USA).

2.11.3. PPARγ

Binding experiments were carried out with Polarscreen™ PPARγ Competitor Assay Green (Invitrogen, Carlsbad, CA/USA) following the manufacturer's instructions. Black 384-well plates (Nunc, Denmark) were read with EnVision multilabel plate reader (PerkinElmer, Waltham, CA/USA). Data are reported as a percentage of the internal control. Displacement curves were analyzed by fitting curves to the data using a one-site competition binding model (Prism, GraphPad software, La Jolla, CA/USA).

2.12. 3T3-L1 adipocyte differentiation

3T3-L1 cells were grown to confluence in 6-well plates. 48 hours after confluence, the culture medium was replaced and supplemented with 1 μM dexamethasone and 5 μg/mL insulin. After 48 hours, the culture medium was

replaced and supplemented with 5 μg/mL insulin (Sigma, Poole, UK) and the putative PPARγ ligand. Cells were grown for around 10 days checking for differentiation and changing the medium 2-3 times per week. Once differentiation occurred, cells were treated for 10 minutes with 4 % formalin and inoculated with Oil Red O at room temperature for 1 hour. Pictures of the wells were taken from the bottom of the wells with a scanner (Epson, Long Beach, CA/USA).

2.13. Statistical analysis

Statistical differences among treatments were calculated with Prism (GraphPad software, La Jolla, CA/USA), one-way ANOVA with Bonferroni's PostHoc test or two-tailed Student's t-test were applied where appropriate.

3. CELL LINE CHARACTERIZATION

3.1. Introduction

The aim of this study was to check the expression in SH-SY5Y human neuroblastoma and HeLa human carcinoma cells of the various proteins that characterize the endocannabinoid machinery, together with expression of the three different PPARs isotypes. mRNA levels of the biosynthetic enzymes NAPE-PLD and DAGLα, the hydrolysing enzymes FAAH-1/2, NAAA and MGL, as well as the CB_1 and CB_2 receptors were monitored in these cell lines together with PPARα, PPARβ and PPARγ. In order to validate the assay, RNA extracted from tissues known to express the target gene at high levels (human brain, spleen or liver, see Table 3.1) were compared. Expression of PPARs and FAAH was then confirmed at the protein level by Western Blotting.

In order to assess the capability of the cell lines used in the study to break down endocannabinoids, hydrolysis of AEA and ODA was monitored in cell homogenates using rat liver as a positive control.

3.1.1. qRT-PCR

qRT-PCR is based on the 5' exo-nuclease activity of Taq polymerase. This activity leads to break down of a probe labelled with a fluorescent (FAM) and a quencher (TAMRA) tag and subsequent increase in the signal at the wavelength specific for the fluorophore. Primers and probe were designed with Primer Express II (Applied Biosystems); software that allows the design of effective primers and probe pairs. The amplicon (PCR product) or, ideally, the

probe was designed to span an intron-exon boundary in order to avoid the amplification of a false positive product from genomic DNA. Selectivity of both primers and probes was checked by aligning the sequences to the human transcriptome with BLAST N (NCBI).

Serial dilutions of a standard cDNA are required in order to construct a standard curve for each primers-probe pair following the *"Relative Standard Curves"* method. The slope of these curves is directly related to the PCR efficiency of each reaction. Comparable PCR efficiencies give the possibility of comparing relative expression of different genes. A mix of cDNAs from different samples was used as a standard in this study. Dilutions of the standard and the samples needed to be determined empirically. As a starting point, a 4-fold serial dilution of the cDNA mix was used for the β-actin (reference gene) standard curve while the samples were diluted five times. Results were interpolated from the reference gene standard curve, normalised to the reference gene expression and compared in terms of relative expression of each target gene.

3.1.2. Western Blotting

In this study, a polyclonal rabbit anti-FAAH antibody (Millipore) was used. This antibody recognized a 17 amino acid peptide sequence near the N-terminus of human FAAH. Working concentration for this antibody was 5 µg/ml (1/200 dilution). A monoclonal anti-PPARα antibody (Sigma) raised in mice with a synthetic peptide corresponding to AA residues 1-18 of mouse

PPARα (1 mismatch with human PPARα) was used at a working concentration of 2 µg/ml (1/500). Rabbit polyclonal Anti-PPARβ antibody (Santa Cruz) recognised AA sequence 2-75 at the N-terminus of human PPARβ and the working concentration was 2 µg/ml (1/100). The polyclonal antibody against PPARγ was raised in rabbit (Cell Signaling) and recognised a sequence around Asp69 of human PPARγ. Working dilution for this antibody was 1/1000.

3.1.3. Enzymatic assays

In order to check the capability of the cells to break down endocannabinoids, two separate enzymatic assays were performed. The first one was a radioactivity based assay that exploits the hydrophilic properties of the tritiated ethanolamine moiety released from hydrolysis of tritiated AEA. Separation of product from the substrate was achieved with activated charcoal *(Boldrup et al.*, 2004). This avoids the use of toxic solvents such as methanol and chloroform. The second enzymatic assay carried out in this study measured hydrolysis of ODA, a preferred FAAH-2 substrate (Wei *et al.*, 2006). This assay monitors ammonia liberation from ODA hydrolysis, exploiting the fluorescent product of the reaction between ammonia and OPA (Mana *et al.*, 2001).

3.2. Results

3.2.1. Endocannabinoid system

3.2.1.1. RNA expression

RNA levels of both NAPE-PLD and DAGLα, the two endocannabinoid synthetic enzymes, were relatively high in SH-SY5Y cells compared to HeLa cells (Table 3.1). FAAH expression was again much higher in neuroblastoma cells compared to HeLa cells, while FAAH-2 RNA was not detected in SH-SY5Y and moderately expressed in HeLa cells. The two other catabolic enzymes monitored in this study, NAAA and MGL, were expressed in both cell lines with HeLa cells showing the higher RNA levels for these genes. The situation was inverted for CB_1 and CB_2 RNA expression. These receptors were indeed expressed in both cells but the neuroblastoma showed the highest RNA levels (Table 3.1).

3.2.1.2. Protein expression

Expression of the endocannabinoid hydrolysing enzyme FAAH was confirmed by Western blotting. The expected size for the FAAH protein was 63 kDa. SH-SY5Y neuroblastoma cells showed a clear band just below 64 kDa while HeLa cells showed only a faint band at this size (Figure 3.1).

target/β-actin (a.u.)	SH-SY5Y	HeLa	Positive control	Tissue
NAPE-PLD	**1.80E-04** ±1.90E-05	**3.49E-05** ±2.57E-06	**5.92E-04** ±4.37E-05	**Human Brain**
DAGLα	**1.23E-03** ±3.11E-04	**4.14E-04** ±5.66E-05	**6.10E-03** ±1.35E-03	**Human Brain**
FAAH	**2.53E-03** ±1.35E-04	**1.44E-04** ±1.74E-05	**1.83E-02** ±1.24E-03	**Human Brain**
FAAH-2	**Undetermined**	**4.01E-04** ±5.77E-05	**1.40E-03** ±8.88E-05	**Human Liver**
NAAA	**6.69E-05** ±1.51E-05	**3.44E-04** ±4.58E-05	**9.65E-03** ±2.44E-04	**Human Liver**
MGL	**3.73E-05** ±1.83E-06	**5.60E-04** ±8.77E-05	**2.60E-02** ±6.15E-03	**Human Brain**
CB1	**8.15E-04** ±4.14E-05	**2.11E-05** ±3.40E-06	**3.53E-02** ±4.03E-03	**Human Brain**
CB2	**3.34E-04** ±3.90E-05	**2.68E-05** ±6.87E-06	**1.18E-02** ±1.39E-03	**Human Spleen**

Table 3.1: qRT-PCR analysis of RNA expression in SH-SY5Y cells. Results are expressed as average arbitrary units normalised by β-actin and were conducted in triplicate. mRNA or total RNA was extracted from SH-SY5Y or HeLa cells and either human liver, spleen or brain as a positive control.

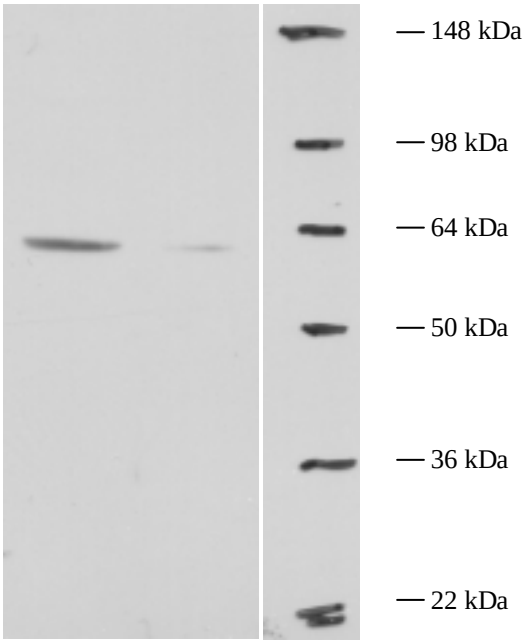

Figure 3.1: Western blotting of either 30 µg SH-SHY5Y (lane **1**) or 30 µg HeLa (lane **2**) protein using antibodies against FAAH (Millipore). The membrane was developed using the ECL Western blotting detection system (Amersham). The lane on the right molecular represents molecular weight markers (SeeBlue Plus2 ladder, Invitrogen)

3.2.1.3. Activity assay

3.2.1.3.1. [^{3}H]-AEA Hydrolysis

In a radioactivity based assay, SH-SY5Y cells were able to hydrolyse exogenously administered AEA. This activity was almost completely reversed by pre-incubation with the FAAH inhibitor URB597 (1 µM, $P<0.05$, Figure 3.2). By contrast, HeLa cells showed no measurable AEA hydrolysis activity with or without URB597 pre-incubation. In the same assay, URB597 was able

to completely reverse AEA hydrolysis in rat liver microsomes (P<0.01, Figure 3.2).

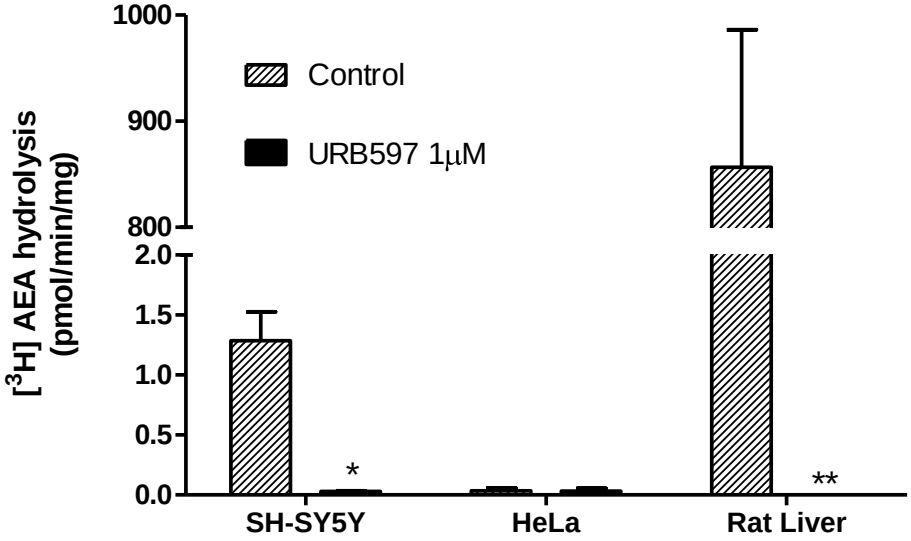

Fig 3.2: AEA hydrolysis measured in particulate preparations from either SH-SY5Y or HeLa cells or rat liver microsomes as a positive control. Samples were pre-incubated for 30 minutes with either DMSO (n=at least 6) as a control or URB597 1 μM (n≥ 3, * P<0.05, ** P<0.01, unpaired Student's t-test, two-tailed, compared to control)

3.2.1.3.2. ODA Hydrolysis

Monitoring of ODA hydrolysis showed measurable activity in both SH-SY5Y and HeLa cells. In both cases, pre-incubation with URB597 almost completely inhibited ODA hydrolysis (P<0.05, Figure 3.3). In the same experiment, URB597 was able to inhibit ODA hydrolysis in rat liver microsomes, albeit only partially.

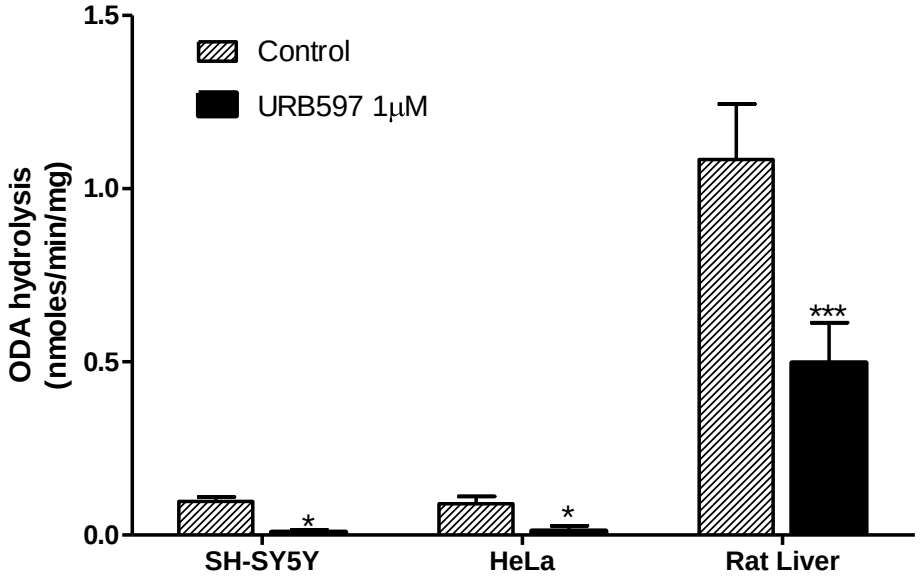

Fig 3.3: ODA hydrolysis measured in particulate preparations from either SH-SY5Y or HeLa cells, or rat liver microsomes as a positive control. Samples were pre-incubated for 10 minutes with either DMSO as a control or URB597 (1 μM, n=6, * $P<0.05$, *** $P<0.001$, unpaired Student's t-test, two-tailed, compared to control).

3.2.2. PPAR expression

Expression of the three PPAR isotypes was measured in neuroblastoma and HeLa cells, both at the RNA level by qRT-PCR and at the protein level by Western blotting.

3.2.2.1. RNA expression

Analysis of mRNA levels of the three PPAR isotypes from SH-SY5Y and HeLa cells revealed a similar pattern of relative expression in the two cell lines

(Table 3.2). In neuroblastoma cells, PPARβ was the most abundant isotype. PPARα was expressed at lower levels in these cells while PPARγ RNA was almost undetected. The expression relative to PPARγ was: PPARβ (11600-fold) > PPARα (374-fold) > PPARγ (1.00). In HeLa cells, PPARβ was again the most expressed isotype followed by much lower levels of PPARα and PPARγ. The fold expression in this case was: PPARβ (142-fold) > PPARα (2.8-fold) > PPARγ (1.00).

target/β-actin (a.u.)	SH-SY5Y	HeLa	Positive ctrl	Tissue
PPARα	**1.24E-03** ±3.24E-05	**1.17E-04** ±8.30E-06	**6.25E-03** ±1.73E-03	**Human Liver**
PPARβ	**3.85E-02** ±2.45E-03	**5.90E-03** ±3.99E-04	**2.57E-02** ±7.45E-03	**Human Liver**
PPARγ	**3.31E-06** ±9.93E-07	**4.16E-05** ±4.36E-06	**6.69E-04** ±1.94E-04	**Human Liver**

Table 3.2: qRT-PCR analysis of mRNA expression in SH-SY5Y cells. Results are expressed as average arbitrary units normalised by β-actin, measured in triplicate. mRNA or total RNA was extracted from SH-SY5Y cells, HeLa cells as control cell line and either human liver, spleen or brain as a positive control.

3.2.2.2. Protein expression

Differential expression among the PPARs isotypes was confirmed by Western blotting of protein preparations from cells separated by SDS polyacrylamide gel electrophoresis (Figure 3.4). Expected sizes were: 52 kDa (PPARα), 50

kDa (PPARβ), and 58 kDa (PPARγ). All the antibodies used showed staining at slightly larger molecular sizes than expected. PPARβ and PPARα proteins were detected in both cell lines while PPARγ staining was apparent only in HeLa cells. Levels of relative protein expression of the various PPARs isotypes were consistent with RNA levels reported in the previous section.

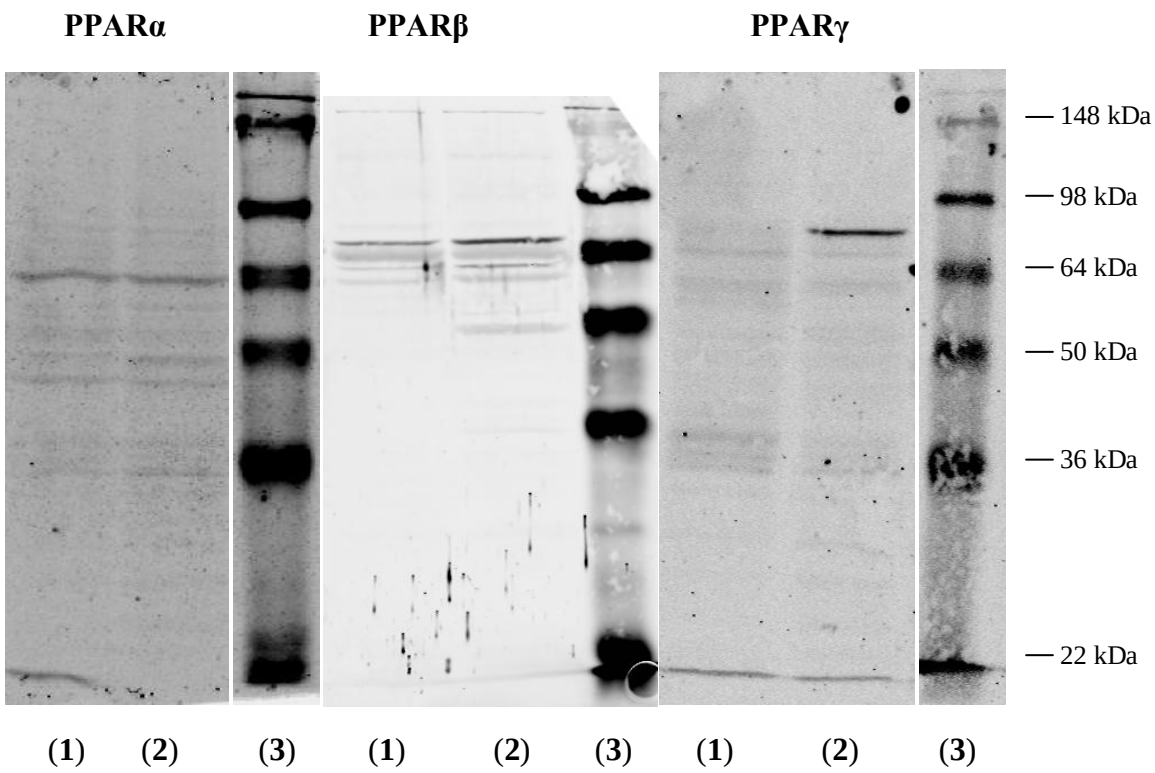

Figure 3.4: Western blotting of either 30 µg SH-SHY5Y (lanes **1**) or 30 µg HeLa (lanes **2**) protein using antibodies against PPARα (Sigma), PPARβ (SantaCruz) and PPARγ (Cell Signalling). The membrane was scanned with an Odyssey scanner (LI-COR Biosciences). Lanes **3** show SeeBlue Plus2 MW ladder (Invitrogen).

3.3. Discussion

The presence of the machinery to synthesize and break down endocannabinoids was revealed in both neuroblastoma SH-SY5Y and HeLa cells together with the two cannabinoid receptors, at least at the mRNA level. These results are consistent with very recent findings showing expression of a fully functional endocannabinoid system in SH-SY5Y neuroblastoma cells (Marini *et al.*, 2009; Pasquariello *et al.*, 2009). FAAH expression was confirmed at the protein level in SH-SY5Y cells, but not in HeLa cells; the latter observation confirming a previous report (Day *et al.*, 2001). Differential FAAH expression was also reflected in AEA hydrolysis activity that was absent in HeLa cells and present in neuroblastoma cells (Figure 3.2). However, the presence of mRNA encoding other enzymes involved in endocannabinoid hydrolysis (most notably FAAH-2 in HeLa cells), prompted us to monitor hydrolysis of ODA, the main substrate for this enzyme (Wei *et al.*, 2006). Results showed that both cell lines could hydrolyse ODA and this activity was reversed by URB597, which inhibits both FAAH and FAAH-2 with similar potency (Wei *et al.*, 2006). HeLa cells appeared to selectively catabolise ODA over AEA under the conditions used in this study.

Expression of PPAR nuclear receptors measured at both mRNA and protein levels revealed that PPARβ was the most abundant isotype in both cell lines, followed by PPARα. This pattern of expression might reflect a role for PPARβ in the regulation of tumour cell growth even if the literature reports conflicting data (Bishop-Bailey *et al.*, 2009). Moreover, activation of PPARβ receptors

has previously been linked with SH-SY5Y cell differentiation into neuronal-like cells (Di Loreto *et al.*, 2007). Data in the present study showed that PPARγ was expressed in HeLa cells while RNA levels of this receptor in SH-SY5Y cells were really low and protein was not detected by immunoblotting in these cells. These findings are partially inconsistent with previous studies showing PPARγ expression in SH-SY5Y cells (Valentiner *et al.*, 2005). However, among the various neuroblastoma cell types tested, SH-SY5Y cells showed the lowest level of expression in both immunohistochemistry and western blot analysis with nuclear staining in these cells virtually negative. Moreover, the PPARγ ligand rosiglitazone could inhibit cell adhesion, invasiveness and apoptosis in SK-N-AS, a PPARγ positive neuroblastoma cell line, while it was ineffective in SH-SY5Y cells (Cellai *et al.*, 2006)

4. EFFECTS OF FAAH INHIBITION ON FAAs LEVELS

4.1. Introduction

In the previous section, SH-SY5Y cells were shown to express functional FAAH activity, while HeLa cells were shown to be FAAH negative. Given that FAEs appear to be hydrolysed to ethanolamine and fatty acids principally through the action of FAAH, inhibition of FAAH should lead to accumulation of a variety of intracellular FAEs. In this study, this possibility was tested in SH-SY5Y cells as a model of neuronal cells and HeLa cells as an FAAH negative control.

4.1.1. FAAH expression and activity

SH-SY5Y cells were treated with the FAAH inhibitor URB597 for 24 hours and changes in FAAH expression were monitored at both the RNA and the protein levels. For the qRT-PCR measurements, the geometric mean of two separate reference genes (β-actin-B2M) was used to normalise RNA values. Time-course of inhibition of FAAH activity was monitored following liberation of tritiated ethanolamine from labelled AEA in either cell homogenates or intact cells. In addition to URB597, two structurally and functionally distinct FAAH inhibitors, OL135 and PF750, were tested (Lichtman *et al.*, 2002) (Ahn *et al.*, 2007). Changes in 2OG hydrolysis rate were also monitored in intact cells.

4.1.2. ECs measurement

ECs measurements were performed by Dr. Leonie Norris in the School of Pharmacy (University of Nottingham). Intracellular ECL levels were monitored after 24 hours of URB597 treatment in both SH-SY5Y and HeLa cells by LC-MS/MS as previously described (Richardson *et al.*, 2007). Data were normalised by cell number in order to account for morphological differences between cell types.

4.1.3. RNA interference

In order to show that the pharmacological treatments used in this study were selectively targeting FAAH, FAAH knock down by RNA interference in SH-SY5Y cells was attempted. Various technologies were applied including miRNA, siRNA and shRNA (see Chapter 2).

4.1.4. Cell viability

In order to check whether the FAAH inhibitors were affecting cell viability at the concentrations used in the study, neutral red uptake by SH-SY5Y cells was monitored. This widely used assay is based on the ability of viable cells to incorporate the supravital dye neutral red, a weakly cationic dye. Neutral red penetrates cell membranes by non-ionic passive diffusion and concentrates in the lysosomes, where it binds by electrostatic hydrophobic bonds to anionic and/or phosphate groups of the lysosomal matrix. When the cell dies or the pH gradient is reduced, the dye cannot be retained. Consequently, the amount of retained dye is proportional to the number of viable cells (Repetto *et al.*, 2008).

4.1.5. Calcium mobilization

Recently, URB597 was proposed to activate TRPA1 and inhibit TRPM8 receptors (Niforatos *et al.*, 2007). These receptors are ligand-activated non-selective cation channels able to gate calcium influx. In order to rule out the possibility of this mechanism being involved in this study, intracellular calcium mobilization was monitored in both SH-SY5Y and HeLa cells in response to URB597 administration.

4.2. Results

4.2.1. FAAH expression

Expression of FAAH in SH-SY5Y cells was monitored after 24 hours of 1 μM URB597 treatment at the mRNA and protein levels. FAAH mRNA expression was 1.04 ± 0.15 after vehicle (DMSO 0.1%) treatment and remained at a value of 0.93 ± 0.11 after URB597 treatment (arbitrary units, normalised to expression of β-actin-B2M, n=3). Western blotting of protein preparations from treated SH-SY5Y cells showed no difference in FAAH protein levels after either vehicle (DMSO 0.1%) or URB597 treatment (n=2, Figure 4.1)

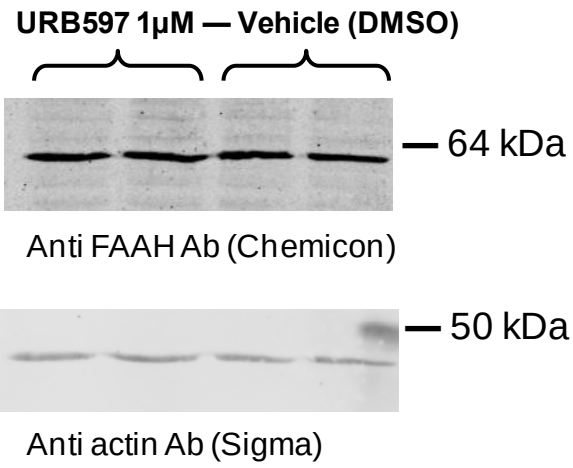

Figure 4.1: Western blotting of 30 µg SH-SHY5Y protein using antibodies against FAAH (Millipore) or actin (Sigma). The membranes were scanned with an Odyssey scanner (LI-COR biosciences). The protein sizes indicated on the right result from MW markers of the SeeBlue Plus2 ladder (Invitrogen).

4.2.1.1. AEA hydrolysis

4.2.1.1.1. Cell homogenate

Cells were treated with 1 µM URB597 either with continuous exposure for different times up to 24 hours or for 30 mins after which the medium was changed, following which AEA hydrolysis was measured in SH-SY5Y cell homogenates. Inhibition of FAAH activity (AEA hydrolysis) was achieved inside 30 minutes and sustained over time following either 30 minutes or continuous URB597 treatment ($P<0.001$, Figure 4.2).

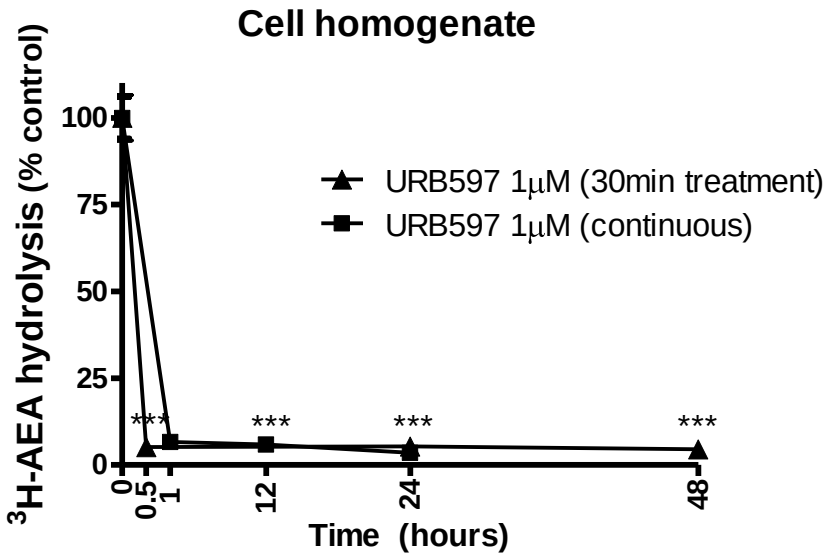

Figure 4.2: Time course of URB597-evoked inhibition of AEA hydrolysis in SH-SY5Y cell homogenates. Results are expressed as a percentage of control at t=0 (***P<0.001 compared to control, n=3).

4.2.1.1.2. Intact cells

4.2.1.1.2.1. Time course

Cells were treated with 1 μM URB597 as above, either continuously for different times up to 24 hours or for 30 mins after which the medium was changed, measuring AEA hydrolysis in intact SH-SY5Y cells. Inhibition of FAAH activity (AEA hydrolysis) was achieved inside 30 minutes and sustained over time by either 30 minutes or continuous URB597 treatment (P<0.001 and P<0.01 respectively, Figure 4.3). A residual activity of around 25% of control was detected.

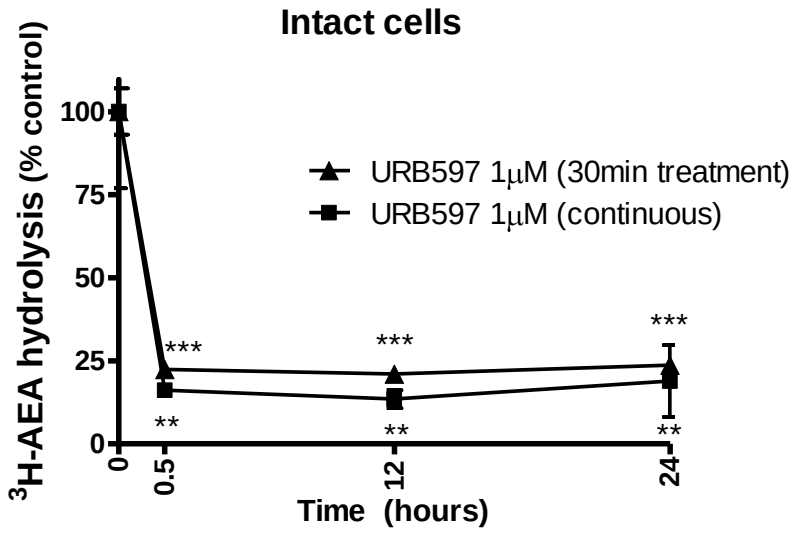

Figure 4.3: Time course measurement of AEA hydrolysis in intact SH-SY5Y cells. Results are expressed as percentage of control at t=0 (**P<0.01 and ***P<0.001 compared to control, n=3).

4.2.1.1.2.2. Concentration-response]

Cells were treated for 24 hours with increasing concentrations of three different FAAH inhibitors (OL135, URB597 and PF750). All the FAAH inhibitors tested were able to inhibit AEA hydrolysis in a concentration-dependent fashion. IC_{50} (95% C.I.) values were $4.2x10^{-6}$ M ($2.3x10^{-6}$ to $7.5x10^{-6}$) for OL135, $3.4x10^{-9}$ M ($2.1x10^{-9}$ to $5.4x10^{-9}$) for URB597 and $3.2x10^{-10}$ M ($1.9x10^{-10}$ to $5.6x10^{-10}$) for PF750. A residual activity of around 25% of control was detected that only the highest concentration of URB597 (-4.5 log M) could inhibit (Figure 4.4).

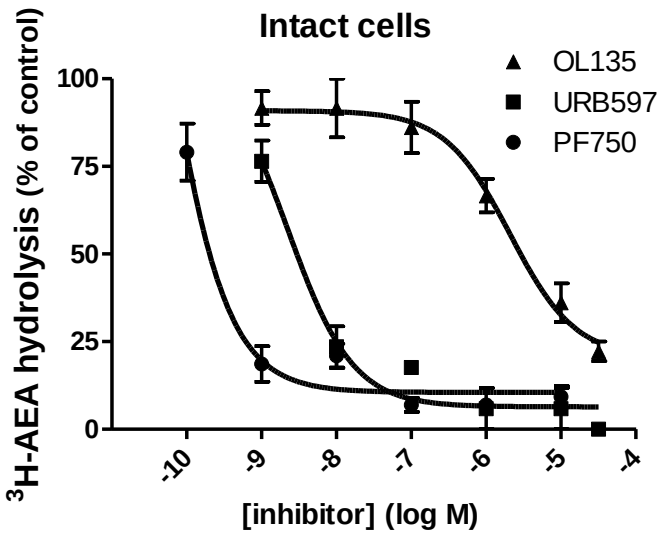

Figure 4.4: Concentration-response effects of FAAH inhibitors on AEA hydrolysis in intact SH-SY5Y cells. Results are expressed as percentage of control (n=3).

4.2.1.1.2.3. Extended and brief FAAH inhibition

Measurement of AEA hydrolysis in intact SH-SY5Y cells showed that extended (24 hours) treatment with 10 μM URB597 could not completely inhibit AEA hydrolysis ($P<0.001$, Figure 4.5 **a** and **b**). Acute (30 minutes) pre-incubation of cells with either 10 or 30 μM URB597 following 24 hour treatment with 10 μM URB597 could almost completely inhibit the residual activity down to levels achieved by 24 hour treatment with 30 μM URB597 ($P<0.05$, **a**). Moreover, acute pre-incubation of cells with 60 μM of the NAAA inhibitor CCP following 24 hour treatment with 10 μM URB597 could almost completely inhibit the residual activity down to levels achieved by 24 hour treatment with 30 μM URB597 (#$P<0.05$, **b**).

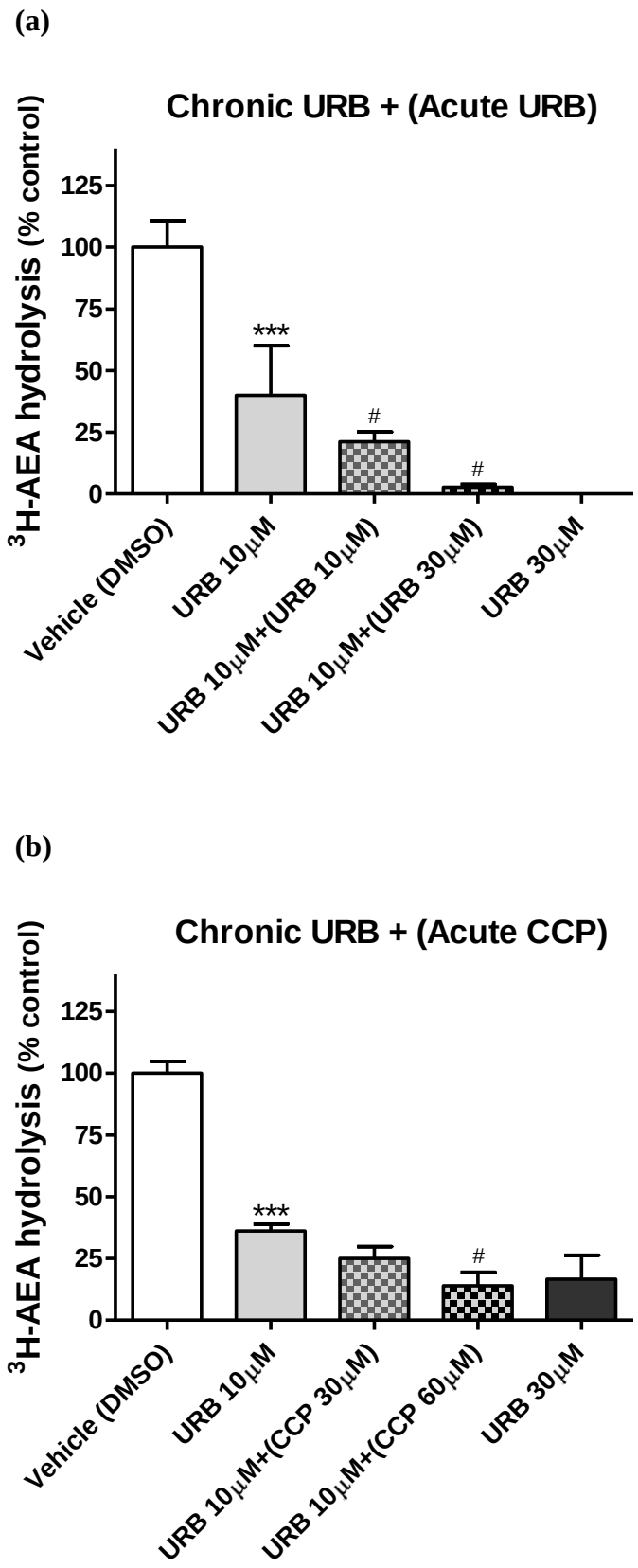

Figure 4.5: Measurement of AEA hydrolysis in intact SH-SY5Y cells following extended (24 hours) and brief (30 mins pre-incubation, in brackets)

treatment with either URB597 **(a)** or CCP **(b)**. Results are expressed as percentage of control (n=3, *** P<0.001 compared to control, # P<0.05 compared to 10 μM URB597). Typical basal AEA hydrolysis was 1.2 ± 0.1 pmol/min/well (mean ± SD).

4.2.1.2. 2OG hydrolysis

Measurement of 2OG hydrolysis in intact SH-SY5Y cells following extended (24 hours) or brief (30 mins pre-incubation) treatment, showed that 10 μM MAFP could inhibit 2OG hydrolysis in SH-SY5Y cells both acutely (P<0.001) or after 24 hour treatment (P<0.05, Figure 4.6). By contrast, 30 μM URB597 was unable to inhibit 2OG hydrolysis. Basal 2OG hydrolysis was 1.37 ± 0.38 pmol/min/well (mean ± SD).

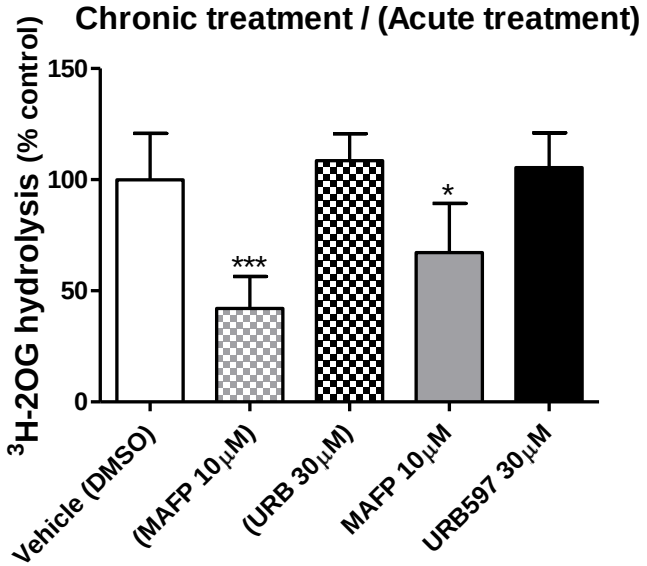

Figure 4.6: Measurement of 2OG hydrolysis in intact SH-SY5Y cells following extended (24 hours) or brief (30 min pre-incubation, in brackets)

treatment with either 10 μM MAFP or 30 μM URB597. Results are expressed as percentage of control (n≥5 * P<0.05, *** P<0.001 compared to control).

4.2.2. ECL measurements

Cells were treated with either DMSO or 10 μM URB597 for 24 hours. Cells were then harvested and lipids were extracted, together with internal standards. LC-MS/MS measurements of AEA, OEA, PEA and 2AG levels in SH-SY5Y cells showed that AEA, PEA and 2AG levels were significantly increased after 10 μM URB597 treatment (P<0.01, P<0.05 and P<0.01 respectively), while OEA levels were unaffected. In HeLa cells, PEA levels were significantly increased after 24 hours of 10 μM URB597 treatment (P<0.05, Table 4.1) while AEA, OEA and 2AG levels were unaffected.

	SH-SY5Y		HeLa	
	Vehicle (DMSO) *fmol/10⁶cells median (range)*	**URB597 10μM** *fmol/10⁶cells median (range)*	**Vehicle (DMSO)** *fmol/10⁶cells median (range)*	**URB597 10μM** *fmol/10⁶cells median (range)*
AEA	**338** (282 / 431)	**648**** (467 / 729)	**503** (194 / 598)	**436** (385 / 502)
OEA	**4850** (2940 / 6590)	**5810** (4590/ 10300)	**4250** (2350 / 5870)	**4030** (3220 / 7110)
PEA	**11100** (7430 / 16800)	**17000*** (14400 / 19900)	**9100** (5240 / 13400)	**15500*** (12200 / 23000)
2AG	**6590** (5490 / 8050)	**13800**** (11100 / 16100)	**2070** (1470 / 4870)	**2000** (1520 / 4180)

Table 4.1: LC-MS/MS measurements of AEA, OEA, PEA and 2AG levels in SH-SY5Y and HeLa cells. Results are expressed as fmol/10^6 cells, median values (range). (measured by Dr Leonie Norris. *P<0.05, **P<0.01 and **P<0.01, n=5)

4.2.3. RNA interference

SH-SY5Y cells were treated with siRNAs, miRNAs or shRNAs and FAAH expression was determined at the mRNA level. siRNAs delivered by Nucleofection (see Chapter 2) successfully knocked down actin as a positive control (25.9 ± 5.9 % of control) while they could only knock down FAAH levels to 61.6 ± 21.7% of control. siRNAs delivered with Dharmacon reagent successfully knocked down the positive control GAPDH (13.7 ± 0.8% of control) while the best construct tested (14) could knock down FAAH levels to 49.1 ± 9.7 % of control. miRNA-expressing plasmids were unsuccessful in knocking down FAAH (no positive control used). Finally, shRNAs delivered as viral particles knocked down the positive control B2M to 64.1 ± 5.0 % of control while the best construct against FAAH (36FAAH) could only knock its RNA levels down to 70.2 ± 10.9 % of control when transduced at MOI=3 (Table 4.2).

Technology	Construct ID	FAAH % of control Mean±SD	Positive % control Mean±SD (gene)
siRNA Ambion+Nucleofector	**1+3**	**61.6±21.7** n=7	**25.9±5.9 (Actin)** n=2
siRNA	**14**	**49.1±9.7**	**13.7±0.8 (GAPDH)**

Dharmacon		n=6	n=6
	15	**68.3±11.5** n=6	
	16	**53.5±2.5** n=6	
	17	**63.6±5.7** n=6	
	SmartPool (14+15+16+17)	**75.7±8.7** n=6	
miRNA Invitrogen	**293 (1)**	**106.4** n=1	**N.D.**
	293 (2)	**152.6** n=1	
	590 (1)	**93.2** n=1	
	590 (2)	**93.2** n=1	
shRNA Sigma	**34FAAH MOI=1**	**77.7±6.2** n=3	**64.1±5.0 (B2M)** n=3
	34FAAH MOI=3	**73.9±7.6** n=3	
	35FAAH MOI=1	**72.7±6.4** n=3	
	35FAAH MOI=3	**74.7±3.7** n=3	
	36FAAH MOI=1	**73.2±7.8** n=3	
	36FAAH MOI=3	**70.2±10.9** n=3	
	37FAAH MOI=1	**74.5±6.6** n=3	
	37FAAH MOI=3	**82.4±4.0** n=3	
	38FAAH MOI=1	**95.0±7.8** n=3	
	38FAAH MOI=3	**84.3±2.9** n=3	

Table 4.2: Expression of either FAAH or a control gene after various RNAi treatments in SH-SY5Y cells.

4.2.4. Cell viability

Neutral Red uptake was measured in SH-SY5Y cells after treatment with either DMSO, increasing concentrations of URB597, OL135, PF750 or 0.1 % saponin as a positive control. Results showed that none of the FAAH inhibitors affected cell viability at all concentrations tested (Figure 4.7).

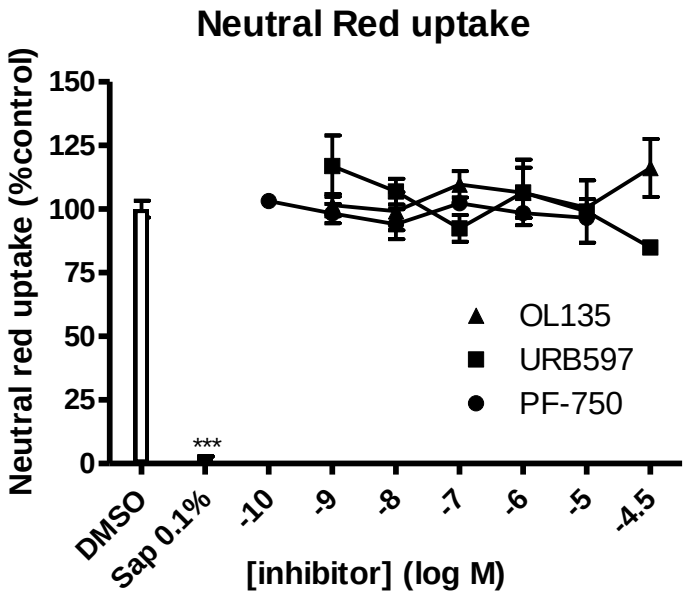

Figure 4.7: Neutral Red uptake was measured in SH-SY5Y cells after 24 hours treatment with the FAAH inhibitors. Results are expressed as percentage of control (n=3)

4.2.5. Calcium mobilization

Intracellular Ca^{2+} measurements showed that, although carbachol evoked significant elevations in $[Ca^{2+}]_i$ in both SH-SY5Y and HeLa cells ($P<0.001$) compared to vehicle control (not shown, 0%), 100 μM URB597 and the

TRPM8 ligand menthol (100 nM) were without effect. 1 mM ATP significantly elevated $[Ca^{2+}]_i$ in HeLa cells ($P<0.001$, Figure 4.8 **a** and **b**) while it could only slightly elevate $[Ca^{2+}]_i$ in SH-SY5Y cells.

(**a**)

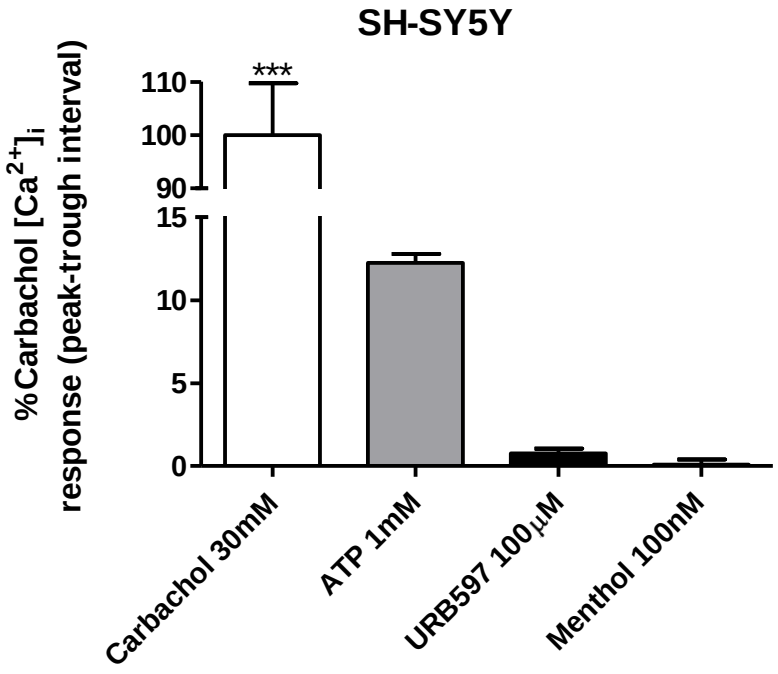

(**b**)

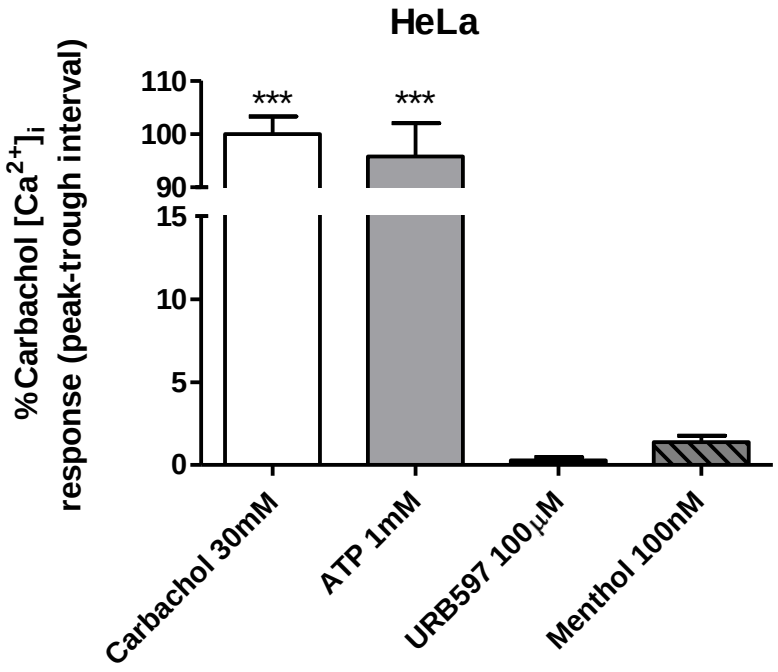

Figure 4.8: Intracellular Ca^{2+} mobilization in SH-SY5Y (**a**) and HeLa cells (**b**). Results are expressed as a percentage of carbachol response (*** P<0.001 compared to control, not shown, n=6).

4.3. Discussion

In this section, inhibition of FAAH activity in SH-SY5Y cells was achieved by 1 µM URB597 treatment for either 30 minutes or 24 hours continuous treatment as shown by AEA hydrolysis inhibition in cell homogenates (Figure 4.2). In order to verify this inhibition in a more physiologically relevant way, AEA hydrolysis was measured in intact SH-SY5Y cells. The same URB597 treatment elicited FAAH inhibition that was achieved inside 30 minutes and sustained over time. However, a residual FAAH activity of around 25% was still detected (Figure 4.3). It has been previously shown that sustained and

nearly complete FAAH inhibition is required to maintain elevated ECs levels *in vivo* (Fegley *et al.,* 2005). Concentration-response experiments treating SH-SY5Y cells with URB597, OL135 and PF750 showed that these compounds could all inhibit FAAH activity in neuroblastoma cells to similar levels although with different potencies. PF750 appeared to be the most potent FAAH inhibitor, with OL135 the least potent. However, a residual AEA hydrolysis activity was measurable after treatment with all three inhibitors (Figure 4.4). Acute re-exposure to 10 μM URB597 or extended treatment with a higher concentration of URB597 (30 μM) could further inhibit the residual AEA hydrolysis (Fig 4.5a) pointing towards the possibility of newly synthesised FAAH being responsible for this activity. A potential alternative is that URB597 is being hydrolysed or accumulated in other compartments where it cannot inhibit FAAH, which might explain the need for either higher chronic concentrations or freshly administered URB97. However, acute treatment with the NAAA inhibitor CCP 30-60 μM could also knock down the residual AEA hydrolysis activity (Figure 4.5b). CCP has been shown to selectively inhibit NAAA without inhibiting FAAH up to concentration of at least 100 μM (Tsuboi *et al.*, 2004), with which local studies concur (Patel & Alexander, personal communication). More recently, a more selective NAAA inhibitor, (*S*)-OOPP, has been reported to augment PEA levels in activated leukocytes (Solorzano *et al.,* 2009). On the contrary, URB597 has very recently been shown to weakly inhibit (around 25%) recombinant rat NAAA at 100 μM (Solorzano *et al.*, 2009). Moreover, expression of NAAA has been confirmed in SH-SY5Y cells at least at the mRNA level (see Chapter 2). Taken together,

these data would indicate that the residual AEA hydrolysis activity after URB597 treatment in SH-SY5Y cells might be due to NAAA activity.

Increased levels of intracellular AEA, PEA and 2AG but not OEA were measured in SH-SY5Y cells after 24 hours of 10 μM URB597 exposure (Table 4.1). URB597 is reported not to inhibit MGL, the main enzyme hydrolysing 2AG, up to concentrations of at least 30 μM (Kathuria *et al.*, 2003). However, 2AG has been previously showed to be hydrolysed by FAAH under particular circumstances (Di Marzo *et al.*, 2008). This appeared not to be the case in SH-SY5Y cells. Indeed, 30 μM URB597 did not alter hydrolysis of 2OG, a close analogue of 2AG widely used in radioactivity-based MGL assays. On the contrary, 10 μM MAFP, an inhibitor of both FAAH and MGL, could significantly diminish 2OG hydrolysis (Figure 4.6). Expression of MGL has been confirmed at the mRNA level in both SH-SY5Y and HeLa cells (see Chapter 3). However, the possibility of 2AG being hydrolysed by FAAH selectively over 2OG has not been addressed.

Surprisingly, PEA levels were elevated in HeLa cells after URB597 treatment (Table 4.1). PEA is hydrolysed primarily by FAAH and NAAA, and it is thought to be the main substrate for the latter enzyme (Ueda *et al.*, 2001). Another enzyme, FAAH-2, can also break down PEA (Wei *et al.*, 2006) and inhibition of either its activity or NAAA activity by URB597 might well be responsible for intracellular PEA levels elevation. In Chapter 3, HeLa cells were indeed shown to express both FAAH-2 and NAAA RNA. Moreover,

HeLa cells were able to hydrolyse exogenous ODA, the main substrate for FAAH-2. This activity was reversed by URB597 pre-incubation.

A recent publication showed that URB597 can activate TRPA1 receptors and inhibit TRPM8 receptors (Niforatos *et al.*, 2007). Intracellular calcium ion measurements reported in the present study ruled out the involvement of TRPA1 receptor in the mechanism by which URB597 elevated ECL levels in SH-SY5Y or HeLa cells. Indeed, 100 μM URB597 (a concentration 10 times higher than the one used for ECL levels measurement) had no effect on calcium mobilization in both SH-SY5Y and HeLa cells. Menthol, a TRPM8 ligand, did not affect intracellular calcium levels either, indicating that this receptor is either not expressed or not functional in either SH-SY5Y nor HeLa cells (Figure 4.8 **a** and **b** respectively). Moreover, a recent publication (Vetter *et al.*, 2009) reported that capsaicin could not affect calcium measurements in SH-SY5Y cells, possibly suggesting that TRPV1 receptors are also not present in this cell line. There is strong debate in literature about the notion of ECLs being synthesised on demand after an external stimulus. The activity of the anabolic enzyme NAPE-PLD was indeed shown to be activated by high concentrations of Ca^{2+} (Wang *et al.*, 2006). Another study recently reported intracellular elevation of ECs in mixed cultures of neurones and astrocytes after AMPA or NMDA treatment (Loría *et al.*, 2009). AEA, 2AG and PEA were elevated in quantities comparable to the ones shown in the present study. The elevation of AEA, PEA and 2AG in SH-SY5Y cells and of PEA in HeLa cells reported here after inhibition of either FAAH or FAAH-2 and possibly NAAA, indicates that it is possible to modulate ECL levels in cultured cells by

simply modulating their metabolism. This would point in favour of an underlying ECL tone, regardless of external stimulation. Notably, all the FAAH inhibitors were shown not to affect SH-SY5Y cell viability at any concentration tested (Figure 4.7).

RNA interference targeting FAAH in SH-SY5Y cells was able to produce a knockdown of the FAAH gene but at levels that were not considered good enough for our purposes. miRNA expressing plasmid transfection or shRNA plasmid viral transduction could only slightly diminish FAAH mRNA levels. siRNA transfection, exploiting either nucleofection or Dharmacon passive delivery, appeared to be the most reliable technique to knock down this enzyme in SH-SY5Y neuroblastoma cells. However, FAAH mRNA levels were only knocked down to 49.1 ± 9.7% of control (Table 4.2) with the best construct out of four. As already mentioned, it would appear that a complete inhibition of FAAH is required in order to maintain elevated ECL levels (Kathuria *et al.*, 2003). Thus, only pharmacological inhibition of this enzyme was conducted for the next experiments of this study.

5. EFFECT OF THE FAAH INHIBITORS ON PPARs ACTIVATION

5.1. Introduction

In the previous chapter, URB597 and two other structurally and functionally distinct FAAH inhibitors, OL135 and PF750, were shown to inhibit FAAH activity in SH-SY5Y cells. It was then demonstrated how 10 μM URB597 augmented AEA, PEA and 2AG levels in this cell line. In HeLa cells, URB597 inhibited ODA hydrolysis and augmented only PEA levels in this cell line. In this section, the possibility of transactivating PPAR nuclear receptors following pharmacological inhibition of FAAH in both SH-SY5Y and HeLa cells was addressed.

5.1.1. Reporter gene assay

In the literature, two distinct reporter gene assays are usually conducted in order to measure PPAR activation. The first one exploits expression of PPARs as GAL4-DBD (DNA binding domain) fusion protein, which binds to the UAS promoter containing generally four copies of a synthetic GAL4 binding site upstream to the minimal thymidine kinase (TK) promoter. The GAL4-DBD/PPAR fusion protein activates the reporter gene in response to agonist binding (Liu *et al.*, 2003). However, this method does not take into consideration any interaction with co-activators or co-repressors. Transactivation of PPARs measured in this way might not actually reflect a real activation in a more physiologically relevant situation that can be created with the presence of co-regulators. For this reason, a firefly luciferase reporter gene assay was used in this study. The plasmid construct was transiently transfected in the cells and was under the control of three copies of PPRE

(peroxisome proliferator responsive element) upstream to the minimal TK promoter. Ligand binding induced transcription of the reporter gene. A major drawback of this method is the possibility of endogenous PPARs contributing to the measured reporter gene activation . For this reason and in order to test selectivity of activation, pharmacological studies employing selective PPAR antagonists were carried out. Some authors use a dual luciferase assay to normalise their data. This method is based on co-transfection of a plasmid expressing renilla luciferase in order to monitor the quality of transfection. Other authors co-transfect a β-galactosidase expressing plasmid instead. The substrate is then added and detection of the yellow product allows normalisation of data to a value directly correlated with the quality of transfection. However, previous data from the labs in Nottingham indicated that these co-transfection protocols might interact and interfere with the experimental setup giving unstable reporter gene readings. For this reason, data in this study were normalised to protein levels. This also allowed us to exclude data sets that differed from the control protein levels, an indication of possible toxicity of the tested compound.

5.1.2. PPAR binding assays

The PPAR binding assays used in this section are based on displacement of either *cis*-parinaric acid (PPARα) or Fluormone™, a pan-PPAR fluorescent agonist (PPARβ and PPARγ), from the PPAR ligand binding domain. Assays based on Fluormone™ displacement are commercially available (Invitrogen)

and exploit either TR-FRET technology (PPARβ) or fluorescence polarization (PPARγ)

5.2. Results

5.2.1. Transactivation of endogenous PPARs

Cells were treated with either DMSO, 10 μM URB597 or two applications of of 10 μM OL135 for 24 hours. 10 μM WY14643, 1 μM GW0742 and 1 μM rosiglitazone were used as positive controls for PPARα, PPARβ and PPARγ, respectively. In SH-SY5Y cells, both URB597 and OL135 caused significant activation of endogenous PPARs ($P<0.01$ and $P<0.001$ respectively). Both the PPARβ ligand GW0742 and the PPARγ ligand rosiglitazone elevated endogenous PPAR activation ($P<0.001$ and $P<0.01$, respectively), while the PPARα ligand WY14643 had only a small effect. In HeLa cells, neither of the FAAH inhibitors tested had any effect on endogenous PPAR activation. However, both the PPARβ ligand GW0742 and the PPARγ ligand rosiglitazone stimulated endogenous PPAR activation ($P<0.001$, Figure 5.1) while the PPARα ligand WY14643 had no effect.

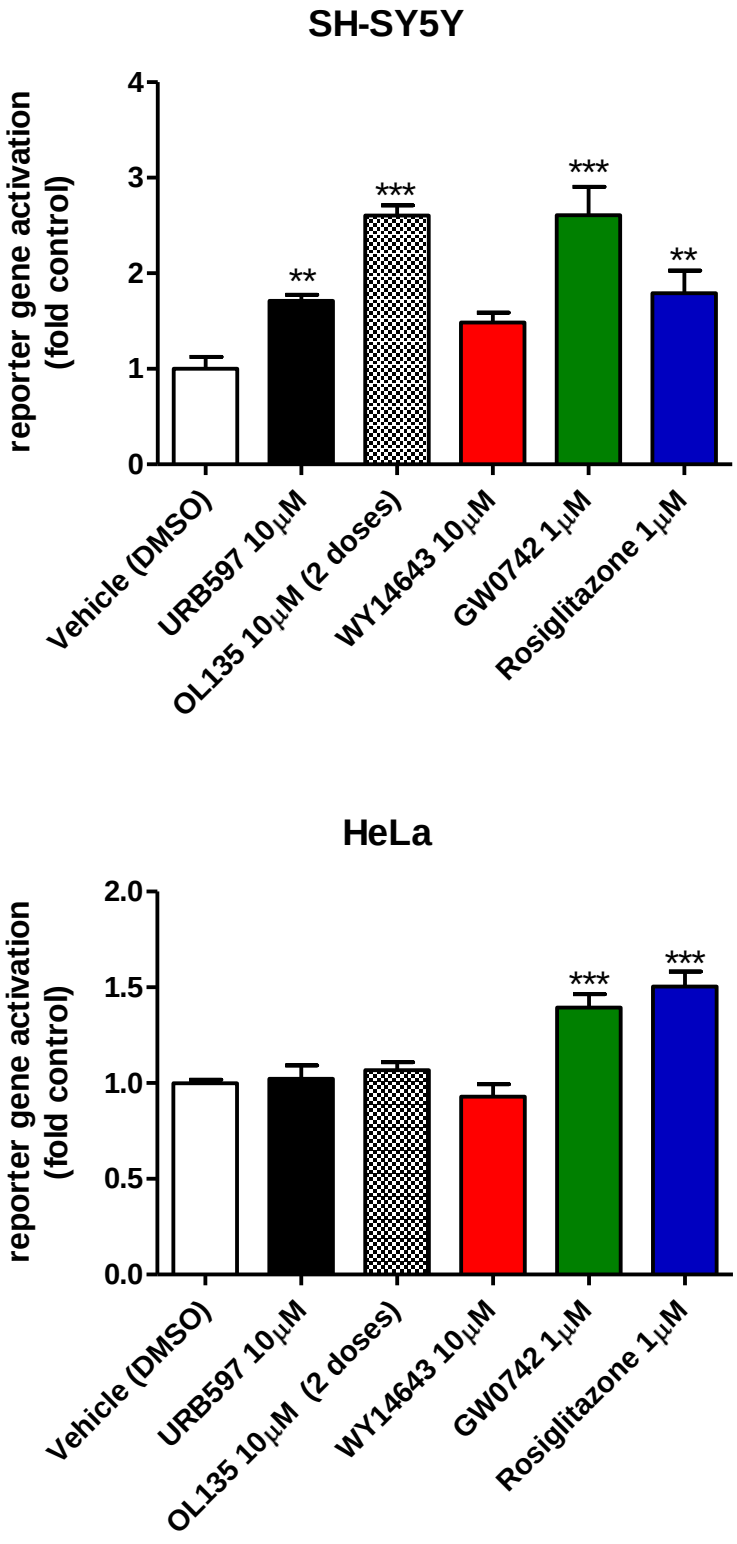

Fig 5.1: Reporter gene activation in SH-SY5Y and HeLa cells transfected with a 3xPPRE-TK Luciferase construct. OL135 was applied two times over 24

hours. Results are expressed as fold activation from control (**P<0.01 and ***P<0.001 compared to vehicle, n ≥ 6).

5.2.2. Transactivation of over-expressed PPARs

5.2.2.1. SH-SY5Y cells

Cells were treated with DMSO, 10 μM OL135 or increasing concentrations of URB597 for 24 hours. URB597 appeared to be able to induce activation of PPARβ and PPARγ in a concentration dependent fashion while it had a biphasic effect on PPARα activation. URB597 appeared to be more potent in activating PPARβ out of the three different isotypes. Indeed, the threshold URB597 concentration to activate PPARβ was 10 μM (P<0.001, Figure 5.2). Another FAAH inhibitor, OL135 at 10 μM, could transactivate all three PPAR isotypes. When expressed as a proportion of the response to the isotype-selective ligand, both URB597 and OL135 appeared to be most efficacious in activating PPARβ, compared to the other two isotypes.

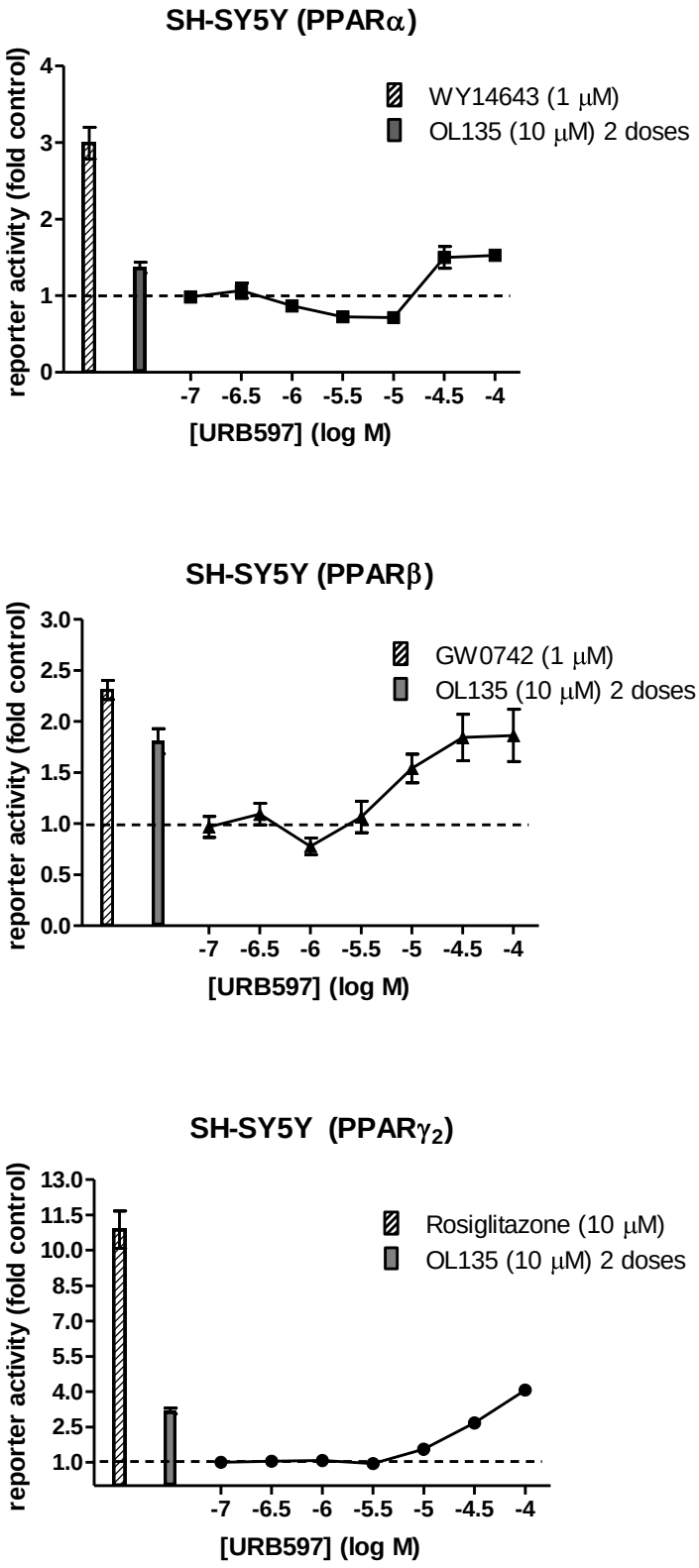

Fig 5.2: Reporter gene activation in SH-SY5Y cells transfected with a 3xPPRE-TK Luciferase construct in combination with a PPARα, PPARβ or

PPARγ_2 expressing plasmid. OL135 was applied two times over 24 hours. Results are expressed as fold activation relative to control (*P<0.05, **P<0.01 and ***P<0.001 compared to control, n=6, representative of two separate experiments).

5.2.2.2. HeLa cells

Cells were treated with DMSO, 10 μM OL135 or increasing concentrations of URB597 for 24 hours. URB597 did not show a clear concentration dependency in PPAR activation. Indeed, URB597 appeared to be either ineffective at low concentrations or to diminish basal activation at high concentrations in both PPARα- and PPARβ-overexpressing HeLa cells. In PPARγ-expressing cells, URB597 had a bell-shaped effect, augmenting basal activation at mid-micromolar concentrations. The most efficacious concentration was 10 μM (P<0.01). Similarly, 10 μM OL135 activated PPARγ (P<0.001), although it was ineffective in PPARα- and PPARβ-overexpressing cells.

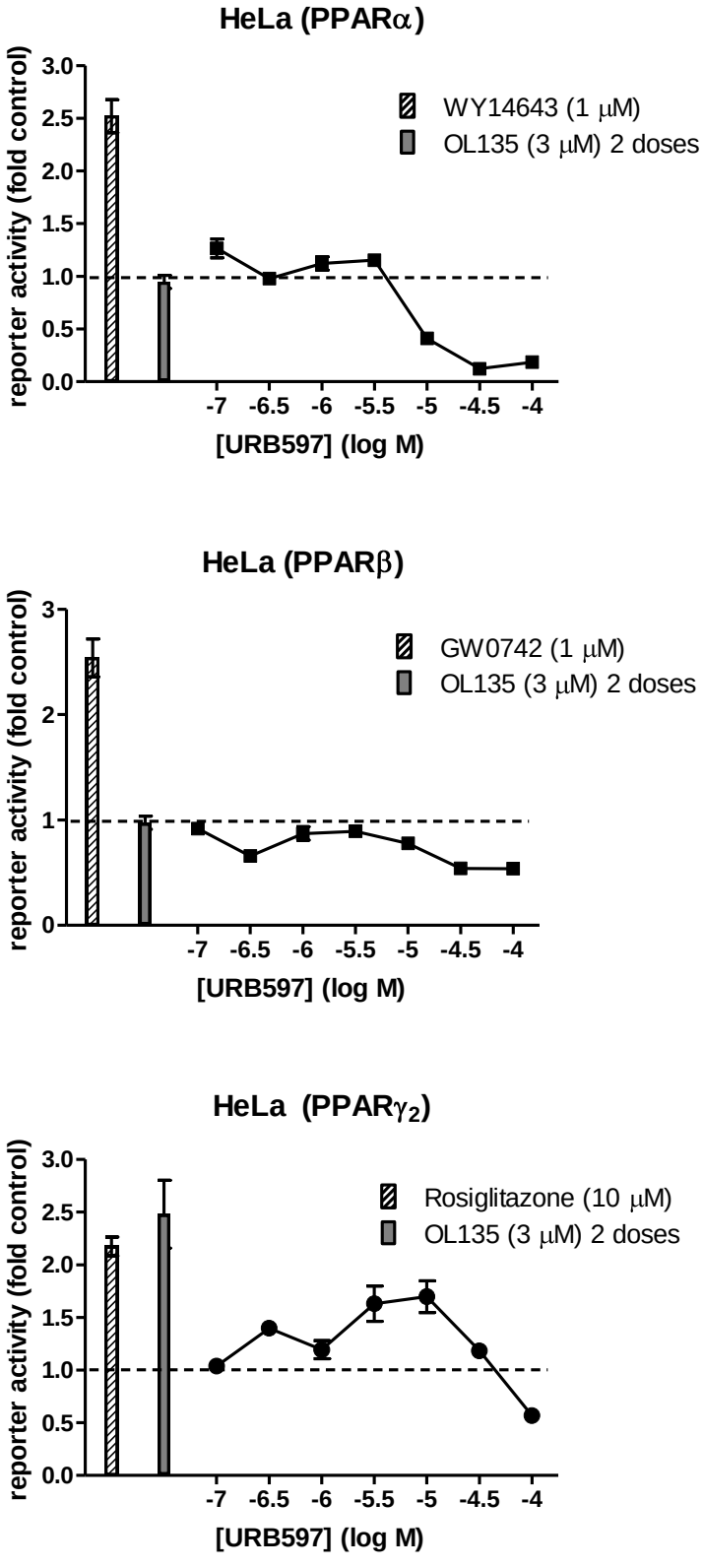

Fig 5.3: Reporter gene activation in HeLa cells transfected with a 3xPPRE-TK Luciferase construct in combination with a PPARα, PPARβ or PPARγ_2

expressing plasmid. OL135 was applied two times over 24 hours. Results are expressed as fold relative to control (*P<0.05, **P<0.01 and ***P<0.001 compared to control, n=6, representative of two separate experiments)

5.2.3. Selectivity of PPAR activation in SH-SY5Y cells

The selectivity of exogenous PPARα, PPARβ and PPARγ activation by 20 μM URB597 in SH-SY5Y cells was confirmed by treating cells with selective antagonists. The PPARα antagonist GW6471 (10 μM) was able to reverse PPARα activation by both 20 μM URB597 and 10 μM WY14643 (P<0.001). However, 10 μM GW6471 was also able to inhibit basal reporter gene activation on its own (P<0.001). The PPARβ antagonist GSK0660 (1 μM), could inhibit basal PPARβ activation on its own and completely reverse activation by 20 μM URB597 (P<0.05 and P<0.001 respectively). In PPARγ-overexpressing cells, the PPARγ antagonist GW9662 inhibited transactivation by 1 μM rosiglitazone (P<0.001). However, the selective PPARγ antagonist was not able to reverse transactivation by 20 μM URB597.

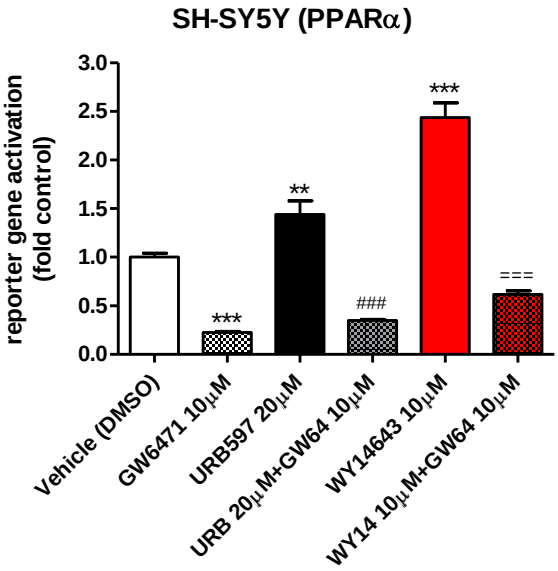
SH-SY5Y (PPARα)
reporter gene activation (fold control)
3.0
2.5
2.0
1.5
1.0
0.5
0.0
***
**
***
###
===
Vehicle (DMSO)
GW6471 10μM
URB597 20μM
URB 20μM+GW64 10μM
WY14643 10μM
WY14 10μM+GW64 10μM

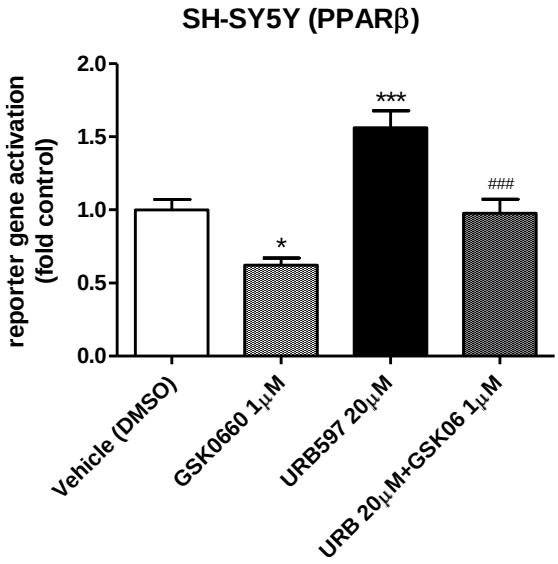
SH-SY5Y (PPARβ)
reporter gene activation (fold control)
2.0
1.5
1.0
0.5
0.0
***
*
###
Vehicle (DMSO)
GSK0660 1μM
URB597 20μM
URB 20μM+GSK06 1μM

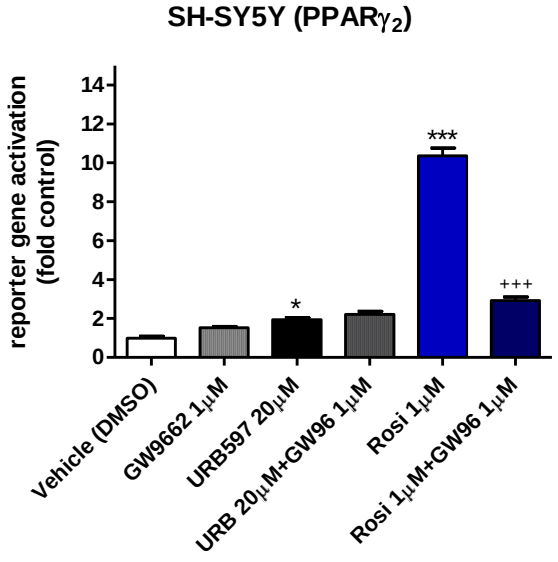
SH-SY5Y (PPARγ2)
reporter gene activation (fold control)
14
12
10
8
6
4
2
0
***
*
+++
Vehicle (DMSO)
GW9662 1μM
URB597 20μM
URB 20μM+GW96 1μM
Rosi 1μM
Rosi 1μM+GW96 1μM

Fig 5.5: Reporter gene activation in SH-SY5Y cells transfected with a 3xPPRE-TK Luciferase construct in combination with a PPARα, PPARβ or PPARγ expressing plasmid. Results are expressed as fold relative to control. (*P<0.05, **P<0.01 and ***P<0.001 compared to control, ###P<0.001 compared to 20 μM URB597 , ===P<0.001 compared to 10 μM WY14643, +++P<0.001 compared to 1 μM rosiglitazone, n≥6)

5.2.4. PPAR activation by PF750 in SH-SY5Y cells

Cells were treated with either DMSO or three separate FAAH inhibitors for 24 hours. 10 μM URB597, 10 μM PF750 or two doses of 10 μM OL135 significantly activated either endogenous PPAR activation (**a**, P<0.01, P<0.001 and P<0.001 respectively) or activation of heterologously expressed PPARβ (**b**, ***P<0.001, *P<0.05 and ***P<0.001 respectively).

(**a**)

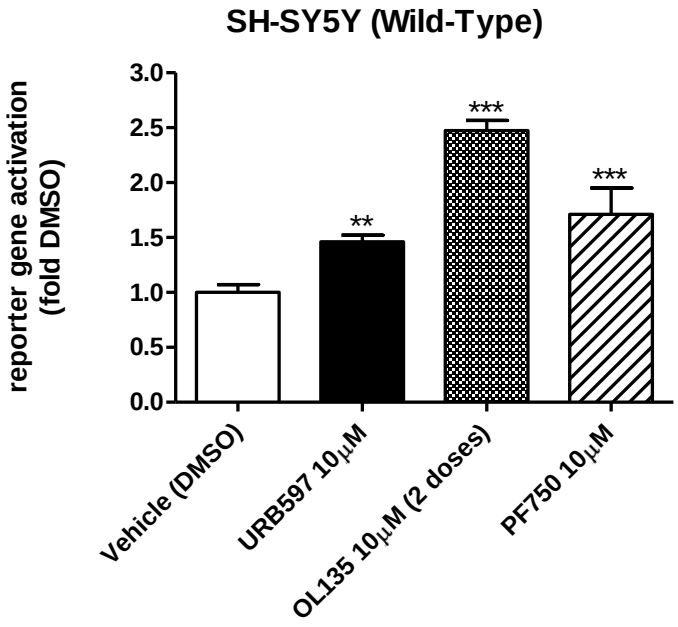

(**b**)

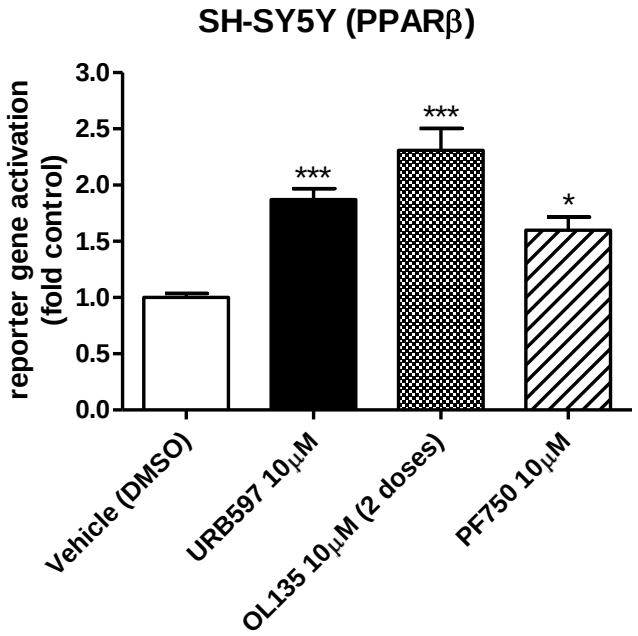

Fig 5.4: Reporter gene activation in SH-SY5Y cells transfected with a 3xPPRE-TK Luciferase construct either alone (**a**) or in combination with a PPARβ expressing plasmid (**b**). OL135 was applied two times over 24 hours.

Results are expressed as fold relative to control. (*P<0.05, **P<0.01 and ***P<0.001 compared to vehicle, $n \geq 6$).

5.2.5. PPAR binding assays

5.2.5.1. FAAH inhibitors

Binding of FAAH inhibitors to PPARα, PPARβ and PPARγ ligand binding domains was tested using as positive controls WY14643, GW0742 and rosiglitazone, respectively. IC_{50} (95% C.I.) values: WY14643 $3.1x10^{-6}$ M ($1.6x10^{-6}$ to $6.2x10^{-6}$) GW0742 $3.3x10^{-10}$ M ($1.7x10^{-10}$ to $6.6x10^{-10}$) and rosiglitazone $3.5x10^{-8}$ M ($3.1x10^{-8}$ to $4.0x10^{-8}$). Increasing concentrations of URB597, OL135 or PF750 failed to displace the competing ligand from the PPARβ ligand binding domain. Moreover, URB597 was not able to bind to either the PPARα or the PPARγ ligand binding domain.

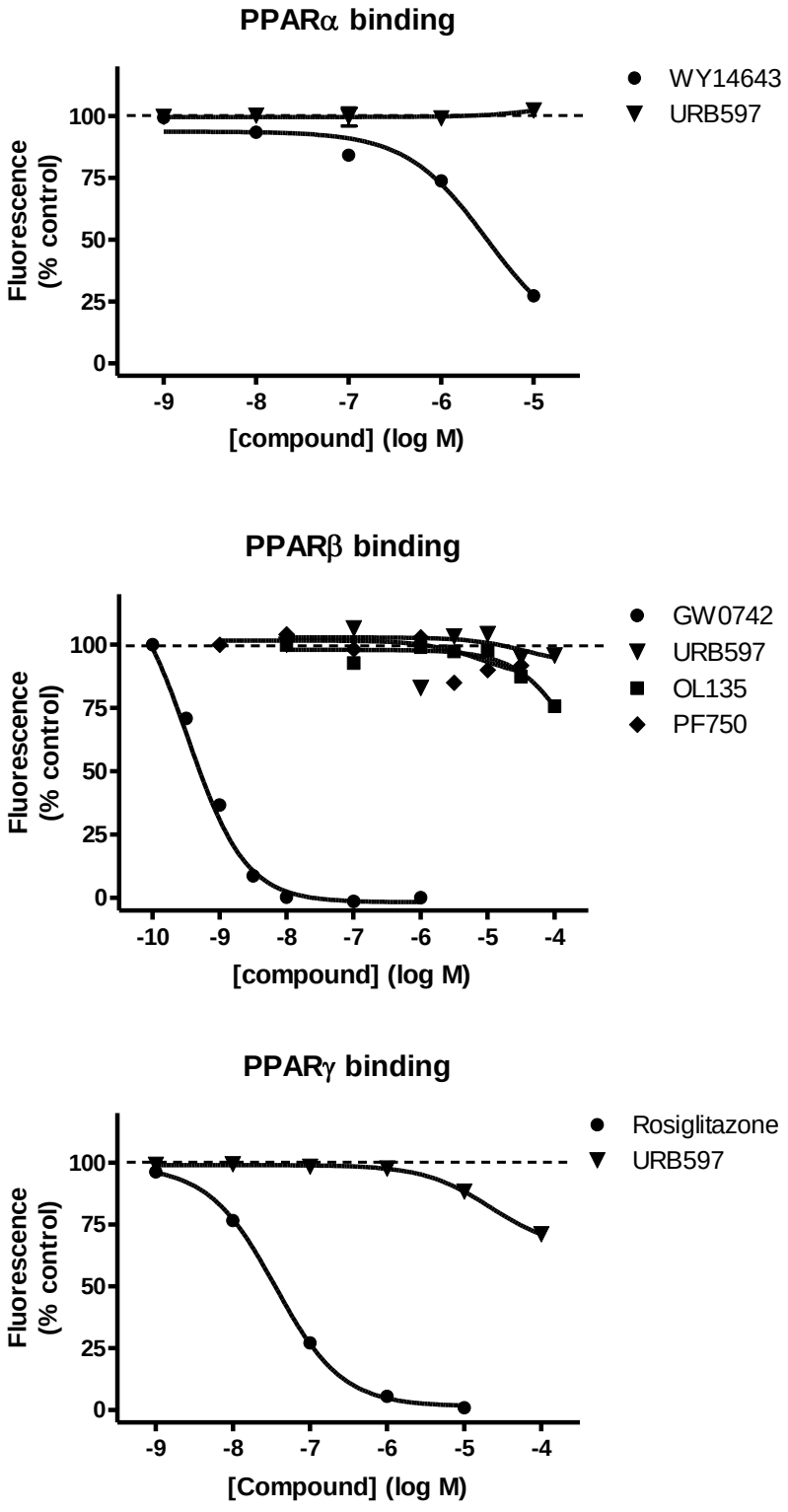

Fig 5.6: TR-FRET (PPARα and PPARβ) or Fluorescence Polarisation (PPARγ) based competition displacement assays (Invitrogen) for the PPAR ligand binding domains (PPARα n=3; PPARβ/γ n=2)

5.2.5.2. ECs and fatty acids

Binding of a variety of ECLs (**a**) and fatty acids (**b**) to the PPARβ ligand binding domain was tested using GW0742 as a positive control (IC_{50} value = $6.7x10^{-10}$ M in **a** and IC_{50} value = $4.2x10^{-10}$ M in **b**). OEA and PEA failed to bind to the PPARβ ligand binding domain, while AEA and 2AG were both ligands (IC_{50} values = $1.4x10^{-5}$ and $8.3x10^{-5}$ M, respectively). Arachidonic acid (AA), palmitic acid (PA) and oleic acid (OA) could all displace the fluorescent ligand from the PPARβ ligand binding domain. IC_{50} (95% C.I.) values: AA $1.8x10^{-6}$ M ($1.1x10^{-6}$ to $3.0x10^{-6}$); PA $1.7x10^{-6}$ M ($9.0x10^{-7}$ to $3.4x10^{-6}$); OA $6.8x10^{-7}$ M ($3.8x10^{-7}$ to $1.2x10^{-6}$).

(**a**)

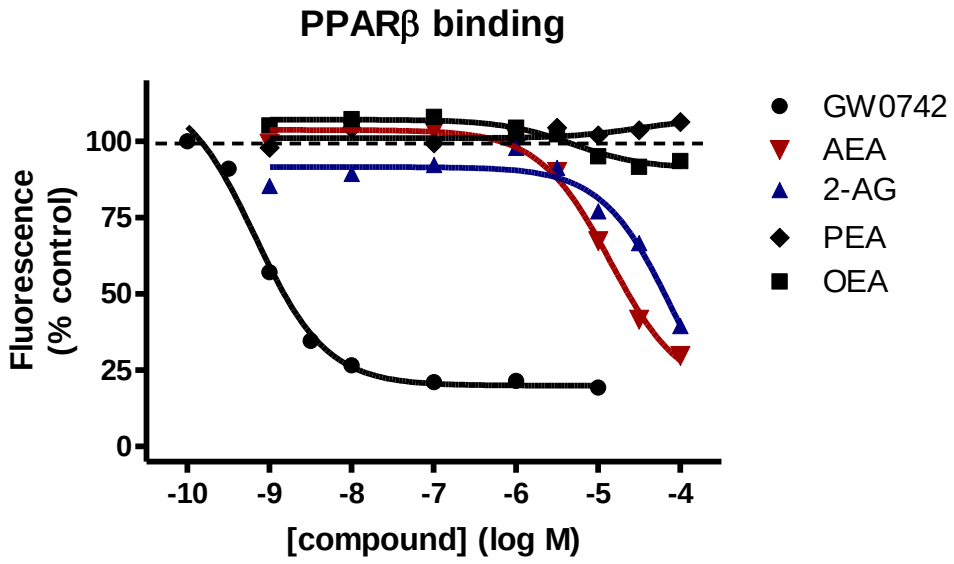

(**b**)

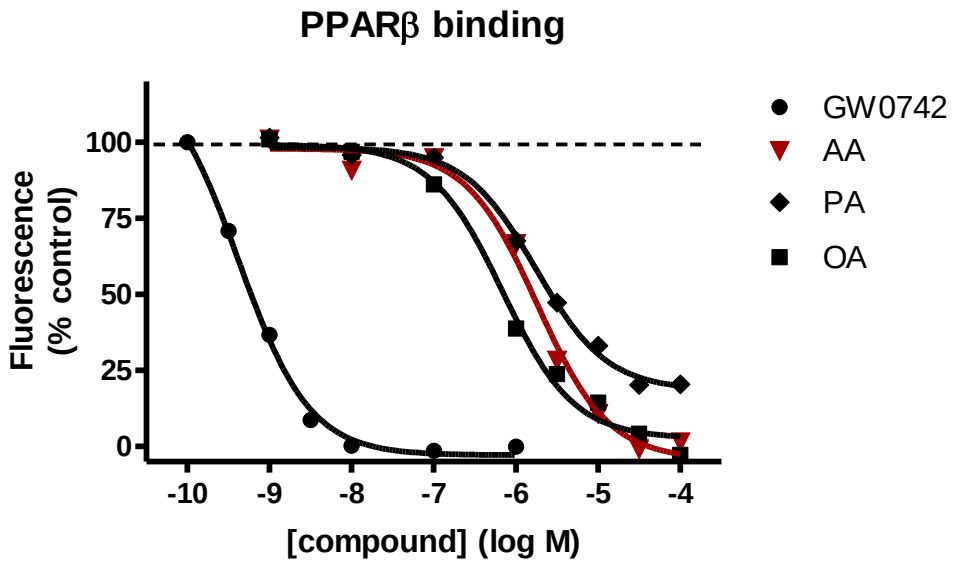

Fig 5.7: TR-FRET based displacement assay for the PPARβ ligand binding domain by ECLs (**a**) and fatty acids (**b**, n=2)

5.3. Discussion

Reporter gene assays of transiently transfected cells showed that both 10 μM URB597 and 10 μM OL135 could induce transactivation of PPARs endogenously expressed in SH-SY5Y cells. In contrast, both FAAH inhibitors were ineffective in HeLa cells (Figure 5.1). The earlier characterization of SH-SY5Y cells in Chapter 3 indicated that PPARβ was by far the most abundant PPAR isotype expressed in these cells. PPARα was expressed at lower levels while PPARγ levels were almost undetected. Surprisingly, 1 μM rosiglitazone induced elevation of basal PPAR activation in SH-SY5Y cells. However, PPARγ ligands such as rosiglitazone and other thiazolidinediones (TZDs) are

reported to activate MAPKs and activation of this pathway is believed to induce activation of PPARs by phosphorylation (Gardner *et al.*, 2005). The PPARα ligand WY14643 10 μM could only slightly increase basal PPAR activity in SH-SY5Y. However, this could be explained by a constitutively high PPARα activation by endogenous ligands as well as by components of the serum (FBS concentration could only be lowered down to 0.5% in order to keep the cells viable).

Pharmacological inhibition of FAAH by URB597 and OL135 was also demonstrated to lead to transactivation of overexpressed PPARα, PPARβ and PPARγ in SH-SY5Y cells. However, low concentrations of URB597 appeared to significantly inhibit PPARα and PPARβ basal activation. This effect might once again be explained by high basal activation of these receptors in SH-SY5Y cells. Initial low potency inhibition of ECL hydrolysis by FAAH might lead to depletion of the pool of arachidonic acid and other FAs in the cells. A variety of saturated and unsaturated fatty acids are recognised endogenous ligands at PPARs, which may actually be involved in basal activation of these receptors. Among the FAs that are produced by hydrolysis of ECs and related molecules, arachidonic acid can transactivate all PPAR isotypes, while oleic and palmitic acids are both PPARα and PPARγ ligands (Figure 5.7b) (Berger *et al.*, 2002). Subsequently, a greater inhibition of FAAH by slightly higher concentrations of URB597 might lead to higher accumulation of intracellular ECLs that would in turn activate PPARs. The possibility of URB597 directly binding to PPARs to induce their activation was also addressed in this study. Concentrations of up to 100 μM URB597 were only slightly able to displace

the fluorescent ligand from the PPARβ and PPARγ ligand binding domain (Figure 5.6). This weak effect is highly unlike to be of any pharmacological relevance.

To provide a further link between URB597- and OL135-induced PPAR transactivation and inhibition of FAAH, PF750 was shown to induce activation of both endogenous PPARs and over-expressed PPARβ (Figure 5.4). While both URB597 and OL135 have been shown to have carboxylesterases as off-targets, PF750 has been demonstrated to be very selective and not to interact with such targets (Ahn *et al.*, 2007; Zhang *et al.*, 2007). 10 μM URB597 and 10 μM PF750 appeared to have similar efficacies in activating both endogenous PPARs and over-expressed PPARβ, while 10 μM OL135 appeared to be slightly more efficacious (Figures 5.1, 5.2, 5.4). However, given that OL135 is the only reversible FAAH inhibitor examined in this study, two applications of this compound were used in these experiments in order to be sure of inducing an inhibition sustained over 24 hours. Cumulative or prolonged effects in elevation of intracellular ECLs by two applications of 10 μM OL135 might explain a stronger effect in PPAR activation by this compound. URB597, OL135 and PF750 were demonstrated not to be ligands at the PPARβ ligand binding domain (Figure 5.6)

As already mentioned, reporter gene assays based on plasmids under the control of PPREs might lack selectivity if PPARs are endogenously expressed in the cells at high levels. The selective PPARα antagonist GW6471 (Xu *et al.*,

2002) and GSK0660, a selective PPARβ antagonist (Shearer *et al.*, 2008), were identified to completely reverse reporter gene activation by URB597 in SH-SY5Y cells overexpressing PPARα and PPARβ respectively (Figure 5.3). In contrast, although the selective PPARγ antagonist GW9662 (Leesnitzer *et al.*, 2002) was able to almost completely reverse reporter gene activation by rosiglitazone, it was ineffective in inhibiting transactivation of over-expressed PPARγ (Figure 5.3). This lack of selectivity of the reporter gene assay based on co-transfection of PPARγ might reflect the low endogenous expression of this receptor isotype compared to PPARα and PPARβ in SH-SY5Y cells (see Chapter 3). While over-expressing one of these two receptors might be enough to confer selectivity over the other isotypes, overexpressing PPARγ might not.

In the previous chapter, levels of AEA, PEA and 2AG were demonstrated to be augmented in SH-S5Y after FAAH inhibition by URB597. Here, inhibition of FAAH was showed to transactivate all PPARs isotypes, or at least selectively activate both PPARα and PPARβ. AEA has been previously reported to transactivate and bind to both PPARα and PPARγ (Bouaboula *et al.*, 2005; Sun *et al.*, 2006). Moreover, 2AG was also demonstrated to transactivate both PPARα and PPARγ (Kozak *et al.*, 2002; Rockwell *et al.*, 2006a). For completeness, in this study both AEA and 2AG were shown to be PPARβ ligands while both PEA and OEA were not able to displace the fluorescent competitor (Figure 5.7a). This is in contrast with the reported activation of a GAL4-DBD/PPARβ fusion protein by OEA previously reported by (Fu *et al.*, 2003). Reporter gene activity was measured after 7 hours following administration of exogenous OEA. Thus, activation of PPARβ in this

timeframe might be due to OEA metabolites. However in the same study, the authors reported that OEA was able to both bind to and transactivate PPARα. Finally, PEA is also reported to transactivate PPARα (LoVerme *et al.*, 2006); however, binding to the PPARα ligand binding domain is still to be demonstrated.

In FAAH-negative HeLa cells, URB597 and OL135 were unable to transactivate overexpressed PPARα or PPARβ. Surprisingly though, both URB597 and OL135 induced activation of over-expressed PPARγ in these cells (Figure 5.3). URB597 was shown to inhibit exogenous ODA hydrolysis in HeLa cells and these cells appeared indeed to express FAAH-2 (see Chapter 3). Differential patterns in intracellular accumulation of ECLs after enzyme inhibition in SH-SY5Y and HeLa cells (see Chapter 4) might indeed explain a differential activation among the three PPAR isotypes in the two cell lines. However, PEA was shown to be elevated in HeLa cells after URB597 treatment. This endocannabinoid analogue has been shown to transactivate PPARα and its anti-inflammatory actions have been demonstrated to be mediated by PPARα activation (LoVerme *et al.*, 2005). Given that in HeLa cells, URB597 and OL135 elicited transactivation only of the PPARγ isotype, it would appear that other ECs or indeed other FAAH-2 products are involved in this mechanism. However, it remains unclear why higher concentrations of URB597 were ineffective in transactivating PPARγ as shown by the bell-shaped curve (Figure 5.3). On the contrary, URB597 appeared to inhibit the basal activation of both PPARα and PPARβ, once again indicating how some

of the FAAH-2 substrates might represent a pool of endogenous ligands to these receptors.

6. ACTIVATION OF PPARs BY OLEAMIDE

6.1. Introduction

In the previous sections of this thesis, FAAH-2 expression in HeLa cells was reported, together with ODA hydrolysis that was inhibited by URB597 pre-treatment. Although levels of OEA and AEA were not significantly affected, PEA levels were augmented in HeLa cells following URB597 exposure. Treatment with this FAAH-1/2 inhibitor led to PPARγ activation. In order to investigate the potential role of ODA, in this part of the study, the capability of ODA to activate PPAR nuclear receptors was assessed.

6.2. Results

6.2.1. PPAR transactivation in CHO cells

ODA at 10 and 50 μM evoked a significant activation of PPARα, PPARβ and PPARγ receptors in CHO cells over-expressing these nuclear receptors. This activation was concentration-dependent for all three receptors. ODA appeared to have the most marked effects on PPARβ and PPARγ receptors. The higher concentration of ODA tested (50 μM) evoked PPARβ activation to 5.5-fold of control and PPARγ activation to 3.2-fold of control (Figure. 6.1).

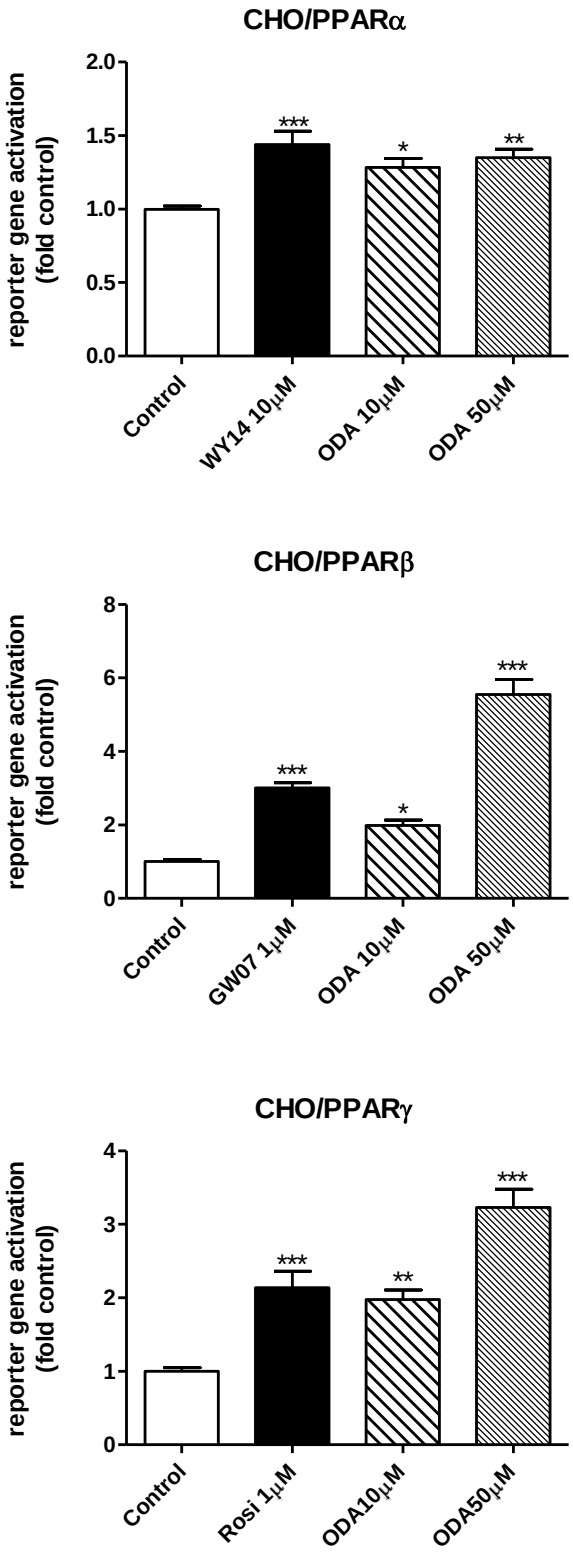

Figure 6.1: PPARα, PPARβ and PPARγ reporter gene assay in transiently transfected CHO cells. ODA, at 10 and 50 μM, was tested alongside DMSO as

vehicle control and either 10 μM WY14643, 1 μM GW0742 or 1 μM rosiglitazone as positive controls, respectively (n=6, * P<0.05, ** P<0.01, *** P<0.001; One-way ANOVA with Bonferroni's PostHoc test).

6.2.2. PPAR ligand binding

The ability of ODA to bind directly to PPARs was then tested *in vitro*. ODA was indeed able to displace fluorescent ligands from the PPARα, PPARβ and PPARγ ligand binding domains in a concentration-dependent fashion. However, ODA was not able to completely displace ligand from the PPARα binding domain at the highest concentration tested (100 μM), while the IC_{50} value for the positive control WY14643 was 3.8×10^{-7} M (1.4×10^{-7} to 1.0×10^{-6}). Similarly, ODA could not completely displace ligand from the PPARβ ligand binding domain either, while the IC_{50} value for the positive control GW0742 was 8.4×10^{-10} M (4.0×10^{-10} to 1.8×10^{-9}). The IC_{50} value for ODA binding to PPARγ was 3.8×10^{-5} M (3.1×10^{-5} to 4.7×10^{-5}), while the IC_{50} value for the positive control rosiglitazone was 2.2×10^{-7} M (2.0×10^{-7} to 2.5×10^{-7}; Figure. 6.2).

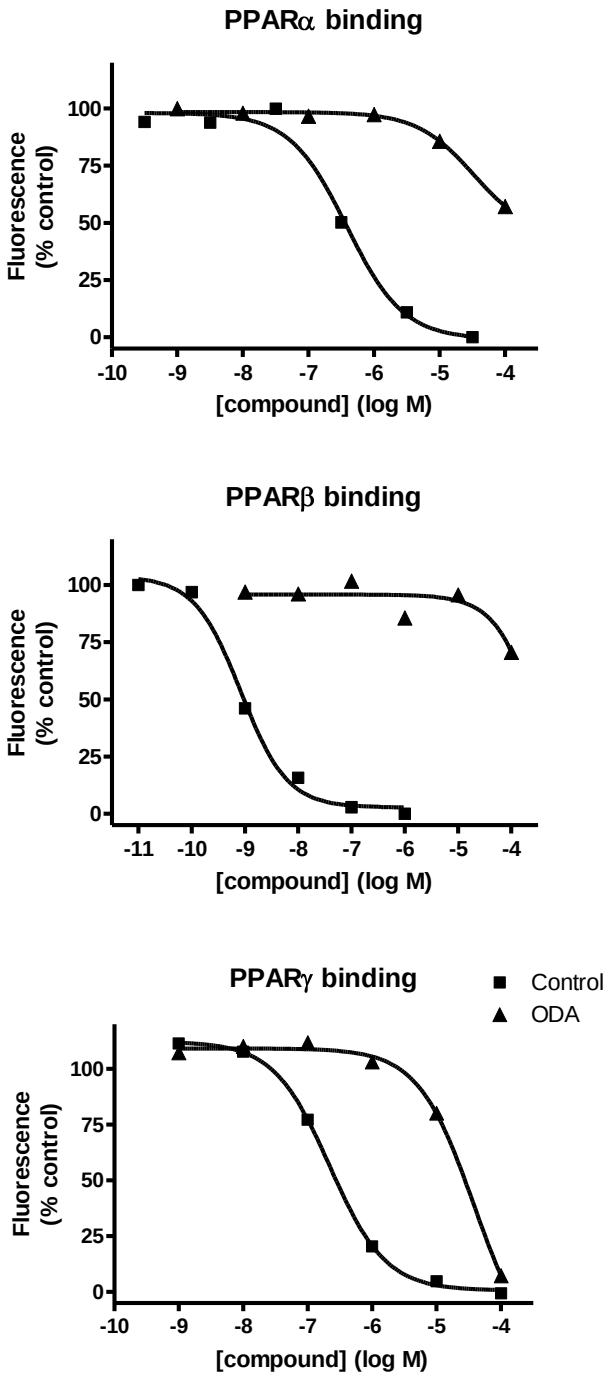

Figure 6.2: PPARα, PPARβ and PPARγ ligand binding assay of increasing concentrations of ODA and either WY14643, GW0742 or rosiglitazone as positive controls respectively (n=2, WY14643 n=1; one-site competition binding)

6.2.3. Differentiation of 3T3-L1 cells

In an Oil Red O uptake-based assay, ODA, at 10-20 µM, was able to induce differentiation of 3T3-L1 mouse fibroblast cells into adipocytes. The number of cells stained by the lipid-sensitive dye was indeed much higher in the ODA treated wells compared to the vehicle treated wells. However, the PPARγ ligand rosiglitazone (10 µM) had a more marked effect on the treated cells (Figure.6.3).

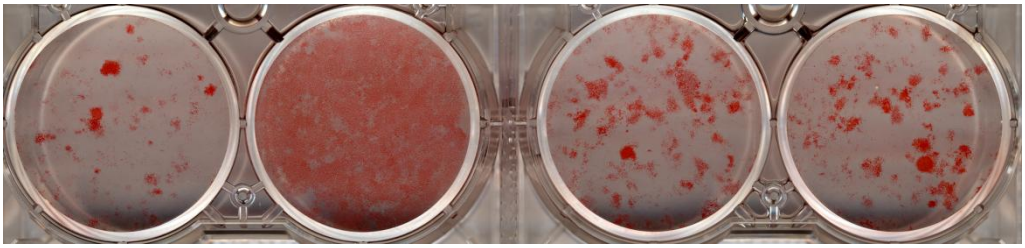

Control **Rosiglitazone 10µM** **ODA 10µM** **ODA 20µM**

Figure 6.3: 3T3-L1 differentiation into adipocytes after treatment with ODA 10-20 µM, rosiglitazone 10 µM as a positive control or DMSO as vehicle control (Picture shows one of three replicates).

6.3. Discussion

In this study, a further endocannabinoid-like molecule, oleamide, was shown to be able to occupy and activate PPAR nuclear receptors. As well as the

phytocannabinoids THC (O'Sullivan *et al.*, 2005), the major psychoactive ingredient in cannabis, and cannabidiol (O'Sullivan et al., 2009), a number of endogenous cannabinoids have been shown to activate PPARs. In particular, anandamide, virodhamine, *N*-arachidonoyldopamine, noladin and 2-arachidonoylglycerol, as well as *N*-oleoylethanolamine and *N*-palmitoylethanolamine, have been shown to activate various members of the PPAR family (O'Sullivan, 2007). Δ^9-tetrahydrocannabinol (THC), the main active ingredient found in the Cannabis plant, has been shown to produce a time dependent vasorelaxation in vitro in isolated rat blood vessels through activation of PPARγ (O'Sullivan et al., 2005). ODA has also been reported to induce vasorelaxation in the rat small mesenteric artery in vitro through activation of an undefined receptor which may be coupled to Ca^{2+}-sensitive K+ channels and Gi/o (Hoi et al., 2006). However, the mechanism by which it elicits vasorelaxation has not been fully explained. ODA can inhibit gap junction formation (Boger *et al.*, 1998), modulate GABA (Yost *et al.*, 1998) and 5-HT (Thomas *et al.*, 1998) receptors *in vitro*. Moreover, ODA has been demonstrated to bind to the CB1 receptor *in vitro* (Leggett et al., 2004).

Results from the present study showed that ODA was able to transactivate PPARα, PPARβ and PPARγ nuclear receptors in a concentration-dependent-fashion with a lower potency than the respective selective ligands WY14643, GW0742 and rosiglitazone (Figure 6.1). ODA itself was able to occupy the ligand binding domain of all three receptors, implying that the enzymatic generation of oleic acid from ODA is not a simple explanation for the observed effects. Of the three subtypes of PPAR, the potency of ODA appeared highest

at PPARγ (Figure 6.2), although functional effects on PPARβ appeared higher in reporter gene assays (Figure 6.1). This may be attributed to greater amplification of PPARβ-evoked responses, or alternatively, to relatively elevated background levels of PPARγ activity.

In order to explore the possibility of ODA being responsible for the reported PPARγ activation by the FAAH inhibitor URB597 in HeLa cells (see Chapter 5), attempts to measure ODA levels in these cells by LC-MS/MS have been made by Dr Leonie Norris in the School of Pharmacy (University of Nottingham). Unfortunately, measurements of ODA internal standards were not linear.

The actual physiological significance of PPAR activation by ODA remains to be addressed. In order to at least partly address this issue, the ability of ODA to induce 3T3-L1 differentiation into adipocytes was demonstrated in this study (Figure 6.3). Adipogenesis is a well recognised PPARγ mediated activity (Mueller et al., 2002). The proposed novel site of action for ODA through PPAR activation might be involved in some of the previously reported ODA effects. The onset of the vasorelaxation by ODA shown by (Hoi *et al.*, 2006) was described to be too quick (on a time scale of *ca.* 5 min) to involve activation of nuclear receptors. The reported vasorelaxant effect of THC through PPARγ in isolated rat blood vessels has also been shown to be time-dependent (O'Sullivan *et al.*, 2005). However, there is strong debate around the possibility of PPARs having non-genomic effects that would have a quicker

onset. Moreover, a late component of the vasorelaxation elicited by ODA might be due to nuclear receptor activation and this possibility has not been tested yet. Effects of *N*-oleoylethanolamine (OEA) and *N*-palmitoylethanolamine, two other endocannabinoid-related molecules, *in vivo* have been demonstrated to be mediated through PPARα activation (Fu et al., 2003) (LoVerme et al., 2006). OEA has also been reported to elicit loss of appetite and to reduce body weight gain in mice with a mechanism dependent on PPARα (Fu et al., 2003) (Fu et al., 2003; Sun et al., 2006). Moreover, it has been previously shown that OEA pre-treatment reduced infarct volume from middle cerebral artery occlusion in wild-type, but not in PPARα-null, mice (Sun et al., 2007). In these two studies, OEA was shown to bind to the ligand binding domain of PPARα and to transactivate both PPARα and PPARβ, however it had no effect on PPARγ. Data from the present study show that ODA binds to all three PPAR LBDs showing higher affinity for PPARγ over the two other receptors (Figure 6.2). OEA and ODA share the same fatty acid chain, oleic acid, which, together with a variety of other saturated and unsaturated fatty acids, is one of the PPARα natural ligands. By contrast, PPARγ is less tolerant of structural variety than PPARα and is usually activated by polyunsaturated fatty acids (Berger *et al.*, 2002). Even if the limiting factor for PPAR binding is usually the length and saturation level of the fatty acid chain, in this case the head residue would appear to confer selectivity between OEA and ODA in PPARγ binding. However, no direct evidence is available in the literature of OEA binding (or not) to the ligand binding domain of PPARγ.

In summary, PPARs were identified as a novel site of action of ODA. Data in this study indicated that ODA could be regarded as a low affinity pan-PPAR ligand in vitro, being able to transactivate all three isotypes of this nuclear receptor family. ODA appeared to be most potent as a ligand of PPARγ.

7. GENERAL DISCUSSION

Fatty Acid Amide Hydrolyse (FAAH) is the enzyme that hydrolyses ECLs of the NAE family. It plays a major role in controlling ECL physiological concentrations and signalling (McKinney *et al.*, 2005). Neurones expressing FAAH in the rat brain are usually found in close proximity to axon terminals containing CB_1 receptors, highlighting the role of FAAH in synaptic AEA inactivation (Suárez *et al.*, 2008). Moreover, FAAH knockout mice have higher levels of AEA in the brain and show signs of an exaggerated endocannabinoid tone, such as reduced pain sensation (Cravatt *et al.*, 2001). These findings suggest that inhibition of FAAH might augment AEA levels in discrete brain regions where this endogenous lipid is constitutively active, for example those engaged in the processing of pain. Indeed, FAAH inhibition is anti-nociceptive in models of acute and inflammatory pain (Fegley *et al.*, 2005; Holt *et al.*, 2005; Kathuria *et al.*, 2003; Russo *et al.*, 2007). FAAH is a promising drug target for pain treatment because it might allow the avoidance of undesirable central side effects associated with CB receptor activation. For example, its inhibition by URB597 increases AEA levels in the brain without inducing immobility, hypothermia or over-eating at doses that are effective at abrogating pain (Kathuria *et al.*, 2003; Piomelli *et al.*, 2006). Moreover, no rewarding effects are produced after FAAH inhibition by URB597 and this compound does not substitute for cannabinoid agonists in a rat drug discrimination test (Gobbi *et al.*, 2005). Recently, *in vivo* effects of FAAH inhibition by URB597 such as analgesia, enhancement of memory acquisition and suppression of nicotine-induced excitation of dopamine cells have been linked to PPAR activation *(Jhaveri et al., 2008; Mazzola et al., 2009; Melis et al.*, 2008).

Other authors previously reported how a variety of ECs and related molecules can bind to and activate PPARs when administered exogenously (O'Sullivan, 2007). The aim of the present work was to test the possibility of elevating intracellular levels of ECLs by inhibiting their metabolism and check whether this augmentation in ECLs levels would lead to activation of PPARs nuclear receptors. In this study, it was indeed demonstrated that in intact SH-SY5Y human neuroblastoma cells (a model of neuronal cells), sustained FAAH inhibition by URB597 (~75 %) leads to accumulation of AEA, 2AG & PEA, but not OEA (see Chapter 4). Treatment with URB597, OL135 or PF750, three structurally and functionally distinct FAAH inhibitors, induces activation of endogenously expressed PPARs while no activation is observed in FAAH-1 negative HeLa cells. Furthermore, exposure to URB597, OL135 or PF750 leads to activation of over-expressed PPARs in SH-SY5Y cells. In the case of over-expressed PPARβ, this activation was clearly concentration-dependent and it was reversed by a selective antagonist. However, concentrations of URB597 required to evoke PPARβ activation exceeded concentrations needed to inhibit FAAH activity (see Chapter 5). Higher concentrations of URB597 might be required to either inhibit the activity of newly synthesised FAAH or to inhibit the residual AEA hydrolysing activity that seems to be due to NAAA activity. To rule out direct activation of PPARs by URB597, cell-free binding assays showed that URB597 could not bind to PPARα, PPARβ or PPARγ. URB597, OL135 and PF750 were all unable to bind to PPARβ binding domain, while AEA and 2-AG are ligands. In conclusion, activation of PPARs and, in particular of PPARβ, with URB597 in intact cells appears to be

mediated through elevations of AEA and/or 2AG via FAAH-dependent and -independent (NAAA) mechanisms. Surprisingly, treatment with URB597 in HeLa cells led to intracellular PEA accumulation but not AEA, OEA or 2AG. This might be due to inhibition of either FAAH-2 or NAAA that are both expressed in HeLa cells (see Chapter 3). Moreover, both URB597 and OL135 could activate PPARγ receptors over-expressed in HeLa cells. ODA, the main substrate for FAAH-2, was shown to bind to and activate all three PPARs *in vitro* (see Chapter 6). Thus, it is possible that either PEA or ODA were responsible for PPARγ activation in HeLa cells after URB597 treatment. However, there is no evidence that PEA can bind to PPARγ and this isotype is usually selectively activated by polyunsaturated fatty acids (Berger *et al.*, 2002). Moreover, it is reported that PEA could not transactivate PPARγ in a reporter gene assay in HeLa cells (LoVerme *et al.*, 2005).

In the present study, transactivation of PPARs was monitored by measuring luciferase expression after 24 hours treatment in order to allow accumulation of intracellular ECs and transcription of the reporter gene (see Chapter 2). However, it is likely that in this time course ECL metabolism through oxidative metabolism via COX-2, 12-LOX or 15-LOX (Bisogno *et al.*, 2005) could generate oxy-metabolites that might be PPAR ligands in their own right. Indeed, it has been demonstrated that a COX-2 metabolite of 2AG inhibits IL-2 secretion in activated T cells through PPARγ activation independent of the cannabinoid receptors (Rockwell *et al.*, 2006b). Moreover, a 15-LOX metabolite of 2AG (15-HETE-G) has been identified as a PPARα agonist (Kozak *et al.*, 2002). Furthermore, inhibition of IL-2 in murine splenocytes

was suggested to be mediated through activation of PPARγ by a COX-2 metabolite of AEA (Rockwell *et al.*, 2004). Another possible mechanism of PPAR activation after elevation of intracellular ECLs is the activation of CB receptors that are linked to downstream activation of the MAP kinase pathway (Demuth *et al.*, 2006). All three of the well known MAPK family members (ERK, p38, and JNK) are known to phosphorylate PPARs leading to changes in transcriptional activity (Gardner *et al.*, 2005)

In the literature, it is widely accepted that AEA and 2AG, the two main ECs, are produced on demand and not stored in vesicles. This assumption is based, at least in the case of AEA, on the low basal concentration compared to other neurotransmitters and on the fact that AEA and *N*-arachidonyl PE biosynthesis is associated with stimulus-dependent release of AEA from neurones itself (Piomelli *et al.*, 1998). Moreover, the activity of the semi-purified biosynthetic enzyme NAPE-PLD was shown to be activated by high concentrations of Ca^{2+} (Wang *et al.*, 2006). The elevation of AEA, PEA and 2AG in SH-SY5Y cells and of PEA in HeLa cells reported here after inhibition of either FAAH or FAAH-2 and possibly NAAA (see Chapter 4), indicates for the first time to my knowledge, that it is possible to elevate ECs levels in cultured cells by simply modulating their metabolism. This would point in favour of an underlying ECL tone, at least in cultured cells, regardless of external stimulation. The failure of the RNAi approach to completely knock down FAAH mRNA levels does not allow an irrefutable link between the reported intracellular ECs elevation and subsequent PPARs activation to inhibition of this enzyme. However, in this study a thorough pharmacological approach was carried out by employing

three structurally and pharmacologically distinct FAAH inhibitors. Involvement of carboxylesterases, off-target actions of URB597 and OL135 (Zhang *et al*., 2007), was ruled out using PF750. This compound belongs to a novel class of FAAH inhibitors whose greater selectivity has been identified in mouse and human proteomes (Ahn *et al.*, 2007)

The increase in AEA, PEA and 2AG levels after URB597 treatment in SH-SY5Y cells reported in this study (see Chapter 4) is not as marked as reported in other *ex vivo* studies. (Fegley *et al.*, 2005) reported that in rat brain AEA levels were trebled and both OEA and PEA levels were around four times higher following URB597 treatment. Here it is reported that in SH-SY5Y cells, AEA and 2AG levels were doubled after URB597 treatment, while PEA levels were only slightly increased. However, these results are in accordance with levels measured in mixed cultures of neurones and astrocytes after AMPA or NMDA treatment. AEA, 2AG and PEA were elevated in quantities comparable to the ones showed in the present study (Loría *et al.*, 2009). Moreover, ECL levels were measured only after 24 hours treatment in the present study. It is likely that the intracellular concentration of ECs will vary after URB597 treatment as a function of time. Moreover, the fact that different ECL appear to be elevated in SH-SY5Y cells after URB597 treatment compared to other *ex vivo* studies can be explained by a different site-specific availability of the various phospholipid precursors as well as possible distinct biosynthetic pathways.

Both AEA and 2AG are reported here to be ligands of PPARβ while ODA appears to be a pan-PPAR ligand (see Chapter 5 and 6). However, their IC_{50} are on the mid-micromolar range and the slight increase observed in ECL levels after URB597 treatment (see Chapter 4) might not appear enough to explain PPAR transactivation. Nevertheless, it was previously shown by a colleague in my lab how heterologous expression of fatty acid binding protein (FABP) 3 and 7 can selectively enhance activation of PPARα and PPARγ by exogenously administered OEA and AEA, respectively (Sun *et al.*, 2008). Moreover, (Kaczocha *et al.*, 2009) recently demonstrated that AEA uptake and hydrolysis were significantly potentiated in N18TG2 neuroblastoma cells after over-expression of FABP5 or FABP7. Taken together, these studies highlight the role of FABPs as AEA carriers. A similar chaperone system would explain how ECs that appear to only weakly bind to PPARs in cell-free systems and minimal differences in their intracellular concentration might lead to PPARs activation.

The notion of a measurable EC tone in human cells and the possibility of a link between variation in intracellular ECs concentrations and PPAR activation might speculatively highlight a new role for these signalling lipids. PPARs are widely recognised as "lipid sensors" providing a ready transcriptional response to changes in the available lipids pool (Berger *et al.*, 2002). Intracellular ECLs would appear to be mainly regulated by FAAH (McKinney *et al.*, 2005). So far, this enzyme has been shown to be regulated by FSH, leptin and progesterone (Maccarrone *et al.*, 2003a; Maccarrone *et al.*, 2003b; Rossi *et al.*,

2007). ECs might represent the substrates that allow a cross-talk between these hormones and PPAR function.

As previously mentioned, increasing evidence points towards a role for PPARs in mediating the anti inflammatory and analgesic effects of FAAH inhibition. The experiments presented in this study might be developed into models that would be useful to study the potential of new inhibitors of the EC metabolism in activating this pathway. Crucially, intracellular ECLs should be monitored after treatment with both OL135 and PF750 other than URB597 in order to strengthen the link between FAAH inhibition and PPARs transactivation. Moreover, timecourse experiments to monitor EC levels and PPARs activation should be carried out in order to better understand the relationship between these systems. The possibility of PPARs mediating the analgesic effect of FAAH inhibition is fascinating. However, this therapeutic approach is not without drawbacks. FAAH inhibition *in vivo* would indeed indiscriminately augment a variety of ECLs in the human body. Studying this mechanism *in vivo* could help us to develop novel FAAH inhibitors with selective effect on PPARs activation over CB receptors activation. As an example, URB597 would also inhibit FAAH-2 in humans, possibly leading to accumulation of ODA other than the rest of ECLs. ODA accumulation might in turn lead to sleep induction, a major and unwanted side effect.

The same model developed in this study might be used to test novel MGL inhibitors. However, inhibition of this enzyme might actually lead to even

more marked central side effects. Indeedm, while FAAH inhibitors are largely inactive in the tetrad test, (Long *et al.*, 2009) showed that a selective MGL inhibitor (JZL184) caused hypomotility when administered in mice. Dual inhibition of FAAH and MGL is not a feasible target either. Indeed, the same authors reported that this approach leads to a stronger analgesic effect than FAAH or MGL inhibition alone, but caused hypomotility, catalepsy and THC-like effects in drug discrimination (Long *et al.*, 2009*)*. Conversely, as already mentioned no rewarding effects are produced after FAAH inhibition by URB597 and this compound does not substitute for cannabinoid agonists in a rat drug discrimination test (Gobbi *et al.*, 2005). Long et al. (2009) concluded that the limited abuse potential of selective FAAH inhibitors compared to direct CB_1 agonists may reflect a requirement for dual stimulation of AEA and 2-AG pathways to produce the subjective effects of marijuana.

Finally, it is worth mentioning that FAAH inhibition might not be a therapeutic strategy for analgesia only. Indeed, it is well recognised that ECLs up-regulation exerts a protective action during inflammatory conditions. In a recent review of the therapeutic applications of the modulation of the EC system (Bifulco, 2009), it is outlined how pharmacological elevation of ECLs levels may be a promising strategy to counteract intestinal inflammation and colon cancer. Moreover, the involvement of the EC system and in particular of the FAAH enzyme in reproduction and fertility is presented as potential new target for infertility treatment (Bifulco, 2009).

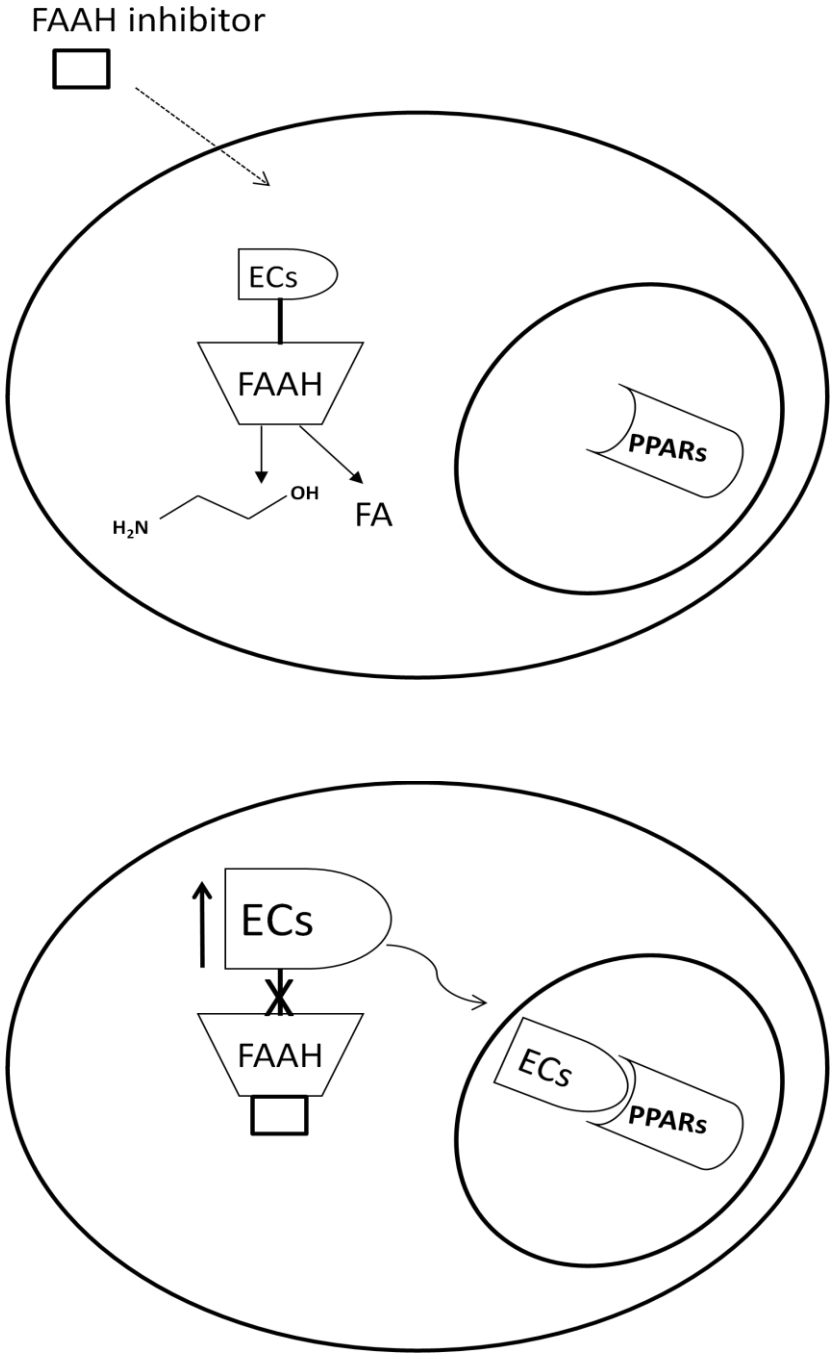

Figure 7.1: Schematic representation of the pharmacological inhibition of FAAH that leads to augmentation of intracellular endocannabinoids (ECs) levels that in turn activate PPARs nuclear receptors.

8. REFERENCES

Ahn K, Johnson DS, Fitzgerald LR, Liimatta M, Arendse A, Stevenson T, *et al.* (2007). Novel Mechanistic Class of Fatty Acid Amide Hydrolase Inhibitors with Remarkable Selectivity *Biochemistry* 46(45): 13019-13030.

Ahn K, Johnson DS, Mileni M, Beidler D, Long JZ, McKinney MK, *et al.* (2009). Discovery and Characterization of a Highly Selective FAAH Inhibitor that Reduces Inflammatory Pain. *Chemistry & Biology* 16(4): 411-420.

Alexander JP, Cravatt BF (2005). Mechanism of Carbamate Inactivation of FAAH: Implications for the Design of Covalent Inhibitors and In Vivo Functional Probes for Enzymes. *Chemistry & Biology* 12(11): 1179-1187.

Alexander SPH, Kendall DA (2007). The complications of promiscuity: endocannabinoid action and metabolism. *British Journal of Pharmacology* Epub: 1-22.

Appendino G, Minassi A, Di Marzo V (2006). Oxyhomologues of Anandamide and Related Endolipids: Chemoselective Synthesis and Biological Activity. *Journal of Medicinal Chemistry* 49: 2333-2338.

Berger J, Moller DE (2002). The Mechanisms of Action of PPARs. *Annual Reviews Medicine* 53: 409-435.

Bifulco PM (2009). The endocannabinoid system: From biology to therapy. *Pharmacological Research* 60(2): 75-76.

Bishop-Bailey D, Bystrom J (2009). Emerging roles of peroxisome proliferator-activated receptor-[beta]/[delta] in inflammation. *Pharmacology & Therapeutics* 124(2): 141-150.

Bisogno T, Howell F, Williams G, Minassi A, Cascio MG, Ligresti A, *et al.* (2003). Cloning of the first sn1-DAG lipases points to the spatial and temporal regulation of endocannabinoid signaling in the brain. *J. Cell Biol.* 163(3): 463-468.

Bisogno T, Ligresti A, Di Marzo V (2005). The endocannabinoid signalling system: Biochemical aspects. *Pharmacology, Biochemistry and Behavior* 81: 224 – 238.

Boger D, Miyauchi H, Du W, Cravatt B (2005). Discovery of a Potent, Selective, and Efficacious Class of Reversible alpha-Ketoheterocycle Inhibitors of Fatty Acid Amide Hydrolase Effective as Analgesics. *Journal of Medicinal Chemistry* 48: 1849-1856.

Boger D, Patterson J, Gilula N (1998). Chemical requirements for inhibition of gap junction communication by the biologically active lipid oleamide. *Proceedings of the National Academy of Sciences USA* 95(9): 4810-4815.

Boldrup L, Wilson S, Fowler C (2004). A simple stopped assay for fatty acid amide hydrolase avoiding the use of a chloroform extraction phase. *J. Biochem. Biophys. Methods* 60: 171–177.

Bouaboula M, Hilairet S, Casellas P (2005). Anandamide induced PPARg transcriptional activation and 3T3-L1 preadipocyte differentiation. *European Journal of Pharmacology* 517: 174 – 181.

Brown S, Wager-Miller J, Mackie K (2002). Cloning and molecular characterization of the rat CB2 cannabinoid receptor. *Biochimica et Biophysica Acta* 1576: 255– 264.

Causevic M, Wolf C, Palmer C (1999). Substitution of a conserved amino acid residue alters the ligand binding properties of peroxisome proliferator activated receptors. *FEBS Letters* 463(3): 205-210.

Cellai I, Benvenuti S, Luciani P, Galli A, Ceni E, Simi L, *et al.* (2006). Antineoplastic effects of rosiglitazone and PPAR[gamma] transactivation in neuroblastoma cells. *Br J Cancer* 95(7): 879-888.

Chang L, Luo L, Palmer C, Sutton S, Wilson S, Barbier A, *et al.* (2006). Inhibition of fatty acid amide hydrolase produces analgesia by multiple mechanisms. *British Journal of Pharmacology* 148(1): 102-113.

Cravatt B, Demarest K, Lichtman A (2001). Supersensitivity to anandamide and enhanced endogenous cannabinoid signaling in mice lacking fatty acid amide hydrolase. *Proceedings of the National Academy of Sciences USA* 98(16): 9371–9376.

Cravatt BF, Prospero-Garcia O, Siuzdak G, Gilula NB, Henriksen S, Boger DL, *et al.* (1995). Chemical characterization of a family of brain lipids that induce sleep. *Science* 268(5216): 1506-1509.

Day T, Rakhshan F, Deutsch D, Barkerm E (2001). Role of Fatty Acid Amide Hydrolase in the Transport of the Endogenous Cannabinoid Anandamide. *Molecular Pharmacology* 59: 1369-1375.

De Petrocellis L, Bisogno T, Di Marzo V (2002). Effect on cancer cell proliferation of palmitoylethanolamide, a fatty acid amide interacting with both the cannabinoid and vanilloid signalling systems. *Fundamental & Clinical Pharmacology* 16: 297–302.

Demuth D, Molleman A (2006). Cannabinoid signalling. *Life Sciences* 78: 549 – 563.

Deutsch DG, Chin SA (1993). Enzymatic synthesis and degradation of anandamide, a cannabinoid receptor agonist. *Biochemical Pharmacology* 46(5): 791-796.

Devane W, Hanus L, Breuer, Pertwee, Stevenson, Griffin, *et al.* (1992). Isolation and structure of a brain constituent that binds to the cannabinoid receptor. *Science* 258(5090): 1946-1949.

Di Loreto S, D'Angelo B, Cimini A (2007). PPARb Agonists Trigger Neuronal Differentiation in the Human Neuroblastoma Cell Line SH-SY5Y. *Journal of Cellular Physiology* 211: 837–847.

Di Marzo V, Bifulco M, De Petrocellis L (2004). The endocannabinoid system and its therapeutic exploitation. *Nat Rev Drug Discov* 3(9): 771-784.

Di Marzo V, Maccarrone M (2008). FAAH and anandamide: is 2-AG really the odd one out? ***Trends in Pharmacological Sciences*** **29(5): 229-233.**

Di Marzo V, Melck D, De Petrocellis L (2001). Palmitoylethanolamide inhibits the expression of fatty acid amide hydrolase and enhances the anti-proliferative effect of anandamide in human breast cancer cells. ***Biochemical Journal*** **358: 249-255.**

Dinh T, Freund T, Piomelli D (2002). A role for monoglyceride lipase in 2-arachidonoylglycerol inactivation. ***Chemistry and Physics of Lipids*** **121: 149-158.**

Drew P, Xu J, Racke M (2006). Peroxisome proliferator-activated receptor agonist regulation of glial activation: Relevance to CNS inflammatory disorders. ***Neurochemistry International*** **49: 183–189.**

Fedorova I, Hashimoto A, Basile A (2001). Behavioral Evidence for the Interaction of Oleamide with Multiple Neurotransmitter Systems. ***The Journal of Pharmacology and Experimental Therapeutics*** **299(1): 332-342.**

Fegley D, Gaetani S, Piomelli D (2005). Characterization of the Fatty Acid Amide Hydrolase Inhibitor Cyclohexyl Carbamic Acid 3'-Carbamoyl-biphenyl-3-yl Ester (URB597): Effects on Anandamide and Oleoylethanolamide Deactivation. ***The Journal of Pharmacology and Experimental Therapeutics*** **313(1): 352–358.**

Fowler C (2006). The cannabinoid system and its pharmacological manipulation – a review, with emphasis upon the uptake and hydrolysis of anandamide. ***Fundamental & Clinical Pharmacology*** **20: 549–562.**

Fowler C (2004). Oleamide: a member of the endocannabinoid family? ***British Journal of Pharmacology*** **141: 195-196.**

Fu J, Gaetani S, Piomelli D (2003). Oleylethanolamide regulates feeding and body weight through activation of the nuclear receptor PPAR-a. ***Nature*** **425(2): 90-93.**

Gaoni Y, Mechoulam R (1971). The Isolation and Structure of delta 9'-Tetrahydrocannabinol and Other Neutral Cannabinoids from Hashish. ***Journal of the American Chemical Society*** **93(1): 217-224.**

García-Bueno B, Madrigal J, Leza J (2005). Peroxisome Proliferator-Activated Receptor Gamma Activation Decreases Neuroinflammation in Brain After Stress in Rats. ***Biological Psychiatry*** **57: 885–894.**

Gardner O, Dewar B, Graves L (2005). Activation of Mitogen-Activated Protein Kinases by Peroxisome Proliferator-Activated Receptor Ligands: An Example of Nongenomic Signaling. ***Molecular Pharmacology*** **68(4): 933-941.**

Giuffrida A, Parsons LH, Kerr TM, de Fonseca FR, Navarro M, Piomelli D (1999). Dopamine activation of endogenous cannabinoid signaling in dorsal striatum. ***Nat Neurosci*** **2(4): 358-363.**

Gobbi G, Bambico FR, Mangieri R, Bortolato M, Campolongo P, Solinas M, *et al.* (2005). Antidepressant-like activity and modulation of brain monoaminergic transmission by blockade of anandamide hydrolysis. *Proceedings of the National Academy of Sciences of the United States of America* 102(51): 18620-18625.

Gómez-Ruiz M, Hernández M, de Miguel R, Ramos J (2007). An Overview on the Biochemistry of the Cannabinoid System. *Molecular Neurobiology* 36: 3-14.

Guzman M, Lo Verme J, Piomelli D (2004). Oleoylethanolamide Stimulates Lipolysis by Activating the Nuclear Receptor Peroxisome Proliferator-activated Receptor a (PPAR-a). *The Journal of Biological Chemistry* 279(27): 27849–27854.

Hoi PM, Hiley CR (2006). Vasorelaxant effects of oleamide in rat small mesenteric artery indicate action at a novel cannabinoid receptor. *British Journal of Pharmacology* 147: 560-568.

Holt S, Comelli F, Fowler C (2005). Inhibitors of fatty acid amide hydrolase reduce carrageenan induced hind paw inflammation in pentobarbital-treated mice: comparison with indomethacin and possible involvement of cannabinoid receptors. *British Journal of Pharmacology* 146: 467–476.

Jhaveri M, Richardson D, Chapman V (2006). Analgesic Effects of Fatty Acid Amide Hydrolase Inhibition in a Rat Model of Neuropathic Pain. *The Journal of Neuroscience* 26(51): 13318 –13327.

Jhaveri M, Richardson D, Chapman V (2008). Inhibition of fatty acid amide hydrolase and cyclooxygenase-2 increases levels of endocannabinoid related molecules and produces analgesia via peroxisome proliferator-activated receptor-alpha in a model of inflammatory pain. ***Neuropharmacology*** **55: 85-93.**

Kaczocha M, Glaser ST, Deutsch DG (2009). Identification of intracellular carriers for the endocannabinoid anandamide. ***Proceedings of the National Academy of Sciences*** **106(15): 6375-6380.**

Kathuria S, Gaetani S, Piomelli D (2003). Modulation of anxiety through blockade of anandamide hydrolysis. ***Nature Medicin*** **9(1): 76-81.**

Kim J, Isokawa M, Ledent C, Alger BE (2002). Activation of Muscarinic Acetylcholine Receptors Enhances the Release of Endogenous Cannabinoids in the Hippocampus. ***J. Neurosci.*** **22(23): 10182-10191.**

Klein T, Newton C, Larsen K, Lily Lu, Izabella Perkins, Liang Nong, ***et al.*** **(2003). The cannabinoid system and immune modulation.** ***Journal of Leukocyte Biology*** **74: 486–496.**

Kozak KR, Gupta RA, Moody JS, Ji C, Boeglin WE, DuBois RN, ***et al.*** **(2002). 15-Lipoxygenase Metabolism of 2-Arachidonylglycerol.** ***Journal of Biological Chemistry*** **277(26): 23278-23286.**

Laemmli U (1970). Cleavage of structural proteins during the assembly of the head of bacteriophage T4. ***Nature*** **227(5259): 680-685.**

Leesnitzer LM, Parks DJ, Bledsoe RK, Cobb JE, Collins JL, Consler TG, ***et al.*** **(2002). Functional Consequences of Cysteine Modification in the Ligand Binding Sites of Peroxisome Proliferator Activated Receptors by GW9662.** ***Biochemistry*** **41(21): 6640-6650.**

Leggett JD, Aspley S, Beckett SRG, D'Antona AM, Kendall DA, Kendall DA (2004). Oleamide is a selective endogenous agonist of rat and human CB1 cannabinoid receptors. ***British Journal of Pharmacology*** **141: 253–262.**

Lichtman A, Hawkins E, Cravatt B (2002). Pharmacological Activity of Fatty Acid Amides Is Regulated, but Not Mediated, by Fatty Acid Amide Hydrolase in Vivo. ***The Journal of Pharmacology and Experimental Therapeutics*** **302(1): 73-79.**

Lichtman A, Leung D, Cravatt B (2004). Reversible Inhibitors of Fatty Acid Amide Hydrolase That Promote Analgesia: Evidence for an Unprecedented Combination of Potency and Selectivity. ***The Journal of Pharmacology and Experimental Therapeutics*** **311(2): 441-448.**

Liu J, Li H, Chen D (2003). Activation and Binding of Peroxisome Proliferator-Activated Receptor gamma by Synthetic Cannabinoid Ajulemic Acid. ***Molecular Pharmacology*** **63(5): 983-992.**

Liu J, Wang L, Harvey-White J, Huang BX, Kim H-Y, Luquet S, *et al.* (2008). Multiple pathways involved in the biosynthesis of anandamide. *Neuropharmacology* 54(1): 1-7.

Liu QR, Pan CH, Hishimoto A, Li CY, Xi ZX, Llorente-Berzal A, *et al.* (2009). Species differences in cannabinoid receptor 2 (CNR2 gene): identification of novel human and rodent CB2 isoforms, differential tissue expression and regulation by cannabinoid receptor ligands. *Genes, Brain and Behavior* 8(5): 519-530.

Lo Verme J, La Rana G, Piomelli D (2005). The search for the palmitoylethanolamide receptor. *Life Sciences* 77(1685-1698).

Long JZ, Nomura DK, Vann RE, Walentiny DM, Booker L, Jin X, *et al.* (2009). Dual blockade of FAAH and MAGL identifies behavioral processes regulated by endocannabinoid crosstalk in vivo. *Proceedings of the National Academy of Sciences*: -.

Loría F, Petrosino S, Guaza C (2009). An endocannabinoid tone limits excitotoxicity in vitro and in a model of multiple sclerosis. *Neurobiology of Disease* 37(1): 166-176.

LoVerme J, Fu J, Astarita G, La Rana G, Russo R, Calignano A, *et al.* (2005). The Nuclear Receptor Peroxisome Proliferator-Activated Receptor-α Mediates the Anti-Inflammatory Actions of Palmitoylethanolamide. *Mol Pharmacol* 67(1): 15-19.

LoVerme J, Russo R, La Rana G, Fu J, Farthing J, Mattace-Raso G, *et al.* (2006). Rapid Broad-Spectrum Analgesia through Activation of Peroxisome Proliferator-Activated Receptor-{alpha}. *J Pharmacol Exp Ther* 319(3): 1051-1061.

Maccarrone M, Bari M, Rossi A (2003a). Progesterone Activates Fatty Acid Amide Hydrolase (FAAH) Promoter in Human T Lymphocytes through the Transcription Factor Ikaros. *The Journal of Biological Chemistry* 278(35): 32726–32732.

Maccarrone M, Di Rienzo M, Rossi A (2003b). Leptin Activates the Anandamide Hydrolase Promoter in Human T Lymphocytes through STAT3. *The Journal of Biological Chemistry* 278(15): 13318–13324.

Mana H, Spohn U (2001). Sensitive and selective flow injection analysis of hydrogen sulfite/sulfur dioxide by fluorescence detection with and without membrane separation by gas diffusion. *Analytical Chemistry* 73: 3187-3192.

Marini P, Moriello A, Di Marzo V (2009). Cannabinoid CB1 receptor elevation of intracellular calcium in neuroblastoma SH-SY5Y cells: Interactions with muscarinic and δ-opioid receptors. *Biochimica et Biophysica Acta* 1793: 1289-1303.

Martin B, Mechoulam R, Razdan R (1999). Discovery and characterization of endogenous cannabinoids. *Life Sciences* 65: 573-595.

Matsuda L, Lolait S, Brownstein M, Young A, Bonner T (1990). Structure of a cannabinoid receptor and functional expression of the cloned cDNA. ***Nature*** **346(6284): 561.**

Mazzola C, Medalie J, Scherma M, Panlilio L, Solinas M, Tanda G, ***et al.*** **(2009). Fatty acid amide hydrolase (FAAH) inhibition enhances memory acquisition through activation of PPAR-α nuclear receptors.** ***Learn. Mem.*** **16.**

McKinney MK, Cravatt BF (2005). Structure and Function of Fatty Acid Amide Hydrolase. ***Annual Reviews Biochemistry*** **74: 411-432.**

Mechoulam R, Ben-Shabat S, Hanus L (1995). Identification of an Endogenous 2-Monoglyceride, Present in Canine Gut, That Binds to Cannabinoid Receptors. ***Biochemical Pharmacology*** **50(1): 83-90.**

Melis M, Pillolla G, Pistis M (2008). Endogenous Fatty Acid Ethanolamides Suppress Nicotine-Induced Activation of Mesolimbic Dopamine Neurons through Nuclear Receptors. ***The Journal of Neuroscience*** **28(51): 13985–13994.**

Michalik L, Auwerx J, Wahli W (2006). International Union of Pharmacology. LXI. Peroxisome Proliferator-Activated Receptors. ***Pharmacological Reviews*** **58: 726–741.**

Mueller E, Drori S, Spiegelman B (2002). Genetic Analysis of Adipogenesis through Peroxisome Proliferator-activated Receptor gamma Isoforms. ***The Journal of Biological Chemistry*** **277(44): 41925–41930.**

Munro S, Thomas K, Abu-Shaar M (1993). Molecular characterization of a peripheral receptor for cannabinoids. ***Nature*** **365(6441): 61.**

Niforatos W, Zhang X, Moreland R (2007). Activation of TRPA1 Channels by the Fatty Acid Amide Hydrolase Inhibitor 3-Carbamoylbiphenyl-3-yl cyclohexylcarbamate (URB597). ***Molecular Pharmacology*** **71: 1209-1216.**

O'Sullivan SE (2007). Cannabinoids go nuclear: evidence for activation of peroxisome proliferator-activated receptors. ***British Journal of Pharmacology*** **152: 576-582.**

O'Sullivan SE, Sun Y, Bennett AJ, Randall MD, Kendall DA (2009). Time-dependent vascular actions of cannabidiol in the rat aorta. ***European Journal of Pharmacology*** **612(1-3): 61-68.**

O'Sullivan SE, Tarling EJ, Bennett AJ, Kendall DA, Randall MD (2005). Novel time-dependent vascular actions of Delta9-tetrahydrocannabinol mediated by peroxisome proliferator-activated receptor gamma. ***Biochemical and Biophysical Research Communications*** **337(3): 824-831.**

Onaivi ES, Hiroki I, Jian-Ping G, Sejal P, Alex P, Paul A M, ***et al.*** **(2006). Discovery of the Presence and Functional Expression of Cannabinoid CB2 Receptors in Brain.** ***Annals of the New York Academy of Sciences*** **1074(Cellular and Molecular Mechanisms of Drugs of Abuse and Neurotoxicity: Cocaine, GHB, and Substituted Amphetamines): 514-536.**

Oz (2006). Receptor-independent actions of cannabinoids on cell membranes: Focus on endocannabinoids. ***Pharmacology & Therapeutics*** **111: 114–144.**

Pagotto U, Marsicano G, Cota D, Lutz B, Pasquali R (2006). The Emerging Role of the Endocannabinoid System in Endocrine Regulation and Energy Balance. ***Endocr Rev*** **27(1): 73-100.**

Palmer JA, Higuera ES, Chang L, Chaplan SR (2008). Fatty acid amide hydrolase inhibition enhances the anti-allodynic actions of endocannabinoids in a model of acute pain adapted for the mouse. ***Neuroscience*** **154(4): 1554-1561.**

Pasquariello N, Catanzaro G, Marzano V, Amadio D, Barcaroli D, Oddi S, ***et al.*** **(2009). Characterization of the endocannabinoid system in human neuronal cells, and proteomic analysis of anandamide-induced apoptosis.** ***J. Biol. Chem.*****: M109.044412.**

Piomelli D, Beltramo M, Stella N (1998). Endogenous Cannabinoid Signaling. ***Neurobiology of Disease*** **5: 462–473.**

Piomelli D, Tarzia G, Putman D (2006). Pharmacological Profile of the Selective FAAH Inhibitor KDS-4103 (URB597). ***CNS Drug Reviews*** **12(1): 21-38.**

Repetto G, del Peso A, Zurita JL (2008). Neutral red uptake assay for the estimation of cell viability/cytotoxicity. ***Nat. Protocols*** **3(7): 1125-1131.**

Richardson D, Ortori CA, Chapman V, Kendall DA, Barrett DA (2007). Quantitative profiling of endocannabinoids and related compounds in rat brain using liquid chromatography-tandem electrospray ionization mass spectrometry. ***Analytical Biochemistry*** **360(2): 216-226.**

Rockwell C, Snider N, Kaminski N (2006a). Interleukin-2 Suppression by 2-Arachidonyl Glycerol Is Mediated through Peroxisome Proliferator-Activated Receptor gamma Independently of Cannabinoid Receptors 1 and 2. ***Molecular Pharmacology*** **70(1): 101–111.**

Rockwell CE, Kaminski NE (2004). A Cyclooxygenase Metabolite of Anandamide Causes Inhibition of Interleukin-2 Secretion in Murine Splenocytes. ***Journal of Pharmacology and Experimental Therapeutics*** **311(2): 683-690.**

Rockwell CE, Snider NT, Thompson JT, Vanden Heuvel JP, Kaminski NE (2006b). Interleukin-2 Suppression by 2-Arachidonyl Glycerol Is Mediated through Peroxisome Proliferator-Activated Receptor gamma Independently of Cannabinoid Receptors 1 and 2. ***Molecular Pharmacology*** **70(1): 101-111.**

Rossi G, Gasperi V, Maccarrone M (2007). Follicle-Stimulating Hormone Activates Fatty Acid Amide Hydrolase by Protein Kinase A and Aromatase-Dependent Pathways in Mouse Primary Sertoli Cells. ***Endocrinology*** **148(3): 1431-1439.**

Russo R, Lo Verme J, Piomelli D (2007). The Fatty Acid Amide Hydrolase Inhibitor URB597 (Cyclohexylcarbamic Acid 3-Carbamoylbiphenyl-3-yl Ester) Reduces Neuropathic Pain after Oral Administration in Mice. ***The Journal of Pharmacology and Experimental Therapeutics*** **322(1): 236-242.**

Ryberg E, Larsson N, Greasley P (2007). The orphan receptor GPR55 is a novel cannabinoid receptor. ***British Journal of Pharmacology*** **152(7): 1092-1101.**

Schmid HHO (2000). Pathways and mechanisms of N-acylethanolamine biosynthesis: can anandamide be generated selectively? ***Chemistry and Physics of Lipids*** **108(1-2): 71-87.**

Schmid PC, Zuzarte-Augustin ML, Schmid HH (1985). Properties of rat liver N-acylethanolamine amidohydrolase. ***Journal of Biological Chemistry*** **260(26): 14145-14149.**

Shearer B, Steger D, Billin A (2008). Identification and characterization of a selective PPARbeta (NR1C2) antagonist ***Molecular Endocrinology*** **22(2): 523-529.**

Snider NT, Nast JA, Tesmer LA, Hollenberg PF (2009). A Cytochrome P450-Derived Epoxygenated Metabolite of Anandamide Is a Potent Cannabinoid Receptor 2-Selective Agonist. ***Molecular Pharmacology*** **75(4): 965-972.**

Solorzano C, Zhu C, Battista N, Astarita G, Lodola A, Rivara S, ***et al.*** **(2009). Selective N-acylethanolamine-hydrolyzing acid amidase inhibition reveals a key role for endogenous palmitoylethanolamide in inflammation.** ***Proceedings of the National Academy of Sciences*****: -.**

Straiker A, Mackie K (2006). Cannabinoids, Electrophysiology, and Retrograde Messengers: Challenges for the Next 5 Years. ***AAPS J*** **8(2): Article 31.**

Suárez J, Bermúdez-Silva F, Mackie K, Ledent C, Zimmer A, Cravatt B, ***et al.*** **(2008). Immunohistochemical description of the endogenous cannabinoid system in the rat cerebellum and functionally related nuclei.** ***The Journal of Comparative Neurology*** **509(4): 400-421.**

Sugiura T, Kondo S, Sukagawa A, Nakane S, Shinoda A, Itoh K, ***et al.*** **(1995). 2-Arachidonoylgylcerol: A Possible Endogenous Cannabinoid Receptor Ligand in Brain.** ***Biochemical and Biophysical Research Communications*** **215(1): 89-97.**

Sun Y, Alexander SPH, Garle MJ, Gibson CL, Hewitt K, Murphy SP, ***et al.*** **(2007). Cannabinoid activation of PPARa; a novel neuroprotective mechanism.** ***British Journal of Pharmacology*** **152(5): 734-743.**

Sun Y, Alexander SPH, Bennett AJ (2006). Cannabinoids and PPARα signalling. ***Biomedical society transactions*** **34: 1095-1097.**

Sun Y, Alexander SPH, Kendall DA, Bennett AJ (2008). Involvement of fatty acid binding proteins in the transport of endocannabinoids to peroxisome proliferator activated receptors. ***International Cannabinoid Research Society, Burlington, VT*** **p.17. 1.**

Thomas EA, Carson MJ, Sutcliffe JG (1998). Oleamide-induced modulation of 5-hydroxytryptamine receptor-mediated signaling. ***Annals New York Academy of Sciences*** **861: 183-189.**

Tsou K, Brown S, Sanudo (1998). Immunohistochemical distribution of Cannabinoid CB1 Receptors in the rat central nervous system. *Neuroscience* 83(2): 393–411.

Tsuboi K, Hilligsmann C, Vandevoorde Sv, Lambert DM, Ueda N (2004). N-cyclohexanecarbonylpentadecylamine: a selective inhibitor of the acid amidase hydrolysing N-acylethanolamines, as a tool to distinguish acid amidase from fatty acid amide hydrolase. *Biochem. J.* 379(1): 99-106.

Tsuboi K, Sun Y, Ueda N (2005). Molecular Characterization of N-Acylethanolamine-hydrolyzing Acid Amidase, a Novel Member of the Choloylglycine Hydrolase Family with Structural and Functional Similarity to Acid Ceramidase. *The Journal of Biological chemistry* 280(12): 11082–11092.

Tudor C, Feige J, Gelman L (2007). Association with Coregulators Is the Major Determinant Governing Peroxisome Proliferator-activated Receptor Mobility in Living Cells. *The Journal of Biological Chemistry* 282(7): 4417–4426.

Ueda N, Yamanaka K, Yamamoto S (2001). Purification and Characterization of an Acid Amidase Selective for N-Palmitoylethanolamine, a Putative Endogenous Anti-inflammatory Substance. *Journal of Biological Chemistry* 276(38): 35552-35557.

Valentiner U, Carlsson M, Schumacher U (2005). Ligands for the peroxisome proliferator-activated receptor- have inhibitory effects on growth of human neuroblastoma cells in vitro. *Toxicology* 213: 157–168.

Van der Stelt M, Trevisani M, Di Marzo V (2005). Anandamide acts as an intracellular messenger amplifying Ca2+ influx via TRPV1 channels. ***The EMBO Journal*** **24: 3026-3037.**

Varma N, Carlson GC, Ledent C, Alger BE (2001). Metabotropic Glutamate Receptors Drive the Endocannabinoid System in Hippocampus. ***J. Neurosci.*** **21(24): 188RC-.**

Vetter I, Lewis RJ (2009). Characterization of endogenous calcium responses in neuronal cell lines. ***Biochemical Pharmacology*** **79(6): 908-920.**

Walker JM, Huang SM, Strangman NM, Tsou K, Sanudo-Pena MC (1999). Pain modulation by release of the endogenous cannabinoid anandamide. ***Proceedings of the National Academy of Sciences of the United States of America*** **96(21): 12198-12203.**

Wang J, Okamoto Y, Morishita J, Tsuboi K, Miyatake A, Ueda N (2006). Functional Analysis of the Purified Anandamide-generating Phospholipase D as a Member of the Metallo-Î²-lactamase Family. ***Journal of Biological Chemistry*** **281(18): 12325-12335.**

Wei B, Mikkelsen T, Cravatt B (2006). A second fatty acid amide hydrolase with variable distribution among placental mammals. ***The Journal of Biological chemistry*** **281(48): 36569-36578.**

Wiley JL, Razdan RK, Martin BR (2006). Evaluation of the role of the arachidonic acid cascade in anandamide's in vivo effects in mice. ***Life Sciences*** **80(1): 24-35.**

Xu HE, Stanley TB, Montana VG, Lambert MH, Shearer BG, Cobb JE, *et al.* (2002). Structural basis for antagonist-mediated recruitment of nuclear co-repressors by PPAR[alpha]. *Nature* 415(6873): 813-817.

Yates ML, Barker EL (2009). Inactivation and Biotransformation of the Endogenous Cannabinoids Anandamide and 2-Arachidonoylglycerol. *Mol Pharmacol* 76(1): 11-17.

Yost C, Hampson A, Gray A (1998). Oleamide potentiates benzodiazepine-sensitive gamma-aminobutyric acid receptor activity but does not alter minimum alveolar anesthetic concentration. *Anesthesia and Analgesia* 86: 1294-1300.

Zhang D, Saraf A, Kolasa T, Bhatia P, Zheng GZ, Patel M, *et al.* (2007). Fatty acid amide hydrolase inhibitors display broad selectivity and inhibit multiple carboxylesterases as off-targets. *Neuropharmacology* 52(4): 1095-1105.

APPENDIX

8.1. Vector's inserts

Sequences in this chapter were copied and pasted from VectorNTI files.

Human PPARα (CDS: 124-1530):

1 gttctggagg ctgggaagtt caagatcaaa gtgccagcag attcagtgtc atgtgaggac

61 gtgcttcctg cttcatagat aagagcttgg agctcggcgc acaaccagca ccatctggtc

121 gcgatggtgg acacggaaag cccactctgc cccctctccc cactcgaggc cggcgatcta

181 gagagcccgt tatctgaaga gttcctgcaa gaaatgggaa acatccaaga gatttcgcaa

241 tccatcggcg aggatagttc tggaagcttt ggctttacgg aataccagta tttaggaagc

301 tgtcctggct cagatggctc ggtcatcacg gacacgcttt caccagcttc gagcccctcc

361 tcggtgactt atcctgtggt ccccggcagc gtggacgagt ctcccagtgg agcattgaac

421 atcgaatgta gaatctgcgg ggacaaggcc tcaggctatc attacggagt ccacgcgtgt

481 gaaggctgca agggcttctt tcggcgaacg attcgactca agctggtgta tgacaagtgc

541 gaccgcagct gcaagatcca gaaaaagaac agaaacaaat gccagtattg tcgatttcac

601 aagtgccttt ctgtcgggat gtcacacaac gcgattcgtt ttggacgaat gccaagatct

661 gagaaagcaa aactgaaagc agaaattctt acctgtgaac atgacataga agattctgaa

721 actgcagatc tcaaatctct ggccaagaga atctacgagg cctacttgaa gaacttcaac

781 atgaacaagg tcaaagcccg ggtcatcctc tcaggaaagg ccagtaacaa tccacctttt

841 gtcatacatg atatggagac actgtgtatg gctgagaaga cgctggtggc caagctggtg

901 gccaatggca tccagaacaa ggaggcggag gtccgcatct ttcactgctg ccagtgcacg

961 tcagtggaga ccgtcacgga gctcacggaa ttcgccaagg ccatcccagg cttcgcaaac

1021 ttggacctga acgatcaagt gacattgcta aaatacggag tttatgaggc catattcgcc

1081 atgctgtctt ctgtgatgaa caaagacggg atgctggtag cgtatggaaa tgggtttata

1141 actcgtgaat tcctaaaaag cctaaggaaa ccgttctgtg atatcatgga acccaagttt

1201 gattttgcca tgaagttcaa tgcactggaa ctggatgaca gtgatatctc ccttttgtg

1261 gctgctatca tttgctgtgg agatcgtcct ggccttctaa acgtaggaca cattgaaaaa

1321 atgcaggagg gtattgtaca tgtgctcaga ctccacctgc agagcaacca cccggacgat

1381 atctttctct tcccaaaact tcttcaaaaa atggcagacc tccggcagct ggtgacggag

1441 catgcgcagc tggtgcagat catcaagaag acggagtcgg atgctgcgct gcacccgcta

1501 ctgcaggaga tctacaggga catgtactga gttccttcag atcagccaca ccttttccag

1561 gagttctgaa gctgacagca ctacaaagga gacgggggag cagcacgatt ttgcacaaat

1621 atccaccact ttaaccttag agcttggaca gtctgagctg taggtaaccg gcatattatt

1681 ccatatcttt gttttaacca gtacttctaa gagcatagaa ctcaaatgct g

Cloning Primers:

Forward: ATAGGATCCTCGCGATGGTGGACACGGAA (BamHI)

Reverse: ATAAGGGCCCCCTGGAAAAGGTGTGGCTGATCTG (ApaI)

Lenght: 1443bp

Human PPARβ (CDS: 310-1635):

1 gcggagcgtg tgacgctgcg gccgccgcgg acctggggat taatgggaaa agttttggca

61 ggagcgggag aattctgcgg agcctgcggg acggcggcgg tggcgccgta ggcagccggg

121 acagtgttgt acagtgtttt gggcatgcac gtgatactca cacagtggct tctgctcacc

181 aacagatgaa gacagatgca ccaacgaggc tgatgggaac caccctgtag aggtccatct

241 gcgttcagac ccagacgatg ccagagctat gactgggcct gcaggtgtgg cgccgagggg

301 agatcagcca tggagcagcc acaggaggaa gcccctgagg tccgggaaga ggaggagaaa

361 gaggaagtgg cagaggcaga aggagcccca gagctcaatg ggggaccaca gcatgcactt

421 ccttccagca gctacacaga cctctcccgg agctcctcgc caccctcact gctggaccaa

481 ctgcagatgg gctgtgacgg ggcctcatgc ggcagcctca acatggagtg ccgggtgtgc

541 ggggacaagg catcgggctt ccactacggt gttcatgcat gtgaggggtg caagggcttc

601 ttccgtcgta cgatccgcat gaagctggag tacgagaagt gtgagcgcag ctgcaagatt

661 cagaagaaga accgcaacaa gtgccagtac tgccgcttcc agaagtgcct ggcactgggc

721 atgtcacaca acgctatccg ttttggtcgg atgccggagg ctgagaagag gaagctggtg

781 gcagggctga ctgcaaacga ggggagccag tacaacccac aggtggccga cctgaaggcc

841 ttctccaagc acatctacaa tgcctacctg aaaaacttca acatgaccaa aaagaaggcc

901 cgcagcatcc tcaccggcaa agccagccac acggcgccct ttgtgatcca cgacatcgag

961 acattgtggc aggcagagaa ggggctggtg tggaagcagt tggtgaatgg cctgcctccc

1021 tacaaggaga tcagcgtgca cgtcttctac cgctgccagt gcaccacagt ggagaccgtg

1081 cgggagctca ctgagttcgc caagagcatc cccagcttca gcagcctctt cctcaacgac

1141 caggttaccc ttctcaagta tggcgtgcac gaggccatct tcgccatgct ggcctctatc

1201 gtcaacaagg acgggctgct ggtagccaac ggcagtggct ttgtcacccg tgagttcctg

1261 cgcagcctcc gcaaaccctt cagtgatatc attgagccta agtttgaatt tgctgtcaag

1321 ttcaacgccc tggaacttga tgacagtgac ctggccctat tcattgcggc catcattctg

1381 tgtggagacc ggccaggcct catgaacgtt ccacgggtgg aggctatcca ggacaccatc

1441 ctgcgtgccc tcgaattcca cctgcaggcc aaccaccctg atgcccagta cctcttcccc

1501 aagctgctgc agaagatggc tgacctgcgg caactggtca ccgagcacgc ccagatgatg

1561 cagcggatca agaagaccga aaccgagacc tcgctgcacc ctctgctcca ggagatctac

1621 aaggacatgt actaacggcg gcacccaggc ctccctgcag actccaatgg ggccagcact

1681 ggaggggccc acccacatga cttttccatt gaccagccct tgagcacccg gcctggagca

1741 gcagagtccc acgatcgccc tcagacacat gacacccacg gcctctggct ccctgtgccc

1801 tctctcccgc ttcctccagc cagctctctt cctgtctttg ttgtctccct ctttctcagt

1861 tcctctttct tttctaattc ctgttgctct gtttcttcct ttctgtaggt ttctctcttc

1921 ccttctccct tgccctccct ttctctctcc acccccccacg tctgtcctcc tttcttattc

1981 tgtgagatgt tttgtattat ttcaccagca gcatagaaca ggacctctgc ttttgcacac

2041 cttttcccca ggagcagaag agagtggggc ctgccctctg ccccatcatt gcacctgcag

2101 gcttaggtcc tcacttctgt ctcctgtctt cagagcaaaa gacttgagcc atccaaagaa

2161 acactaagct ctctgggcct gggttccagg gaaggctaag catggcctgg actgactgca

2221 gccccctata gtcatggggt ccctgctgca aaggacagtg ggcaggaggc cccaggctga

2281 gagccagatg cctccccaag actgtcattg cccctccgat gctgaggcca cccactgacc

2341 caactgatcc tgctccagca gcacacctca gccccactga cacccagtgt ccttccatct

2401 tcacactggt ttgccaggcc aatgttgctg atggcccccc gcactggccg ctggacggca

2461 ctctcccagc ttggaagtag gcagggttcc ctccaggtgg gcccccacct cactgaagag

2521 gagcaagtct caagagaagg agggggggatt ggtggttgga ggaagcagca cacccaattc

2581 tgcccctagg actcggggtc tgagtcctgg ggtcaggcca gggagagctc ggggcaggcc

2641 ttccgccagc actcccactg ccccccctgcc cagtagcagc cgcccacatt gtgtcagcat

2701 ccagggccag ggcctggcct cacatccccc tgctcctttc tctagctggc tccacgggag

2761 ttcaggcccc actccccctg aagctgcccc tccagcacac acacataagc actgaaatca

2821 ctttacctgc aggctccatg cacctccctt ccctccctga ggcaggtgag aacccagaga

2881 gaggggcctg caggtgagca ggcagggctg ggccaggtct ccggggaggc aggggtcctg

2941 caggtcctgg tgggtcagcc cagcacctgc tcccagtggg agcttcccgg gataaactga

3001 gcctgttcat tctgatgtcc atttgtccca atagctctac tgccctcccc ttccccttta

3061 ctcagcccag ctggccacct agaagtctcc ctgcacagcc tctagtgtcc ggggaccttg

3121 tgggaccagt cccacaccgc tggtccctgc cctcccctgc tcccaggttg aggtgcgctc

3181 acctcagagc agggccaaag cacagctggg catgccatgt ctgagcggcg cagagccctc

3241 caggcctgca ggggcaaggg gctggctgga gtctcagagc acagaggtag gagaactggg

3301 gttcaagccc aggcttcctg ggtcctgcct ggtcctccct cccaaggagc cattctgtgt

3361 gtgactctgg gtggaagtgc ccagcccctg cccctacggg cgctgcagcc tcccttccat

3421 gccccaggat cactctctgc tggcaggatt cttcccgctc cccacctacc cagctgatgg

3481 gggttggggt gcttcctttc aggccaaggc tatgaaggga cagctgctgg gacccacctc

3541 cccctccccg gccacatgcc gcgtccctgc cccgacccgg gtctggtgct gaggatacag

3601 ctcttctcag tgtctgaaca atctccaaaa ttgaaatgta tatttttgct aggagcccca

3661 gcttcctgtg tttttaatat aaatagtgta cacagactga cgaaacttta aataaatggg

3721 aattaaatat ttaa

Cloning Primers:

Forward: ATAGGATCCAGATCAGCCATGGAGCAGCC (BamHI)

Reverse: ATATCTAGAGCCTGGGTGCCGCCGTTAGT (XbaI)

Lenght: 1331bp

Human PPARγ2 (CDS: 91-1608):

1 tccggttttt ttcttttaac ggattgatct tttgctagat agagacaaaa tatcagtgtg

61 aattacagca aacccctatt ccatgctgtt atgggtgaaa ctctgggaga ttctcctatt

121 gacccagaaa gcgattcctt cactgataca ctgtctgcaa acatatcaca agaaatgacc

181 atggttgaca cagagatgcc attctggccc accaactttg ggatcagctc cgtggatctc

241 tccgtaatgg aagaccactc ccactccttt gatatcaagc ccttcactac tgttgacttc

301 tccagcattt ctactccaca ttacgaagac attccattca caagaacaga tccagtggtt

361 gcagattaca agtatgacct gaaacttcaa gagtaccaaa gtgcaatcaa agtggagcct

421 gcatctccac cttattattc tgagaagact cagctctaca ataagcctca tgaagagcct

481 tccaactccc tcatggcaat tgaatgtcgt gtctgtggag ataaagcttc tggatttcac

541 tatggagttc atgcttgtga aggatgcaag ggtttcttcc ggagaacaat cagattgaag

601 cttatctatg acagatgtga tcttaactgt cggatccaca aaaaaagtag aaataaatgt

661 cagtactgtc ggtttcagaa atgccttgca gtggggatgt ctcataatgc catcaggttt

721 gggcggatgc cacaggccga gaaggagaag ctgttggcgg agatctccag tgatatcgac

781 cagctgaatc cagagtccgc tgacctccgg gccctggcaa aacatttgta tgactcatac

841 ataaagtcct tcccgctgac caaagcaaag gcgagggcga tcttgacagg aaagacaaca

901 gacaaatcac cattcgttat ctatgacatg aattccttaa tgatgggaga agataaaatc

961 aagttcaaac acatcacccc cctgcaggag cagagcaaag aggtggccat ccgcatcttt

1021 cagggctgcc agtttcgctc cgtggaggct gtgcaggaga tcacagagta tgccaaaagc

1081 attcctggtt ttgtaaatct tgacttgaac gaccaagtaa ctctcctcaa atatggagtc

1141 cacgagatca tttacacaat gctggcctcc ttgatgaata aagatggggt tctcatatcc

1201 gagggccaag gcttcatgac aagggagttt ctaaagagcc tgcgaaagcc ttttggtgac

1261 tttatggagc ccaagtttga gtttgctgtg aagttcaatg cactggaatt agatgacagc

1321 gacttggcaa tatttattgc tgtcattatt ctcagtggag accgcccagg tttgctgaat

1381 gtgaagccca ttgaagacat tcaagacaac ctgctacaag ccctggagct ccagctgaag

1441 ctgaaccacc ctgagtcctc acagctgttt gccaagctgc tccagaaaat gacagacctc

1501 agacagattg tcacggaaca cgtgcagcta ctgcaggtga tcaagaagac ggagacagac

1561 atgagtcttc acccgctcct gcaggagatc tacaaggact tgtactag

Cloning Primers:

Forward: ATTGGTACCCCATGCTGTTATGGGTGAAA (KpnI)

Reverse: ACGTCTAGACTAGTACAAGTCCTTGTAGA (XbaI)

Lenght: 1528bp

8.2. Primers and Probes

Sequences in this chapter were copied and pasted from Primer Express files

Human β-actin:

FW Primer: CCTGGCACCCAGCACAAT

Tm: 59 % G/C: 61 Length: 18

RV Primer: GCCGATCCACACGGAGTACT

Tm: 59 % G/C: 60 Length: 20

TaqMan Probe: ATCAAGATCATTGCTCCTCCTGAGCGC

Tm: 69 % G/C: 52 Length: 27

Amplicon:

Tm: 82 %G/C: 56 Length: 70

Human B2M:

FW Primer: TGACTTTGTCACAGCCCAAGATA

Tm: 58.9 % G/C: 43.5 Length: 23

RV Primer: AATCCAAATGCGGCATCTTC

Tm: 55.3 % G/C: 45 Length: 20

TaqMan Probe: TGATGCTGCTTACATGTCTCGATCCCA

Tm: 65.0 % G/C: 48.1 Length: 27

Amplicon:

Length: 85

Human GAPDH:

FW Primer: CAACAGCCTCAAGATCATCAGC

Tm: 60.3 % G/C: 50 Length: 22

RV Primer: TGGCATGGACTGTGGTCATGAG

Tm: 62.1 % G/C: 54.5 Length: 22

TaqMan Probe: CCTGGCCAAGGTCATCCATGACAAC

Tm: 66.3 % G/C: 56 Length: 25

Amplicon:

Length: 119

Human CB1:

FW Primer: GCCCATGTGGCTAAAAAAGC

Tm: 58 % G/C: 50 Length: 20

RV Primer: CAATGCCAAGTGTATCGGTTCTT

Tm: 59 % G/C: 43 Length: 23

TaqMan Probe: AGACAGTGGATGAGACACACAACGGCA

Tm: 69 % G/C: 52 Length: 27

Amplicon:

Tm: 79 %G/C: 48 Length: 79

Human CB2:

FW Primer: GCAGCGTGACTATGACCTTCAC

Tm: 58 % G/C: 55 Length: 22

RV Primer: GAGCTTTGTAGGAAGGTGGATAGC

Tm: 59 % G/C: 50 Length: 24

TaqMan Probe: TGACCGCCATTGACCGATACCTCTG

Tm: 69 % G/C: 56 Length: 25

Amplicon:

Tm: 83 %G/C: 58 Length: 99

Human FAAH:

FW Primer: TCGTTCGGCTGGAAAACTCT

Tm: 59 % G/C: 50 Length: 20

RV Primer: CTGGGCAATCACGGTTTTG

Tm: 59 % G/C: 53 Length: 19

TaqMan Probe: AACTGCAGCACGAGATCGAGGTGTACC

Tm: 68 % G/C: 56 Length: 27

Amplicon:

Tm: 82 %G/C: 56 Length: 70

Human FAAH2:

FW Primer: GCCGAGCAGCTTTAGTCTTAGG

Tm: 58 %G/C: 54.5 Length: 22

RV Primer: CAACATCTATACATTTCACCTTTCTCTGT

Tm: 58 %G/C: 34.5 Length 29

TaqMan Probe: CAAAGTTTGCCTCAAAGACCCCTCGG

Tm: 69 %G/C: 53.8 Length: 26

Amplicon:

Tm: 81 Length: 138

Human NAAA:

FW Primer: CAGGAACTACTTTTATTGGCTATGTAGGA

Tm: 59 %G/C: 37.9 Length: 29

RV Primer: CCAGCCTTTATCTCGTTCATCAC

Tm: 59 %G/C: 47.8 Length: 23

TaqMan Probe: ACTGGCCAGAGCCCACACAAGTTTACAGTT

Tm: 70 %G/C: 50 Length: 30

Amplicon:

Tm: 78 Length: 92

Human MGL:

FW Primer: CAGGACAAGACTCTCAAGATTTATGAA

Tm: 58% %G/C: 37 Length: 27

RV Primer: TGTCCTTTGAGAGACCCACATG

Tm: 59% %G/C: 50 Length 22

TaqMan Probe: CTTCCTGAAGTCACCAACTCCGTCTTCCAT

Tm: 69 %G/C: 50 Length: 30

Amplicon:

Tm: 78 Length: 114

Human DAGLa:

FW Primer: CCGGTGACCAGAAACACCAA

Tm: 60% %G/C: 55 Length: 20

RV Primer: GAGCATGTAGTAGCAGACCTCTTTG

Tm: 58% %G/C: 48 Length 25

TaqMan Probe: TCGACCTCAAGAATTCACAAGAGATGCTCC

Tm: 69 %G/C: 46.7 Length: 30

Amplicon:

Tm: 80 Length: 84

Human PPARα:

FW Primer: GCTTCCTGCTTCATAGATAAGAGCTT

Tm: 61.6 % G/C: 42.3 Length: 26

RV Primer: CACCATCGCGACCAGATG

Tm: 58.2 % G/C: 61.1 Length: 18

TaqMan Probe: AGCTCGGCGGCACAACCAGCA

Tm: 65.7 % G/C: 66.7 Length: 21

Human PPARβ:

FW Primer: TGCGGCCATCATTCTGTGT

Tm: 56.7 % G/C: 52.6 Length: 19

RV Primer: CAGGATGGTGTCCTGGATAGC

Tm: 61.8 % G/C: 57.1 Length: 21

TaqMan Probe: ACCGGCCAGGCCTCATGAACG

Tm: 65.7 % G/C: 66.7 Length: 21

Human PPARγ:

FW Primer: GATTCTCCTATTGACCCAGAAAGC

Tm: 64.8 % G/C: 46 Length: 24

RV Primer: GCATCTCTGTGTCAACCATGGT

Tm: 66.2 % G/C: 50 Length: 22

TaqMan Probe: ATTCCTTCACTGATACACTGTCTGCAAACATAT

Tm: 69.9 % G/C: 36 Length: 33

8.3. RNAi constructs

Anti-FAAH siRNA (Ambion):

ID: s496**1**

Sequence:

Sense: **GGCCUGGGAAGUGAACAAAtt**

Antisense: **UUUGUUCACUUCCCAGGCCtt**

ID: s496**3**

Sequence:

Sense: **CUAUGAGACUGACAACUAUtt**

Antisense: **AUAGUUGUCAGUCAGUCUCAUAGta**

Anti-FAAH siRNA (Dharmacon):

ID: A-009907-**14**

Sequence: GUCUCAAUUCUGAAGCUUC

ID: A-009907-**15**

Sequence: GCUUGAGCCUGAAUGAAGG

ID: A-009907-**16**

Sequence: CUUCAAAGGUGAUUUCGUG

ID: A-009907-**17**

Sequence: GGCUUAGGCACUGAUAUCG

Anti-FAAH shRNA (Sigma):

ID: TRCN0000050633

Sequence:

CCGGCCACAGTCCATGTTCAGCTATCTCGAGATAGCTGAACATG

GACTGTGGTTTTTG

ID:TRCN0000050634

Sequence:

CCGGGCTCTTCACCTATGTGGGAAACTCGAGTTTCCCACATAGG

TGAAGAGCTTTTTG

ID:TRCN0000050635

Sequence:

CCGGCGTCAGCTACACTATGCTGTACTCGAGTACAGCATAGTGT

AGCTGACGTTTTTG

ID:TRCN0000050637

Sequence:

CCGGAGAAGAGTTGTGTCTGCGGTTCTCGAGAACCGCAGACAC

AACTCTTCTTTTTTG